


1998

Studies in robust control: analysis of sampled-data systems and aircraft pitch control

Liping Zou
Iowa State University

Follow this and additional works at: <https://lib.dr.iastate.edu/rtd>

 Part of the [Aerospace Engineering Commons](#), and the [Electrical and Computer Engineering Commons](#)

Recommended Citation

Zou, Liping, "Studies in robust control: analysis of sampled-data systems and aircraft pitch control " (1998). *Retrospective Theses and Dissertations*. 11830.
<https://lib.dr.iastate.edu/rtd/11830>

This Dissertation is brought to you for free and open access by the Iowa State University Capstones, Theses and Dissertations at Iowa State University Digital Repository. It has been accepted for inclusion in Retrospective Theses and Dissertations by an authorized administrator of Iowa State University Digital Repository. For more information, please contact digirep@iastate.edu.

INFORMATION TO USERS

This manuscript has been reproduced from the microfilm master. UMI films the text directly from the original or copy submitted. Thus, some thesis and dissertation copies are in typewriter face, while others may be from any type of computer printer.

The quality of this reproduction is dependent upon the quality of the copy submitted. Broken or indistinct print, colored or poor quality illustrations and photographs, print bleedthrough, substandard margins, and improper alignment can adversely affect reproduction.

In the unlikely event that the author did not send UMI a complete manuscript and there are missing pages, these will be noted. Also, if unauthorized copyright material had to be removed, a note will indicate the deletion.

Oversize materials (e.g., maps, drawings, charts) are reproduced by sectioning the original, beginning at the upper left-hand corner and continuing from left to right in equal sections with small overlaps. Each original is also photographed in one exposure and is included in reduced form at the back of the book.

Photographs included in the original manuscript have been reproduced xerographically in this copy. Higher quality 6" x 9" black and white photographic prints are available for any photographs or illustrations appearing in this copy for an additional charge. Contact UMI directly to order.

UMI

A Bell & Howell Information Company
300 North Zeeb Road, Ann Arbor, MI 48106-1346 USA
313/761-4700 800/521-0600

**Studies in robust control: Analysis of sampled-data systems
and aircraft pitch control**

by

Liping Zou

A dissertation submitted to the graduate faculty
in partial fulfillment of the requirements for the degree of
DOCTOR OF PHILOSOPHY

Major: Electrical Engineering (Control Systems)

Major Professor: Mustafa H. Khammash

Iowa State University

Ames, Iowa

1998

Copyright © Liping Zou, 1998. All rights reserved.

UMI Number: 9826591

UMI Microform 9826591
Copyright 1998, by UMI Company. All rights reserved.

**This microform edition is protected against unauthorized
copying under Title 17, United States Code.**

UMI
300 North Zeeb Road
Ann Arbor, MI 48103

Graduate College
Iowa State University

This is to certify that the Doctoral dissertation of
Liping Zou
has met the dissertation requirements of Iowa State University

Signature was redacted for privacy.

Major Professor

Signature was redacted for privacy.

For the Major Program

Signature was redacted for privacy.

For the Graduate College

TABLE OF CONTENTS

ACKNOWLEDGMENTS	vi
ABSTRACT	vii
CHAPTER 1 GENERAL INTRODUCTION	1
PART I ROBUST STEADY-STATE TRACKING OF SAMPLED-DATA SYSTEMS	
CHAPTER 2 INTRODUCTION	4
CHAPTER 3 LITERATURE REVIEW	8
3.1 Robust Stability and Performance	8
3.2 Robust Stability and Performance of Sampled-Data Systems	9
3.3 Robust Steady-State Tracking of Sampled-Data Systems	10
CHAPTER 4 DEFINITIONS AND NOTATIONS	12
CHAPTER 5 ROBUST STEADY-STATE TRACKING OF DISCRETE-TIME SYSTEMS	15
5.1 Single-Input Tracking (LSI Discrete-Time Systems)	18
5.2 Multi-Input Tracking (LSI Discrete-Time Systems)	20
5.2.1 Problem Set-Up	20
5.2.2 Robust Steady-State Tracking	22
5.3 Linear Periodic Discrete-Time Systems	28

5.3.1	Lifting Technique	31
5.3.2	Robust Steady-State Tracking	37
CHAPTER 6 ROBUST STEADY-STATE TRACKING OF		
SAMPLED-DATA SYSTEMS		42
6.1	Sampled-Data Systems	42
6.2	Approximation of the Sampled-Data System	45
6.3	Steady-State Norm $\ \cdot\ _{ss}$ as Performance Measure	46
6.3.1	Steady-State Norm: $\ \cdot\ _{ss}$	46
6.3.2	System Set-Up and Lifting Technique	47
6.3.3	Robust Steady-State Tracking ($\ \cdot\ _{ss}$ Case)	52
6.4	Steady-State Norm $\ \cdot\ _{cs}$ as Performance Measure	60
6.4.1	Steady-State Norm: $\ \cdot\ _{cs}$	60
6.4.2	Robust Steady-State Tracking ($\ \cdot\ _{cs}$ Case)	63
CHAPTER 7 COMPUTATIONAL ALGORITHM AND		
SIMULATIONS		67
7.1	Computation Algorithm	67
7.2	An Example and Simulation	74
CHAPTER 8 CONCLUSIONS		77
PART II ROBUST AIRCRAFT PITCH CONTROL		78
CHAPTER 9 INTRODUCTION		79
CHAPTER 10 AIRCRAFT DYNAMICS AND		
PERFORMANCE CRITERIA		81
10.1	Aircraft Dynamics	81
10.2	Performance Criteria	83

CHAPTER 11 NOMINAL PERFORMANCE	86
11.1 Model Matching	86
11.1.1 Model Matching: Set-Up I	87
11.1.2 A Modified Set-Up for Model Matching	88
11.1.3 Discussion and Analysis	90
11.2 Desired Model as Prefilter	91
11.3 Results	93
CHAPTER 12 ROBUST PERFORMANCE	95
12.1 Parametric Variations of State-Space Model	95
12.2 Plant Variation in Frequency Domain Set-Up	100
12.3 Robust Design vs. Nominal Design	104
CHAPTER 13 CONCLUSIONS	106
CHAPTER 14 GENERAL CONCLUSIONS	107
APPENDIX A SET-UP: DISCUSSION AND ANALYSIS	109
APPENDIX B NOMINAL PERFORMANCE	112
APPENDIX C VARIABLE DEPENDENCE TABLES	127
APPENDIX D PLOTS OF WEIGHTING FUNCTIONS	128
APPENDIX E ROBUST PERFORMANCE	129
BIBLIOGRAPHY	147

ACKNOWLEDGMENTS

Many thanks to my major professor, Dr. Mustafa H. Khammash, for having been a constant source of inspiration and encouragement during my study and research. I am grateful to him for his intellectual guidance throughout this research. I would also like to thank him for funding my study and research at Iowa State University.

I extend special appreciation to Dr. Degang Chen. Dr. Ping Lu. Dr. Bion L. Pierson. and Dr. Vijay Vittal for serving on my thesis committee. I would like to thank them for their time, support, and valuable comments and suggestions.

I also sincerely appreciate the helpful discussions with my fellow students in the control lab as well as their suggestions.

My deepest thanks are due to my lovely wife, Mrs. Lin Xu. for her constant support.

ABSTRACT

This research consists of two parts: (1) robust steady-state tracking of sampled-data systems and (2) robust aircraft pitch control.

In Part I, robust steady-state tracking of linear shift-invariant and periodic discrete-time systems in the presence of structured norm-bounded discrete-time uncertainty is discussed first. Using the results for discrete-time systems, robust steady-state tracking of sampled-data systems, which are considered as continuous-time systems, in the presence of structured norm-bounded continuous-time uncertainty is addressed. Exact conditions are derived for robust steady-state tracking of known inputs for sampled-data systems by using the lifting technique. Sampled-data systems are approximated by fast sampling of the input and output. The resulting systems are in discrete time. Based on the analysis of the resulting approximate discrete-time systems, an approximate converging computation algorithm is given. The same results also apply to general periodic linear time-varying continuous-time systems.

In Part II, robust aircraft pitch control is presented. The discussion focuses on the longitudinal attitude control problem when aircraft weight and center of gravity are unavailable as control inputs. Due to the variation of weight and center of gravity in aircraft models, multiplicative uncertainty models for different flight conditions (three different altitudes/airspeeds) are derived for robust synthesis. Longitudinal attitude robust controllers are designed to provide consistent performance under varying weight and varying center of gravity locations.

CHAPTER 1 GENERAL INTRODUCTION

Two topics will be discussed in this dissertation: (1) robust steady-state tracking of sampled-data systems and (2) robust aircraft pitch control.

In the first part, robust steady-state tracking of sampled-data systems is considered. The performance is considered in a robust manner subject to the system's robust stability. Robustness of sampled-data systems has received a lot of attention recently. A sampled-data control system consists of a continuous-time plant to be controlled, a discrete-time controller, and ideal continuous-to-discrete and discrete-to-continuous transformers. Instances of sampled-data systems can be found in numerous control applications. Sampled-data systems are difficult to analyze because in continuous time they are time varying, or more precisely they are periodic, even when the plant and controller are both time invariant. Therefore the lifting technique is used to deal with periodic systems.

Robust performance of steady-state tracking to input signals is studied in our research of sampled-data systems. Even though zero tracking can be achieved for a nominal system, the steady-state tracking error may no longer be zero in the presence of system uncertainty. Based on the results of robust stability of sampled-data systems, conditions of robust tracking to known inputs in the presence of structured norm-bounded uncertainty will be developed in the following chapters, using some appropriately defined performance measures.

Chapter 2 introduces sampled-data systems and the robust steady-state tracking problem. Relevant research can be found in Chapter 3, the literature review. A collec-

tion of definitions and notations is given in Chapter 4. Robust steady-state tracking for discrete-time systems is considered in Chapter 5. Results are derived for multi-input tracking of linear shift-invariant and periodic discrete-time systems, respectively. Then in Chapter 6, exact conditions of robust steady-state tracking of sampled-data systems are obtained. Chapter 7 discusses a convergent computation algorithm by an approximation method when sampled-data systems are related to the approximated discrete-time systems; a simulation example is shown. Conclusions can be found in Chapter 8.

In the second part, we will address the robust controller design for the longitudinal altitude control of aircraft. This research focuses on the longitudinal altitude control of aircraft with variations in weight and center of gravity throughout the flight regime. The objective is to develop a robust control algorithm that provides consistent aircraft performance in the duration of flight.

Chapter 9 introduces the \mathcal{H}_∞ design for aircraft. Aircraft dynamics and performance criteria are given in Chapter 10. The aircraft model is given as a state-space model with variations in weight and center of gravity. Before the robust controller is designed, nominal models are investigated in Chapter 11. Two controller design set-ups are given: model matching and desired model as prefilter. Nominal controllers are designed using those two set-ups. Based on knowledge of the nominal design, a robust controller is synthesized using the prefilter approach in Chapter 12.

PART I

**ROBUST STEADY-STATE TRACKING OF
SAMPLED-DATA SYSTEMS**

CHAPTER 2 INTRODUCTION

Traditionally, the design of effective controllers for real systems requires accurate mathematical models of the physical systems. The design is based on the specific models of interest. However, the exact physical models cannot be obtained, only the approximated ones. On the other hand, the more accurate the models, the more complicated the design and analysis procedure is for the controllers. Therefore, simple but less accurate approximate systems should be studied. Besides the approximation of real systems, we cannot avoid the existence of uncertainty around the nominal systems. The uncertainty drives the real systems from the nominal models. Perturbations from outside will affect system performance as well. In general, a well-designed controller that achieves stability and performance for the nominal system may fail to achieve the designed objectives for the real system and may even make the closed-loop system unstable. For these reasons, robust control is introduced to deal with model uncertainty and perturbation.

Since digital techniques provide many benefits, modern control systems usually employ them for controllers. The fact that most new industrial controllers are digital provides strong motivation for studying digital control systems. Essentially, there are three approaches to the synthesis of digital controllers. (1) An analog controller is designed for the continuous-time plant and then is implemented as a discrete-time controller obtained by discretization. Analog specifications can be recovered as the sampling period of the discretization goes to 0. (2) We can also discretize the continuous-time plant and obtain an approximate discrete-time system. A discrete-time controller is designed for the resulting discrete-time system, and then this designed discrete-time controller is im-

plemented to control the original plant. The designed controller depends on the choice of sampling period. Both of these approaches ignore the system's behavior between the sampling instants and may result in designs that do not meet the specifications. (3) We can design controllers directly for sampled-data systems. This direct approach to studying sampled-data systems requires considering them as periodic continuous-time systems. Thus, this approach is harder than the previous two approaches because systems are time varying, but it will solve the problem with no approximation.

A sampled-data system arises when a discrete-time feedback controller, K_d , is introduced to control a continuous-time plant, G , through the connection by the sampler, S_T , and the hold device, H_T . S_T and H_T are synchronized (see Figure 2.1). The sampler S_T periodically samples and converts continuous-time signals into discrete-time signals. On the other hand, the hold operator H_T converts discrete-time signals into continuous-time

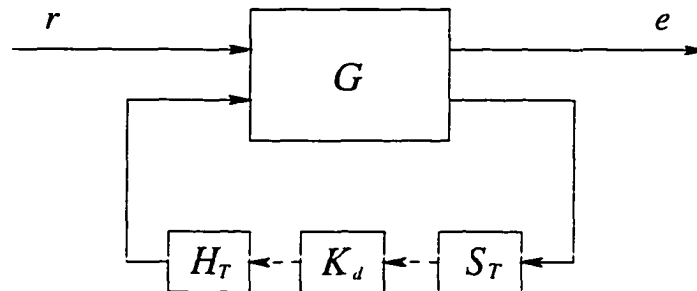


Figure 2.1 A sampled-data system

signals by holding them constant over the sampling period. Sampled-data systems operate in continuous time, but some continuous-time signals are sampled at certain instants, producing discrete-time signals. Thus, sampled-data systems are hybrid systems, involving both continuous-time and discrete-time signals in a continuous-time framework. A sampled-data system with this configuration, considered as a system in continuous time, is not time invariant even when the plant and the controller both are linear time invariant (LTI). In fact, this system is periodic with the same period T as the sampler

and hold device. A conventional approach to the sampled-data system problem is to use the isomorphic lifting technique, converting the periodic linear time-varying system to a linear time-invariant one.

Consequently, robust stability and performance to model uncertainty and perturbation is a consideration in sampled-data system analysis (see Figure 2.2). Some results have been developed for robust stability and performance. On the basis of the results for

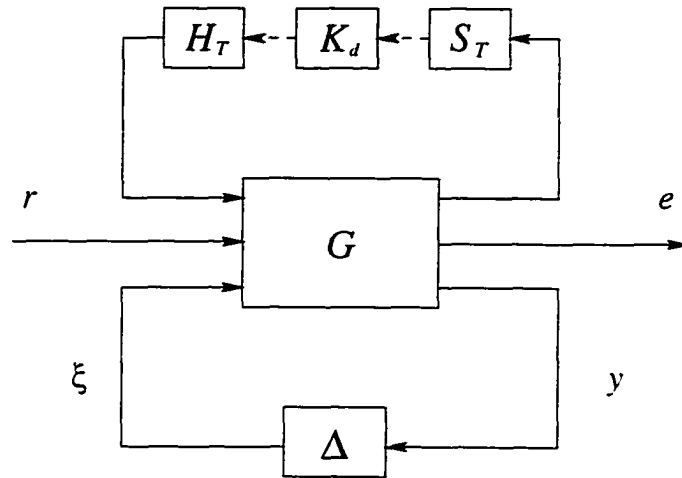


Figure 2.2 A sampled-data system with uncertainty

robust stability, robust steady-state tracking to known inputs, an important performance problem, will be discussed in the following chapters, using some appropriately defined performance measures. By robust steady-state tracking, we mean that the system is robustly stable and the steady-state tracking error in a certain measure is bounded and less than the required value in the presence of structured norm-bounded time-varying uncertainty with finite memory. We can show that even if zero steady-state tracking can be achieved for the nominal system, the steady-state tracking error may no longer be zero in the presence of time-varying uncertainty in the system. In fact, it can be quite large. Like the design approaches we discussed above, the performance analysis of robust steady-state tracking of sampled-data systems can be conducted in different ways.

We will discuss sampled-data systems directly and derive exact conditions of robust steady-state tracking for sampled-data systems. As far as computation is considered, we will discretize the continuous-time plant by fast sampling. Based on the performance analysis of the resulting approximate discrete-time system, a computation algorithm is given in a convergent approximation approach.

CHAPTER 3 LITERATURE REVIEW

Feedback control is necessary for control systems when disturbances and uncertainty are considered. Robustness of control systems in the presence of disturbances and uncertainty is an important issue in feedback control.

3.1 Robust Stability and Performance

Depending on the performance objectives and the nature of the signals affecting a given system, the robust stability and performance of the system can be addressed using approaches that differ according to the definitions of a number of different norms. These norms include the \mathcal{H}_2 norm, which measures the output power when the input is a white Gaussian stochastic process; the \mathcal{H}_∞ norm, which is the induced operator norm measuring energy gain of the operator when \mathcal{L}_2 signals, or bounded energy signals, affect the system; or the \mathcal{L}_1/l_1 norm, which captures the induced operator norm when the $\mathcal{L}_\infty/l_\infty$ signal (bounded signal) norm is used.

The last problem is the so-called \mathcal{L}_1/l_1 problem, which Vidyasagar [32] originally introduced in continuous-time systems when bounded persistent perturbations were presented. Dahleh and Pearson [12, 13] developed a complete solution to the \mathcal{L}_1/l_1 optimal control problem of linear time-invariant systems by minimizing the \mathcal{L}_1/l_1 norm of closed-loop systems. Dahleh and Ohta [11] found necessary and sufficient conditions for the robust stability of LTI systems with unstructured uncertainty. Khammash and Pearson [27, 28] derived the necessary and sufficient conditions for robust stability and per-

formance when nominal systems are LTI with structured uncertainty. The performance robustness problem can be converted to a stability problem, and necessary and sufficient conditions can be provided in the terms of the spectral radius of certain nonnegative matrices.

3.2 Robust Stability and Performance of Sampled-Data Systems

The robustness problem in sampled-data systems has received significant attention in the literature. In their book, Chen and Francis [10] discuss the subject and provide an extensive list of references. Basically, the difficulty in studying a sampled-data system is that it is time varying even when the plant and the controller are both time invariant. A general tool for dealing with sampled-data systems is the lifting technique, which was generalized as a framework in Bamieh and Pearson's paper [4]. These researchers established connection between periodic continuous-time systems and linear shift-invariant (LSI) infinite dimensional discrete-time systems. The same technique can be found in [3, 6]. The resulting infinite dimensional problem was then solved by an approximation procedure.

Robust stability and performance analysis are based on induced norms of the closed-loop operators. Computation and optimization of sampled-data system norms are popular research subjects. Bamieh and Pearson [4, 5] together with Dahleh [3]; Chen and Francis [8]; Dullerud [16] and with Francis [17]; Kabamba, and Hara [23]; Leung, Perry, and Francis [29]; Sivashankar, and Khargonekar [30] et al. have investigated the \mathcal{H}_2 , the \mathcal{H}_∞ , and the \mathcal{L}_∞ induced norms for sampled-data systems. A framework for studying nominal stability of sampled-data systems can be found in Chen and Francis [9] as well as Francis and Georgiou [19]. The robust stability problem of sampled-data systems in the presence of structured norm-bounded uncertainty was addressed by several re-

searchers. In their paper, Dullerud and Glover [18] studied the \mathcal{L}_2 -stable problem with stable structured LTI perturbation. Khammash [24] provided necessary and sufficient conditions for robust stability of linear time-invariant as well as linear time-varying systems when $\mathcal{L}_\infty(l_\infty)$ norm is taken to be the signal norm. Those conditions were given as the spectral radius of certain nonnegative matrices, which consist of induced norms of systems. In the same paper, it was shown that the same result can be applied to sampled-data systems. A similar result for sampled-data systems was developed in Sivashankar and Khargonekar [31] using a different approach. The \mathcal{L}_2 -stable problem for sampled-data systems was also studied there. With robust stability conditions available for sampled-data systems, robust performance problems such as robust tracking can be addressed.

3.3 Robust Steady-State Tracking of Sampled-Data Systems

Steady-state tracking and regulation have been addressed in the literature. Dullerud [16] investigated tracking step signals for sampled-data systems. Design of sampled-data regulators was discussed. A procedure to compute the \mathcal{L}_∞ induced norm of the closed-loop sampled-data systems was also presented. Hara and Sung [21] discussed ripple-free conditions in sampled-data control systems. Chen and Francis [10] also discussed step tracking of sampled-data systems. When the sampled-data system is internally stable, as a special case, tracking to a step input reference for the corresponding discretized system has no steady-state inter-sample ripple. The steady-state tracking errors for sampled-data system and the discretized system are equal. However, this is not the case for general reference signals. Ripple-free tracking cannot be guaranteed when system uncertainty is considered.

Khammash [25] introduced robust steady-state tracking of known inputs for discrete-time systems in the presence of structured norm bounded uncertainty. An appropriate

measure for discrete-time signals was also defined. By using this performance measure, necessary and sufficient conditions for robust steady-state tracking of LSI discrete-time systems were developed. Those conditions are easily computable and fit well with the existing conditions on stability robustness. A multi-reference tracking case was discussed in [33].

CHAPTER 4 DEFINITIONS AND NOTATIONS

- \mathbb{Z}^+ denotes the set of nonnegative integers.
- $\tilde{x}(k)$ and \tilde{x} denote discrete-time signals, while $\tilde{\mathbf{M}}$ and $\tilde{\Delta}$ denote discrete-time operators.
- $x(t)$ and x denote continuous-time signals, while \mathbf{M} and Δ denote continuous-time operators.
- l_∞ denotes the space of sequences $\{\tilde{x}(k)\}_{k=0}^\infty$ with the norm defined as

$$\|\tilde{x}\|_\infty := \sup_k |\tilde{x}(k)| < \infty.$$

- \mathcal{L}_∞ denotes the space of real valued measurable functions on $[0, \infty)$ with the norm defined as

$$\|x\|_{\mathcal{L}_\infty} := \text{ess sup}_t |x(t)| < \infty.$$

- $l_{\mathcal{L}_\infty[0,T]}^\infty$ denotes the space of $\mathcal{L}_\infty[0,T]$ -valued sequences $x = \{x_k\}, x_k \in \mathcal{L}_\infty[0,T]$.

The norm is defined as

$$\|x\|_{l_{\mathcal{L}_\infty[0,T]}^\infty} := \sup_k \|x_k\|_{\mathcal{L}_\infty[0,T]} < \infty.$$

- \mathcal{RC} denotes the space of real valued right continuous functions on $[0, \infty)$.

- c_o denotes the subspace of l_∞ of sequences converging to zero.
- P denotes the truncation operator:

For the discrete-time signal, $P_K: l_\infty \rightarrow l_\infty$,

$$(P_K \tilde{x})(k) := \begin{cases} \tilde{x}(k) & k \leq K. \\ 0 & \text{otherwise.} \end{cases}$$

For the continuous-time signal, $P_T: \mathcal{L}_\infty \rightarrow \mathcal{L}_\infty$.

$$(P_T x)(t) := \begin{cases} x(t) & t \leq T. \\ 0 & \text{otherwise.} \end{cases}$$

- The shift operator S_N (or S_T) acts on l_∞ (or \mathcal{L}_∞) signals by shifting them to the right by N (or T) if N (or T) > 0 and to the left if N (or T) < 0 .
- A linear shift-varying (LSV) discrete-time operator \tilde{M} is said to be periodic with period N if $\tilde{M} = S_{-N} \tilde{M} S_N$. Similarly, a linear time-varying continuous-time operator M is periodic with period T if $M = S_{-T} M S_T$.
- The kernel representation $\tilde{M}(\cdot, \cdot)$ (or $M(\cdot, \cdot)$) of an operator \tilde{M} (or M) is defined as follows:

For the discrete-time case, $\tilde{M}: l_\infty \rightarrow l_\infty$,

$$(\tilde{M} \tilde{x})(k) = \sum_{l=0}^{\infty} \tilde{M}(k, l) \tilde{x}(l).$$

For the continuous-time case, $M: \mathcal{L}_\infty \rightarrow \mathcal{L}_\infty$,

$$(Mx)(t) = \int_0^{\infty} M(t, \tau) x(\tau) d\tau.$$

- For a LTI l_∞ -stable operator $\tilde{M}: l_\infty \rightarrow l_\infty$, its impulse response is an element of l_1 , the space of sequences $\{\tilde{M}(k)\}_{k=0}^\infty$. The induced operator norm is given as

$$\|\tilde{M}\|_1 = \sum_{k=0}^{\infty} |\tilde{M}(k)| < \infty.$$

For a LTI \mathcal{L}_∞ -stable operator $M: \mathcal{L}_\infty \rightarrow \mathcal{L}_\infty$, its impulse response is an element of \mathcal{L}_1 . The induced operator norm is given as

$$\|M\|_1 = \sup_t \int_0^\infty |M(t, \tau)| d\tau < \infty.$$

CHAPTER 5 ROBUST STEADY-STATE TRACKING OF DISCRETE-TIME SYSTEMS

To prepare for the derivation of the solution to the problem of robust steady-state tracking of sampled-data systems, we will first discuss a similar problem for discrete-time systems. As a review, the results for linear shift-invariant discrete-time systems are shown in Section 5.1. For a general multi-input multi-tracking case, the necessary and sufficient conditions will be developed in Section 5.2. Finally, when the discrete-time system is periodic, the problem is solved by using the lifting technique.

First, let us examine the following example shown in Figure 5.1. \tilde{r} is the known reference input, and \tilde{e} is the tracking error. \tilde{G} is a linear shift-invariant discrete-time

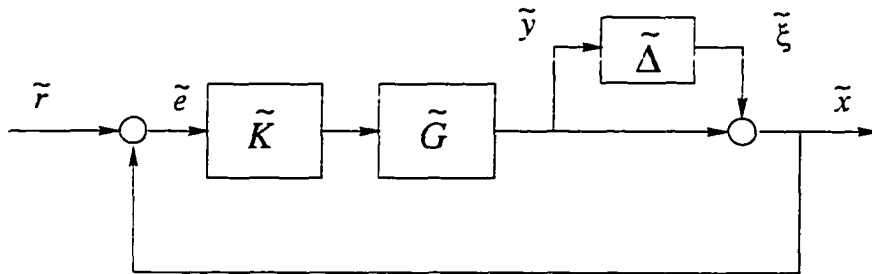


Figure 5.1 A robust tracking problem

plant, while \tilde{K} is a linear shift-invariant stabilizing discrete-time controller. $\tilde{\Delta}$ is a causal norm-bounded uncertainty that belongs to a certain class of perturbation that will be given later. The objective is to make the tracking error, \tilde{e} , as small as possible in the steady-state value. As one possible way, we can pose the robust tracking problem as

the worst-case steady-state value of the tracking error when system uncertainty varies within the uncertainty class to which it belongs.

For the tracking problem, it is natural to use the infinity norm to measure the signals of interest. Infinity norm is defined for the space, denoted as l_∞ , of the bounded sequences. Since steady-state tracking is the problem of interest, a steady-state measure in time domain, namely, steady-state semi-norm, will be defined as the performance measure.

The steady-state value of an error signal is defined as $\lim_{k \rightarrow \infty} |\tilde{x}(k)|$ if it exists. In general, the limit, $\lim_{k \rightarrow \infty} |\tilde{x}(k)|$, may not exist. However, the limit superior of a signal, $\lim_{K \rightarrow \infty} \sup_{k > K} |\tilde{x}(k)|$, always exists if $\tilde{x} \in l_\infty$. Let L_K denote the "tail" operator: $l_\infty \rightarrow l_\infty$ as follows:

$$L_K : L_K \tilde{x} = \begin{cases} \tilde{x}(k) & k > K. \\ 0 & \text{otherwise.} \end{cases}$$

Then, the limit superior can be defined as follows:

$$\lim_{K \rightarrow \infty} \sup_{k > K} |\tilde{x}(k)| = \lim_{K \rightarrow \infty} \|L_K \tilde{x}\|_{l_\infty}.$$

In the following, a steady-state semi-norm is generalized as a performance measure for tracking problems.

Definition 1 [25] (Steady-State Semi-Norm: Discrete-time) For a discrete-time signal $\tilde{x} \in l_\infty$, the steady-state semi-norm, $\|\tilde{x}\|_{ss}$, is given by

$$\|\tilde{x}\|_{ss} := \lim_{K \rightarrow \infty} \sup_{k > K} |\tilde{x}(k)| = \lim_{K \rightarrow \infty} \|L_K \tilde{x}\|_{l_\infty},$$

which is well defined as long as $\tilde{x} \in l_\infty$.

Note that $\|\tilde{x}\|_{ss} = \lim_{k \rightarrow \infty} |\tilde{x}(k)|$ if $\lim_{k \rightarrow \infty} |\tilde{x}(k)|$ exists. One can also see that for any $\tilde{x} \in l_\infty$, $\|\tilde{x}\|_{ss} \leq \|\tilde{x}\|_\infty$. This semi-norm $\|\cdot\|_{ss}$ can be extended to l_∞^p and computed

by $\|\tilde{x}\|_{ss} = \max_i \|\tilde{x}_i\|_{ss}$, where \tilde{x}_i is the i th component of \tilde{x} . Now the robust tracking problem can be evaluated by the quantity, $\sup_{\tilde{\Delta}} \|\tilde{x}\|_{ss}$, as the performance measure.

A conventional way to repose the robust tracking problem in a general form is given in Figure 5.2. \tilde{M} is the linear shift-invariant stable system representing the nominal part in the system that includes the nominal plant \tilde{G} and stabilizing controller \tilde{K} . $\tilde{\Delta}$

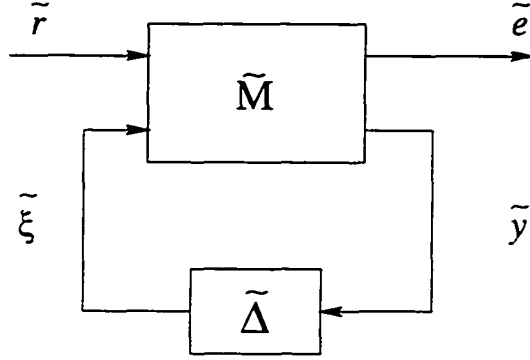


Figure 5.2 The discrete-time system with uncertainty

represents the uncertainty in that system. For a more general class of perturbations defined in the following

$$\tilde{\Delta} := \{\tilde{\Delta} : l_\infty \rightarrow l_\infty : \tilde{\Delta} \text{ is linear, causal, and } \|\tilde{\Delta}\| \leq 1\}.$$

the stability and performance conditions are known (see [11, 27, 28]).

In this research, the system uncertainty is restricted to the class of linear causal norm-bounded structured uncertainty with finite memory. A bounded linear operator, $\tilde{\Delta}$, is said to be a finite memory operator if $\tilde{\Delta}$ maps finite sequences into finite sequences. Let $\tilde{\Delta}_F$ denote the class of linear causal norm-bounded finite memory perturbations. The class of norm-bounded structured uncertainty with finite memory is defined as follows:

$$\tilde{\mathcal{D}}(n) = \{\text{diag}(\tilde{\Delta}_1, \dots, \tilde{\Delta}_n) : \tilde{\Delta}_i \in \tilde{\Delta}_F\},$$

where $\tilde{\Delta}_i : l_\infty \rightarrow l_\infty$ belongs to the class $\tilde{\Delta}_F$ and

$$\|\tilde{\Delta}_i\| := \sup_{\tilde{x} \neq 0} \frac{\|\tilde{\Delta}_i \tilde{x}\|_{l_\infty}}{\|\tilde{x}\|_{l_\infty}} \leq 1,$$

where $\|\tilde{\Delta}_i\|$ is the induced norm. Since $\tilde{\Delta}_F \subset \tilde{\Delta}$, the existing robust stability conditions are still sufficient when the perturbations are restricted to the class of $\tilde{\Delta}_F$. It has been shown in [25] that these same conditions also remain necessary in this situation, meaning that the existing necessary and sufficient conditions for robust stability remain the same when $\tilde{\mathcal{D}}(n)$ is considered as the class of uncertainty for the systems. All results obtained will equally applied to the case when $\tilde{\Delta}$ is fading-memory operator mapping c_0 into c_0 .

Let $\tilde{\mathbf{M}}$ (see Figure 5.3) be an bounded operator: $l_\infty^n \rightarrow l_\infty^n$. Define $\hat{\mathbf{M}}$ as the following:

$$\hat{\mathbf{M}} := \begin{pmatrix} \|\tilde{M}_{11}\|_1 & \cdots & \|\tilde{M}_{1n}\|_1 \\ \vdots & \ddots & \vdots \\ \|\tilde{M}_{n1}\|_1 & \cdots & \|\tilde{M}_{nn}\|_1 \end{pmatrix}.$$

The robust stability problem in Figure 5.3 is solved by the following theorem:

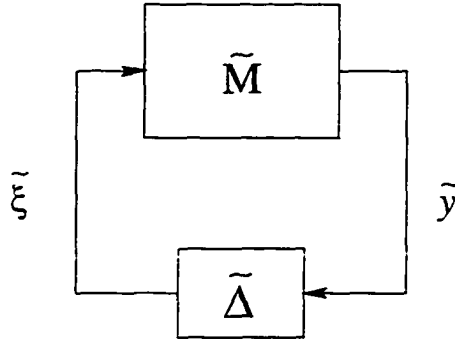


Figure 5.3 The robust stability problem

Theorem 1 [25] Robust Stability (Finite Memory Perturbation) *The system in Figure 5.3 is robustly stable iff $\rho(\hat{\mathbf{M}}) < 1$, where $\rho(\cdot)$ is the spectral radius.*

5.1 Single-Input Tracking (LSI Discrete-Time Systems)

Robust tracking for linear shift-invariant (LSI) discrete-time systems was first introduced by Khammash [25]. Necessary and sufficient conditions were derived for robust

steady-state tracking of known inputs in the presence of structured norm bounded uncertainty. The robust steady-state tracking problem is defined in [25] when $\tilde{\mathbf{M}}$ is a stable linear shift-invariant discrete-time system.

Definition 2 (Single-Input Tracking: LSI Discrete-Time Systems) *The linear shift-invariant discrete-time system $\tilde{\mathbf{M}}$ in Figure 5.2 is said to achieve robust steady-state tracking if*

1. *The interconnection of $\tilde{\mathbf{M}}$ and $\tilde{\Delta}$ is l_∞ -stable for all $\tilde{\Delta} \in \tilde{\mathcal{D}}(n)$.*
2. $\sup_{\tilde{\Delta} \in \tilde{\mathcal{D}}(n)} \|\tilde{e}\|_{ss} < 1$.

Suppose $\tilde{\mathbf{M}}$ (see Figure 5.2) is a linear shift-invariant discrete-time system. \tilde{r} is the single input signal, and \tilde{e} is the corresponding tracking error. Partition $\tilde{\mathbf{M}}$ as a $(n+1) \times (n+1)$ operator matrix:

$$\tilde{\mathbf{M}} = \begin{pmatrix} \tilde{M}_{11} & \tilde{M}_{12} & \dots & \tilde{M}_{1,n+1} \\ \tilde{M}_{21} & \tilde{M}_{22} & \dots & \tilde{M}_{2,n+1} \\ \vdots & \vdots & \ddots & \vdots \\ \tilde{M}_{n+1,1} & \tilde{M}_{n+1,2} & \dots & \tilde{M}_{n+1,n+1} \end{pmatrix}.$$

Let \tilde{M}_{ij} be the ij th element of $\tilde{\mathbf{M}}$. Since \tilde{M}_{ij} is a linear shift-invariant causal operator, it can be represented by the following infinite matrix with lower triangle structure:

$$\tilde{M}_{ij} : \begin{pmatrix} \tilde{M}_{ij}(0) & 0 & 0 & \dots \\ \tilde{M}_{ij}(1) & \tilde{M}_{ij}(0) & 0 & \dots \\ \tilde{M}_{ij}(2) & \tilde{M}_{ij}(1) & \tilde{M}_{ij}(0) & \dots \\ \vdots & \vdots & \vdots & \ddots \end{pmatrix}. \quad (5.1)$$

\tilde{M}_{ij} is a bounded operator: $l_\infty \rightarrow l_\infty$ since $\tilde{\mathbf{M}}$ is. Therefore, the induced norm $\|\tilde{M}_{ij}\|_1$ is well defined and

$$\|\tilde{M}_{ij}\|_1 := \sup_{\tilde{x} \neq 0} \frac{\|\tilde{M}_{ij}\tilde{x}\|_\infty}{\|\tilde{x}\|_\infty} = \sum_{k=0}^{\infty} |\tilde{M}_{ij}(k)| < \infty.$$

where $\tilde{M}_{ij}(\cdot)$ is the kernel representation of \tilde{M}_{ij} shown in (5.1). A fundamental $(n+1) \times (n+1)$ nonnegative matrix is defined as the steady-state norm matrix in the following:

$$\tilde{\mathbf{M}}_{ss} := \begin{pmatrix} \|\tilde{M}_{11}r\|_{ss} & \|\tilde{M}_{12}\|_1 & \cdots & \|\tilde{M}_{1,n+1}\|_1 \\ \|\tilde{M}_{21}r\|_{ss} & \|\tilde{M}_{22}\|_1 & \cdots & \|\tilde{M}_{2,n+1}\|_1 \\ \vdots & \vdots & \ddots & \vdots \\ \|\tilde{M}_{n+1,1}r\|_{ss} & \|\tilde{M}_{n+1,2}\|_1 & \cdots & \|\tilde{M}_{n+1,n+1}\|_1 \end{pmatrix}$$

According to [25], necessary and sufficient conditions of robust tracking for the system in Figure 5.2 were given by the following theorem:

Theorem 2 *The LSI discrete-time system $\tilde{\mathbf{M}}$ in Figure 5.2 achieves robust steady-state tracking iff $\rho(\tilde{\mathbf{M}}_{ss}) < 1$.*

5.2 Multi-Input Tracking (LSI Discrete-Time Systems)

Robust steady-state tracking of discrete-time multi-input multi-tracking systems will be discussed in this section.

5.2.1 Problem Set-Up

Consider the MIMO linear shift-invariant discrete-time system in Figure 5.4. $\tilde{r} \in \mathbb{R}^p$ is the known reference input with dimension p ; $\tilde{e} \in \mathbb{R}^q$ is the tracking error with dimension q . $\tilde{\Delta}$ represents the system uncertainty and belongs to $\tilde{\mathcal{D}}(n)$. The worst-case

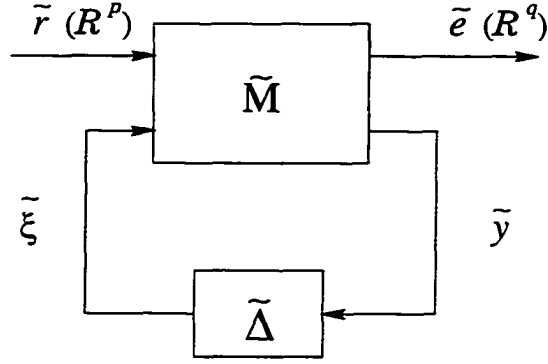


Figure 5.4 The MIMO discrete-time system

steady-state value of error \tilde{e} for $\tilde{\Delta} \in \tilde{\mathcal{D}}(n)$ when \tilde{r} is known is determined by the quantity

$$\max_{0 \leq i \leq q} \sup_{\tilde{\Delta} \in \tilde{\mathcal{D}}(n)} \|\tilde{e}_i\|_{ss}.$$

where \tilde{e}_i is the i th error signal.

$\tilde{\mathbf{M}}$ can be partitioned as $(q+n) \times (p+n)$ operator matrix in the following:

$$\tilde{\mathbf{M}} = \left(\begin{array}{ccc|ccc} \tilde{M}_{1,1} & \dots & \tilde{M}_{1,p} & \tilde{M}_{1,p+1} & \dots & \tilde{M}_{1,p+n} \\ \vdots & \ddots & \vdots & \vdots & \ddots & \vdots \\ \tilde{M}_{q,1} & \dots & \tilde{M}_{q,p} & \tilde{M}_{q,p+1} & \dots & \tilde{M}_{q,p+n} \\ \hline \tilde{M}_{q+1,1} & \dots & \tilde{M}_{q+1,p} & \tilde{M}_{q+1,p+1} & \dots & \tilde{M}_{q+1,p+n} \\ \vdots & \ddots & \vdots & \vdots & \ddots & \vdots \\ \tilde{M}_{q+n,1} & \dots & \tilde{M}_{q+n,p} & \tilde{M}_{q+n,p+1} & \dots & \tilde{M}_{q+n,p+n} \end{array} \right) := \begin{pmatrix} \tilde{\mathbf{M}}_{11} & \tilde{\mathbf{M}}_{12} \\ \tilde{\mathbf{M}}_{21} & \tilde{\mathbf{M}}_{22} \end{pmatrix}. \quad (5.2)$$

Therefore, the following equation holds

$$\begin{pmatrix} \tilde{e} \\ \tilde{y} \end{pmatrix} = \begin{pmatrix} \tilde{\mathbf{M}}_{11} & \tilde{\mathbf{M}}_{12} \\ \tilde{\mathbf{M}}_{21} & \tilde{\mathbf{M}}_{22} \end{pmatrix} \begin{pmatrix} \tilde{r} \\ \tilde{\xi} \end{pmatrix}$$

5.2.2 Robust Steady-State Tracking

The definition of robust steady-state tracking for a multi-input tracking system in Figure 5.4 is defined as follows:

Definition 3 (Multi-Input Tracking: LSI Discrete-Time Systems) *The linear time-invariant system $\tilde{\mathbf{M}}$ in Figure 5.4 is said to achieve robust steady-state tracking if*

1. *The interconnection of $\tilde{\mathbf{M}}$ and $\tilde{\Delta}$ is l_∞ -stable for all $\tilde{\Delta} \in \tilde{\mathcal{D}}(n)$.*
2. $\|\tilde{e}\|_{ss} := \max_{0 \leq i \leq q} \sup_{\tilde{\Delta} \in \tilde{\mathcal{D}}(n)} \|\tilde{e}_i\|_{ss} < 1$.

For different output tracking errors (there are q of them) of the system $\tilde{\mathbf{M}}$ in Figure 5.4, we can construct q different nonnegative matrices $\hat{\mathbf{M}}_{ss}^i \in R^{(n+1) \times (n+1)}$, $1 \leq i \leq q$, which are referred to as the *steady-state norm matrices* as follows:

$$\hat{\mathbf{M}}_{ss}^i = \begin{pmatrix} \left\| \sum_{l=1}^p \tilde{M}_{i,l} \tilde{r}_l \right\|_{ss} & \left\| \tilde{M}_{i,p+1} \right\|_1 & \cdots & \left\| \tilde{M}_{i,p+n} \right\|_1 \\ \left\| \sum_{l=1}^p \tilde{M}_{q+1,l} \tilde{r}_l \right\|_{ss} & \left\| \tilde{M}_{q+1,p+1} \right\|_1 & \cdots & \left\| \tilde{M}_{q+1,p+n} \right\|_1 \\ \vdots & \vdots & \ddots & \vdots \\ \left\| \sum_{l=1}^p \tilde{M}_{q+n,l} \tilde{r}_l \right\|_{ss} & \left\| \tilde{M}_{q+n,p+1} \right\|_1 & \cdots & \left\| \tilde{M}_{q+n,p+n} \right\|_1 \end{pmatrix} \quad (5.3)$$

Define the lower part of $\hat{\mathbf{M}}_{ss}^i$ as

$$\hat{\mathbf{M}}_\Delta = \begin{pmatrix} \left\| \tilde{M}_{q+1,p+1} \right\|_1 & \cdots & \left\| \tilde{M}_{q+1,p+n} \right\|_1 \\ \vdots & \ddots & \vdots \\ \left\| \tilde{M}_{q+n,p+1} \right\|_1 & \cdots & \left\| \tilde{M}_{q+n,p+n} \right\|_1 \end{pmatrix} \quad (5.4)$$

Before robust steady-state tracking is discussed, the stability robustness of the system in the presence of finite memory perturbation must be addressed. According to Theorem

1, the robust stability is determined by the lower part of the steady-state norm matrix. i.e., the necessary and sufficient condition is $\rho(\hat{\mathbf{M}}_\Delta) < 1$.

We will present sufficient conditions for robust steady-state tracking in terms of the above steady-state norm matrix (5.3). First we introduce the following Lemmas, which will be used in the theorem's proof.

Lemma 1 [25] *Let $\tilde{M} : l_\infty \rightarrow l_\infty$ be any bounded linear fading memory operator. Let $\tilde{x} \in l_\infty$. Then*

$$\|\tilde{M}\tilde{x}\|_{ss} \leq \|\tilde{M}\| \|\tilde{x}\|_{ss},$$

where $\|\tilde{M}\|$ is the induced l_∞ operator norm.

Proof: This can be easily seen if one notices that

$$\begin{aligned} \|L_m \tilde{M} \tilde{x}\|_\infty &= \|L_m \tilde{M} L_n \tilde{x} + L_m \tilde{M} P_n \tilde{x}\|_\infty \\ &\leq \|L_m \tilde{M} L_n \tilde{x}\|_\infty + \|L_m \tilde{M} P_n \tilde{x}\|_\infty \\ &\leq \|\tilde{M}\| \|L_n \tilde{x}\|_\infty + \|L_m \tilde{M} P_n \tilde{x}\|_\infty. \end{aligned}$$

The second term vanishes when first m and then n goes to infinity. □

A square nonnegative matrix has the following property:

Lemma 2 [22] *Let A be a square nonnegative matrix (i.e., $a_{ij} \geq 0$). Then $\rho(A) < 1$ if and only if $x \geq 0$ and $x \leq Ax$ imply $x = 0$. where the inequalities are taken component-wise.*

Theorem 3 *If $\rho(\hat{\mathbf{M}}_{ss}^i) < 1$, $1 \leq i \leq q$, then \tilde{M} is robustly stable and $\|\tilde{e}\|_{ss} < 1$ for all $\tilde{\Delta} \in \tilde{\mathcal{D}}(n)$.*

Proof: Define the nonnegative matrix $\hat{\mathbf{M}}_\Delta$ as above (5.4) for the lower part in (5.3), which is associated with the uncertainty.

By Lemma 2, it is easy to see that $\rho(\hat{\mathbf{M}}_{ss}^i) < 1$ implies $\rho(\hat{\mathbf{M}}_\Delta) < 1$, which is exactly necessary and sufficient for robust stability by Theorem 1, guaranteeing that the system is robustly stable.

For the second part of this theorem, we use contraposition. Suppose $\|\tilde{e}_i\|_{ss} \geq 1$ for some $i : 1 \leq i \leq q$ and $\tilde{\Delta} \in \tilde{\mathcal{D}}(n)$. If we define $\tilde{\xi}$ and \tilde{y} as in Figure 5.4, then \tilde{e} and \tilde{y} are given by

$$\tilde{e} = \tilde{\mathbf{M}}_{11}\tilde{r} + \tilde{\mathbf{M}}_{12}\tilde{\xi}, \quad (5.5)$$

$$\tilde{y} = \tilde{\mathbf{M}}_{21}\tilde{r} + \tilde{\mathbf{M}}_{22}\tilde{\xi}. \quad (5.6)$$

By Lemma 1 and using the fact that $\|\cdot\|_{ss}$ satisfies the triangle inequality, we have

$$1 \leq \|\tilde{e}_i\|_{ss} \leq \left\| \sum_{l=1}^p \tilde{M}_{i,l}\tilde{r}_l \right\|_{ss} + \|\tilde{M}_{i,p+1}\|_1 \|\tilde{\xi}_1\|_{ss} + \cdots + \|\tilde{M}_{i,p+n}\|_1 \|\tilde{\xi}_n\|_{ss}. \quad (5.7)$$

Using the fact that $\|\tilde{\Delta}\| \leq 1$, we have

$$\|\tilde{\xi}_j\|_{ss} \leq \|\tilde{y}_j\|_{ss},$$

and the following inequalities for $1 \leq j \leq n$

$$\begin{aligned} \|\tilde{\xi}_j\|_{ss} \leq \|\tilde{y}_j\|_{ss} &\leq \left\| \sum_{l=1}^p \tilde{M}_{q+j,l}\tilde{r}_l \right\|_{ss} + \|\tilde{M}_{q+j,p+1}\|_1 \|\tilde{\xi}_1\|_{ss} + \cdots + \\ &+ \|\tilde{M}_{q+j,p+n}\|_1 \|\tilde{\xi}_n\|_{ss}. \end{aligned} \quad (5.8)$$

Equations (5.7) and (5.8) imply that

$$x = (1, \|\tilde{\xi}_1\|_{ss}, \dots, \|\tilde{\xi}_n\|_{ss})'$$

satisfies $x \leq \hat{\mathbf{M}}_{ss}^i x$ and $x \geq 0$. By Lemma 2, this implies $\rho(\hat{\mathbf{M}}_{ss}^i) \geq 1$, a contradiction to the hypothesis. This completes the proof. \square

To obtain the necessary condition of robust steady-state tracking, we will need the following lemmas. The first lemma shows the effect of adding a c_0 signal on the values of the steady-state semi-norm. The second lemma presents necessary and sufficient

conditions of constructing an admissible uncertainty. Consider the auxiliary system in Figure 5.5.

Lemma 3 [25] *Suppose the interconnection in Figure 5.5 is stable $\forall \tilde{\Delta} \in \tilde{\mathcal{D}}(n)$. Then for any $\tilde{\Delta} \in \tilde{\mathcal{D}}(n)$, $\|\tilde{e}\|_{ss}$ remains unchanged $\forall \tilde{d} \in c_o^n$.*

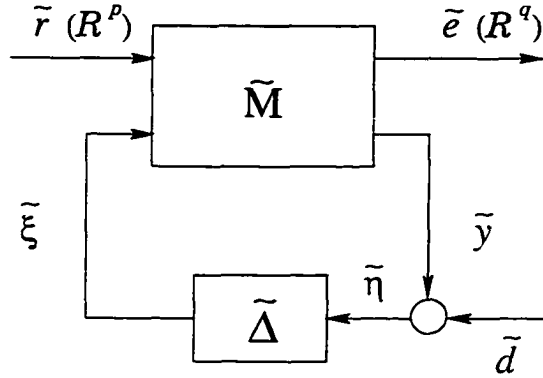


Figure 5.5 The auxiliary system

Lemma 4 [25] *Given any two sequences of real numbers $\tilde{\eta}$ and $\tilde{\xi}$, there exists $\tilde{\Delta} \in \tilde{\Delta}_F$ satisfying $\tilde{\Delta}\tilde{\eta} = \tilde{\xi}$ if and only if*

1. $\|P_k \tilde{\xi}\|_\infty \leq \|P_k \tilde{\eta}\|_\infty, \forall k.$
2. *For any $m \in \mathcal{Z}^+$, there exists $\tilde{m} \in \mathcal{Z}^+$ such that*

$$\|P_k L_{\tilde{m}} \tilde{\xi}\|_\infty \leq \|P_k L_m \tilde{\eta}\|_\infty, \forall k.$$

The following theorem states that the same condition in Theorem 3 remains necessary for robust tracking.

Theorem 4 *Suppose \tilde{M} is robustly stable and that $\|\tilde{e}\|_{ss} < 1$ for all $\tilde{\Delta} \in \tilde{\mathcal{D}}_F(n)$. Then $\rho(\hat{M}_{ss}^i) < 1$ for $1 \leq i \leq q$.*

Proof: We use contraposition.

Suppose $\rho(\hat{\mathbf{M}}_{ss}^i) \geq 1$ for some i . By Lemma 2, this implies that $x \leq \hat{\mathbf{M}}_{ss}^i x$ has a nonzero solution, $x \geq 0$. Suppose $x = (x_1, x_2, \dots, x_{n+1})'$. If $x_1 = 0$, then the inequality $y \leq \hat{\mathbf{M}}_{\Delta} y$ has a nonzero solution, $y = (x_2, x_3, \dots, x_{n+1})'$. Therefore, we have $\rho(\hat{\mathbf{M}}_{\Delta}) \geq 1$, which implies that the system is not robustly stable, a contradiction.

Therefore, we can assume $x_1 \neq 0$. In the following we will show that there exists some admissible uncertainty $\tilde{\Delta} \in \tilde{\mathcal{D}}(n)$ such that $\|\tilde{e}\|_{ss} \geq 1$, i.e., robust tracking is not achieved. This will complete the proof.

Without loss of generality, assume $x_1 = 1$. Then

$$\begin{pmatrix} 1 \\ x_2 \\ \vdots \\ x_{n+1} \end{pmatrix} \leq \hat{\mathbf{M}}_{ss}^i \begin{pmatrix} 1 \\ x_2 \\ \vdots \\ x_{n+1} \end{pmatrix}. \quad (5.9)$$

\tilde{e} , \tilde{y} , and \tilde{d} are defined as in Figure 5.5, where $\tilde{d} \in c_o^n$. According to Lemma 3, the steady-state error will not be changed $\forall \tilde{d} \in c_o^n$. We will construct admissible $\tilde{\xi}$, $\tilde{\Delta} \in \tilde{\mathcal{D}}(n)$ and $\tilde{d} \in c_o^n$, which will result in $\|\tilde{e}\|_{ss} \geq 1$, such that Equations (5.5) and (5.6) are satisfied, and

$$\tilde{\xi} = \tilde{\Delta}(\tilde{y} + \tilde{d}). \quad (5.10)$$

Given a sequence of positive numbers, $\{\epsilon_1, \epsilon_2, \dots\} \in c_o$. We can choose an integer $N_0 > 0$ and construct $\tilde{\xi}_j(k)$ for $0 \leq k \leq N_0$ and $1 \leq j \leq n$ such that $|\tilde{\xi}_j(k)| = x_{j+1}$ and

$$\begin{aligned} |\tilde{e}_i(N_0)| &= |(\sum_{l=1}^p \tilde{M}_{i,l} \tilde{r}_l + \tilde{M}_{i,p+1} \tilde{\xi}_1 + \dots + \tilde{M}_{i,p+n} \tilde{\xi}_n)(N_0)| \\ &\geq \|\sum_{l=1}^p \tilde{M}_{i,l} \tilde{r}_l\|_{ss} + \|\tilde{M}_{i,p+1}\|_1 x_2 + \dots + \\ &\quad + \|\tilde{M}_{i,p+n}\|_1 x_{n+1} - \epsilon_1. \end{aligned}$$

From inequality (5.9), it follows that $|\tilde{e}_i(N_0)| \geq x_1 - \epsilon_1$. Then we can choose $N_1 > N_0$, and construct $\tilde{\xi}_j(k)$ for $N_0 + 1 \leq k \leq N_1$ such that $|\tilde{\xi}_j(k)| = x_{j+1}$ and

$$\begin{aligned} |\tilde{y}_1(N_1)| &= |(\sum_{l=1}^p \tilde{M}_{q+1,l} \tilde{r}_l + \tilde{M}_{q+1,p+1} \tilde{\xi}_1 + \cdots + \tilde{M}_{q+1,p+n} \tilde{\xi}_n)(N_1)| \\ &\geq \|\sum_{l=1}^p \tilde{M}_{q+1,l} \tilde{r}_l\|_{ss} + \|\tilde{M}_{q+1,p+1}\|_1 x_2 + \cdots + \\ &\quad + \|\tilde{M}_{q+1,p+n}\|_1 x_{n+1} - \epsilon_1. \end{aligned}$$

It follows that $|\tilde{y}_1(N_1)| \geq x_2 - \epsilon_1$ from inequality (5.9). We can repeat this process and come up with $N_0 < N_1 < N_2 < \cdots$ and $|\tilde{\xi}_j(k)| = x_{j+1}, \forall k, j$ such that

$$\begin{array}{lll} |\tilde{e}_i(N_0)| \geq x_1 - \epsilon_1 & |\tilde{e}_i(N_{n+1})| \geq x_1 - \epsilon_2 & \cdots \\ |\tilde{y}_1(N_1)| \geq x_2 - \epsilon_1 & |\tilde{y}_1(N_{n+2})| \geq x_2 - \epsilon_2 & \cdots \\ \vdots & \vdots & \vdots \\ |\tilde{y}_n(N_n)| \geq x_{n+1} - \epsilon_1 & |\tilde{y}_n(N_{2n+1})| \geq x_{n+1} - \epsilon_2 & \cdots \end{array}$$

Now we construct $\tilde{d} \in \mathcal{C}_o^n$ by specifying its j th component:

$$\tilde{d}_j(k) := \begin{cases} \|\tilde{\xi}_j\|_\infty \text{sgn}(\tilde{y}_j(0)) & k = 0 \\ \epsilon_1 \text{sgn}(\tilde{y}_j(k)) & 1 \leq k \leq N_n \\ \epsilon_2 \text{sgn}(\tilde{y}_j(k)) & N_n + 1 \leq k \leq N_{2n+1} \\ \vdots & \vdots \end{cases}$$

It follows that

$$\|P_k \tilde{\xi}_j\|_\infty \leq \|P_k(\tilde{y}_j + \tilde{d}_j)\|_\infty \quad \forall k,$$

and $\forall m \in \mathcal{Z}^+, \exists \tilde{m} \in \mathcal{Z}^+$ such that

$$\|P_k L_{\tilde{m}} \tilde{\xi}_j\|_\infty \leq \|P_k L_m(\tilde{y}_j + \tilde{d}_j)\|_\infty \quad \forall k.$$

By Lemma 4, there exists $\tilde{\Delta} \in \tilde{\mathcal{D}}(n)$ such that $\tilde{\xi} = \tilde{\Delta}(\tilde{y} + \tilde{d})$, while $\|\tilde{e}_i\|_{ss} \geq x_1 = 1$, completing the proof. \square

Corollary 1 *The system in Figure 5.4 achieves robust steady-state tracking if and only if $\rho(\hat{M}_i) < 1, \forall i$.*

Proof. If we combine Theorems 3 and 4, we get necessary and sufficient conditions for robust steady-state tracking of the system in Figure 5.4. \square

5.3 Linear Periodic Discrete-Time Systems

To prepare for the discussion of sampled-data systems, we first need to consider robust steady-state tracking for periodic linear discrete-time systems because sampled-data systems are periodic. Suppose the discrete-time system $\tilde{\mathbf{M}}$ in Figure 5.6 is a linear periodic discrete-time system with period N . $\tilde{\Delta}$ belongs to the same class of uncertainty as given before.

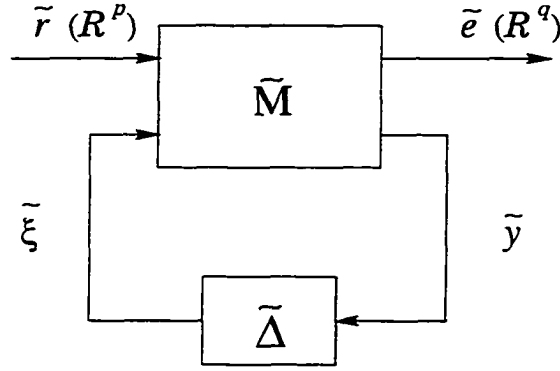


Figure 5.6 The periodic discrete-time system

$\tilde{\mathbf{M}}$ can be partitioned as following, where each element \tilde{M}_{ij} is again periodic with the same period N .

$$\tilde{\mathbf{M}} = \left(\begin{array}{ccc|ccc} \tilde{M}_{1,1} & \dots & \tilde{M}_{1,p} & \tilde{M}_{1,p+1} & \dots & \tilde{M}_{1,p+n} \\ \vdots & \ddots & \vdots & \vdots & \ddots & \vdots \\ \tilde{M}_{q,1} & \dots & \tilde{M}_{q,p} & \tilde{M}_{q,p+1} & \dots & \tilde{M}_{q,p+n} \\ \hline \tilde{M}_{q+1,1} & \dots & \tilde{M}_{q+1,p} & \tilde{M}_{q+1,p+1} & \dots & \tilde{M}_{q+1,p+n} \\ \vdots & \ddots & \vdots & \vdots & \ddots & \vdots \\ \tilde{M}_{q+n,1} & \dots & \tilde{M}_{q+n,p} & \tilde{M}_{q+n,p+1} & \dots & \tilde{M}_{q+n,p+n} \end{array} \right). \quad (5.11)$$

The analogue definition of robust steady-state tracking when $\tilde{\mathbf{M}}$ is a periodic system is given in the following.

Definition 4 (Robust Tracking: Linear Periodic Discrete-Time Systems) *The linear periodic discrete-time system $\tilde{\mathbf{M}}$ in Figure 5.6 is said to achieve robust steady-state tracking if*

1. *The interconnection of $\tilde{\mathbf{M}}$ and $\tilde{\Delta}$ is l_∞ -stable for all $\tilde{\Delta} \in \tilde{\mathcal{D}}(n)$.*
2. $\max_{1 \leq i \leq q} \sup_{\tilde{\Delta} \in \tilde{\mathcal{D}}(n)} \|\tilde{e}_i\|_{ss} < 1$.

In general, a function $\tilde{M}(\cdot, \cdot)$ defined on $\mathcal{Z}^+ \times \mathcal{Z}^+$ defines a linear stable operator $\tilde{\mathbf{M}} : l_\infty^m \rightarrow l_\infty^n$ as follows:

$$\tilde{v}(l) = (\tilde{\mathbf{M}}\tilde{w})(l) = \sum_{h=0}^{\infty} \tilde{M}(l, h)\tilde{w}(h),$$

where $\tilde{w} \in l_\infty^m$ and $\tilde{v} \in l_\infty^n$. Each $\tilde{M}(l, h)$ is a matrix $\in \mathcal{R}^{n \times m}$. If this operator is causal, then $\tilde{M}(l, h) = \mathbf{0}$ for all $h > l$. In this case, the operator can be represented as the following infinite block lower triangle matrix of the form:

$$\begin{pmatrix} \tilde{v}(0) \\ \tilde{v}(1) \\ \tilde{v}(2) \\ \vdots \end{pmatrix} = \begin{pmatrix} \tilde{M}(0,0) & \mathbf{0} & \mathbf{0} & \cdots \\ \tilde{M}(1,0) & \tilde{M}(1,1) & \mathbf{0} & \cdots \\ \tilde{M}(2,0) & \tilde{M}(2,1) & \tilde{M}(2,2) & \cdots \\ \vdots & \vdots & \vdots & \ddots \end{pmatrix} \begin{pmatrix} \tilde{w}(0) \\ \tilde{w}(1) \\ \tilde{w}(2) \\ \vdots \end{pmatrix}. \quad (5.12)$$

Equation (5.12) gives a general representation of linear casual operators. If $\tilde{\mathbf{M}}$ is periodic with period of N , then $\tilde{M}(l+kN, h+kN) = \tilde{M}(l, h)$ for any positive integer k . The matrix representation for a linear periodic operator is shown in Figure 5.7. It has a lower triangular Toeplitz structure. To deal with periodic systems, we use the lifting technique described next.

$$\left(\begin{array}{cccc|cccc|c}
\tilde{M}(0,0) & 0 & \cdots & 0 & 0 & 0 & \cdots & 0 & \cdots \\
\tilde{M}(1,0) & \tilde{M}(1,1) & \cdots & 0 & 0 & 0 & \cdots & 0 & \cdots \\
\vdots & \vdots & \ddots & \vdots & \vdots & \vdots & \ddots & \vdots & \cdots \\
\tilde{M}(N-1,0) & \tilde{M}(N-1,1) & \cdots & \tilde{M}(N-1,N-1) & 0 & 0 & \cdots & 0 & \cdots \\
\hline
\tilde{M}(N,0) & \tilde{M}(N,1) & \cdots & \tilde{M}(N,N-1) & \tilde{M}(0,0) & 0 & \cdots & 0 & \cdots \\
\tilde{M}(N+1,0) & \tilde{M}(N+1,1) & \cdots & \tilde{M}(N+1,N-1) & \tilde{M}(1,0) & \tilde{M}(1,1) & \cdots & 0 & \cdots \\
\vdots & \vdots & \ddots & \vdots & \vdots & \vdots & \ddots & \vdots & \cdots \\
\tilde{M}(2N-1,0) & \tilde{M}(2N-1,1) & \cdots & \tilde{M}(2N-1,N-1) & \tilde{M}(N-1,0) & \tilde{M}(N-1,1) & \cdots & \tilde{M}(N-1,N-1) & \cdots \\
\hline
\vdots & \vdots & \vdots & \vdots & \vdots & \vdots & \vdots & \vdots & \ddots
\end{array} \right)$$

Figure 5.7 Linear periodic discrete-time system $\tilde{\mathbf{M}}$

5.3.1 Lifting Technique

Let $\tilde{v} = \{\tilde{v}(0), \tilde{v}(1), \tilde{v}(2), \dots\}$ be a discrete-time signal in l_∞^m . The lifting operator $W_N(l_\infty^m \rightarrow l_\infty^{m \cdot N})$ is defined as follows:

$$\underline{\tilde{v}} = W_N \tilde{v} := \left\{ \left[\begin{array}{c} \tilde{v}(0) \\ \tilde{v}(1) \\ \vdots \\ \tilde{v}(l) \\ \vdots \\ \tilde{v}(N-1) \end{array} \right], \left[\begin{array}{c} \tilde{v}(N) \\ \tilde{v}(1+N) \\ \vdots \\ \tilde{v}(l+N) \\ \vdots \\ \tilde{v}(N-1+N) \end{array} \right], \dots, \left[\begin{array}{c} \tilde{v}(kN) \\ \tilde{v}(1+kN) \\ \vdots \\ \tilde{v}(l+kN) \\ \vdots \\ \tilde{v}(N-1+kN) \end{array} \right], \dots \right\}. \quad (5.13)$$

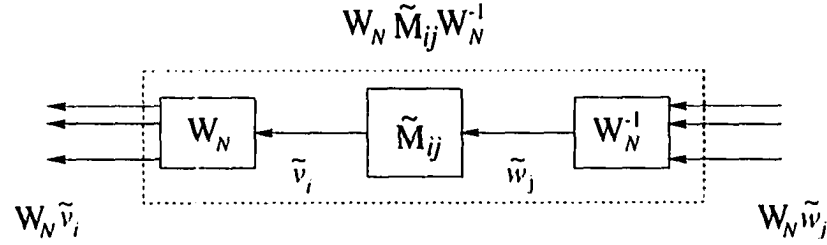
The inverse operator exists and is defined as $\tilde{v} = W_N^{-1} \underline{\tilde{v}}$. Notice that the dimension of the lifted signal, $\underline{\tilde{v}} \in l_\infty^{m \cdot N}$, is N times that of the original signal, \tilde{v} . Define a subsequence of \tilde{v} $\tilde{v}^l = \{\tilde{v}_k^l\}$, where l is an integer $\in [0, N-1]$. \tilde{v}_k^l is given by

$$\tilde{v}_k^l := \tilde{v}(l+kN). \quad (5.14)$$

$\tilde{v}^l = \{\tilde{v}(l), \tilde{v}(l+N), \dots\} \in l_\infty^m$ has the same dimension as that of the original signal, \tilde{v} . Clearly, $\|\tilde{v}\|_{ss} = \max_l \|\tilde{v}^l\|_{ss}$. Notice that the lifting operator W_N (and W_N^{-1}) is norm preserving, meaning that the following equation holds:

$$\|W_N \tilde{v}\|_\infty = \|\tilde{v}\|_\infty.$$

Suppose the system $\tilde{\mathbf{M}}$ in Figure 5.6 is a linear periodic discrete-time system with period N . $\tilde{\mathbf{M}}$ is the $(q+n) \times (p+n)$ operator matrix presented by (5.11). Therefore, each element \tilde{M}_{ij} in (5.11) is a single-input, single-output linear periodic discrete-time operator with period N defined on l_∞ and $\tilde{M}_{ij}(l, h) \in \mathcal{R}^{1 \times 1}$. As shown in Figure 5.8, lifting both the input and output side of \tilde{M}_{ij} , one can get a lifted system, $W_N \tilde{M}_{ij} W_N^{-1}$.



$$W_N \tilde{w}_j \in l_\infty^N$$

$$W_N \tilde{v}_i \in l_\infty^N \left(\begin{array}{cccc|cccc} \tilde{M}_{ij}(0,0) & 0 & \cdots & 0 & 0 & 0 & \cdots & 0 & \cdots \\ \tilde{M}_{ij}(1,0) & \tilde{M}_{ij}(1,1) & \cdots & 0 & 0 & 0 & \cdots & 0 & \cdots \\ \vdots & \vdots & \ddots & \vdots & \vdots & \vdots & \ddots & \vdots & \cdots \\ \tilde{M}_{ij}(N-1,0) & \tilde{M}_{ij}(N-1,1) & \cdots & \tilde{M}_{ij}(N-1,N-1) & 0 & 0 & \cdots & 0 & \cdots \\ \hline \tilde{M}_{ij}(N,0) & \tilde{M}_{ij}(N,1) & \cdots & \tilde{M}_{ij}(N,N-1) & \tilde{M}_{ij}(0,0) & 0 & \cdots & 0 & \cdots \\ \tilde{M}_{ij}(N+1,0) & \tilde{M}_{ij}(N+1,1) & \cdots & \tilde{M}_{ij}(N+1,N-1) & \tilde{M}_{ij}(1,0) & \tilde{M}_{ij}(1,1) & \cdots & 0 & \cdots \\ \vdots & \vdots & \ddots & \vdots & \vdots & \vdots & \ddots & \vdots & \cdots \\ \tilde{M}_{ij}(2N-1,0) & \tilde{M}_{ij}(2N-1,1) & \cdots & \tilde{M}_{ij}(2N-1,N-1) & \tilde{M}_{ij}(N-1,0) & \tilde{M}_{ij}(N-1,1) & \cdots & \tilde{M}_{ij}(N-1,N-1) & \cdots \\ \hline \vdots & \vdots & \vdots & \vdots & \vdots & \vdots & \vdots & \vdots & \ddots \end{array} \right)$$

Figure 5.8 The lifted operator $W_N \tilde{M}_{ij} W_N^{-1}$

and the system matrix representation. Notice that $W_N \tilde{M}_{ij} W_N^{-1}(\cdot, \cdot) \in \mathcal{R}^{N \times N}$ and the resulting lifted system becomes time invariant.

Like the definition of lifted signals in (5.14), if picking the l_i th row of the output of $W_N \tilde{M}_{ij} W_N^{-1}$, one can define the corresponding lifted operator, $(W_N \tilde{M}_{ij} W_N^{-1})^{l_i}$, and the matrix representation in Figure 5.9. Notice that $(W_N \tilde{M}_{ij} W_N^{-1})^{l_i}$ maps l_∞^N into l_∞ and is a linear shift-invariant casual operator. The induced norm can be easily computed.

However, we are really only interested in the one-side lifted operator, which is lifted only on the output side. For each \tilde{M}_{ij} in (5.11): $\tilde{w} \rightarrow \tilde{v}$, if we lift the output side and pick the l_i th output, we can define the corresponding lifted operator, $\tilde{M}_{ij}^{l_i} : \tilde{w} \rightarrow \tilde{v}^{l_i}$, as follows:

$$\tilde{M}_{ij}^{l_i} : (\tilde{M}_{ij}^{l_i} \tilde{w})(k) := \tilde{v}^{l_i}(k) = (\tilde{M}_{ij} \tilde{w})(l_i + kN), \quad (5.15)$$

where l_i is an integer $\in [0, N-1]$. The matrix representation is given in Figure 5.10. The kernel representation for $\tilde{M}_{ij}^{l_i}$ is given by

$$\tilde{M}_{ij}^{l_i}(k, h) := \tilde{M}_{ij}(l_i + kN, h), \quad (5.16)$$

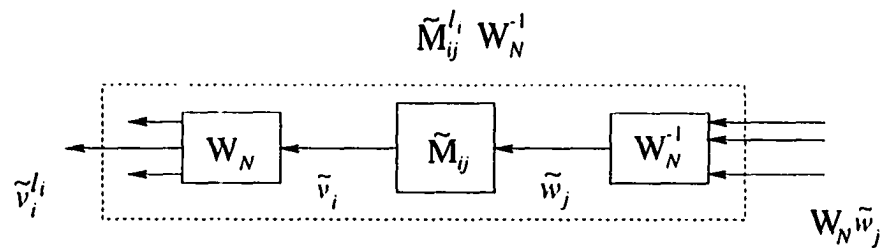
where $\tilde{M}_{ij}(\cdot, \cdot)$ is the kernel representation of \tilde{M}_{ij} .

Note that $\tilde{M}_{ij}^{l_i}$ is related to $(W_N \tilde{M}_{ij} W_N^{-1})^{l_i}$ by the inverse lifting operator, W_N^{-1} . Since $\tilde{M}_{ij}^{l_i}$ is the l_i th output of $W_N \tilde{M}_{ij}$, we have $\tilde{M}_{ij}^{l_i} W_N^{-1} = (W_N \tilde{M}_{ij} W_N^{-1})^{l_i}$.

Therefore, as discussed above, $\tilde{M}_{ij}^{l_i} W_N^{-1}$ is a multi-input (dimension N) single-output linear shift-invariant system. The induced norm is given by

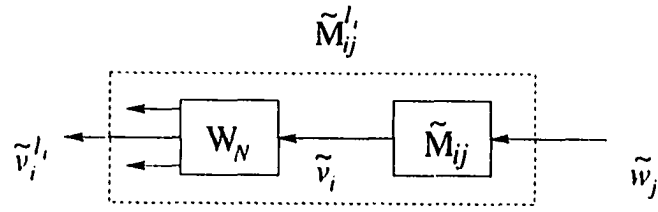
$$\|\tilde{M}_{ij}^{l_i} W_N^{-1}\| := \sum_{k=0}^{\infty} \sum_{h=0}^{N-1} |\tilde{M}_{ij}(l_i + kN, h)| = \sum_{k=0}^{\infty} \sum_{h=0}^{N-1} |\tilde{M}_{ij}^{l_i}(k, h)|.$$

In order to specify \tilde{M}_{ij} completely, it is sufficient to have the knowledge of $\tilde{M}_{ij}(k, h)$, $0 \leq h \leq N-1$, $k = 0, 1, \dots$.



$$\begin{array}{c}
 W_N \tilde{w}_j \in l_\infty^N \\
 \tilde{v}_i^l \in l_\infty \left(\begin{array}{cccc|cccc|c}
 \tilde{M}_{ij}(l_i, 0) & \cdots & \tilde{M}_{ij}(l_i, l_i) & \cdots & 0 & 0 & \cdots & 0 & \cdots & 0 & \cdots \\
 \tilde{M}_{ij}(l_i + N, 0) & \cdots & \tilde{M}_{ij}(l_i + N, l_i) & \cdots & \tilde{M}_{ij}(l_i + N, N - 1) & \tilde{M}_{ij}(l_i, 0) & \cdots & \tilde{M}_{ij}(l_i, l_i) & \cdots & 0 & \cdots \\
 \vdots & \vdots & \vdots & \vdots & \vdots & \vdots & \vdots & \vdots & \vdots & \vdots & \ddots
 \end{array} \right)
 \end{array}$$

Figure 5.9 The lifted operator $\tilde{M}_{ij}^l W_N^{-1}$ or $(W_N \tilde{M}_{ij} W_N^{-1})^l$.



$$\tilde{w}_j \in l_\infty$$

$$\tilde{v}_i^l \in l_\infty \begin{pmatrix} \tilde{M}_{ij}(l_i, 0) & \cdots & \tilde{M}_{ij}(l_i, l_i) & \cdots & 0 & 0 & \cdots & 0 & \cdots & 0 & \cdots \\ \tilde{M}_{ij}(l_i + N, 0) & \cdots & \tilde{M}_{ij}(l_i + N, l_i) & \cdots & \tilde{M}_{ij}(l_i + N, N - 1) & \tilde{M}_{ij}(l_i, 0) & \cdots & \tilde{M}_{ij}(l_i, l_i) & \cdots & 0 & \cdots \\ \vdots & \vdots & \vdots & \vdots & \vdots & \vdots & \vdots & \vdots & \vdots & \vdots & \ddots \end{pmatrix}.$$

Figure 5.10 The lifted operator \tilde{M}_{ij}^l

Finally, the induced norm for the defined lifted operator, $\tilde{M}_{ij}^{l_i}$, can be computed as follows by using the fact that the lifting operator, W_N (and W_N^{-1}), preserves norms.

$$\begin{aligned}
\|\tilde{M}_{ij}^{l_i}\| &= \sup_{\tilde{x} \neq 0} \frac{\|\tilde{M}_{ij}^{l_i} \tilde{x}\|}{\|\tilde{x}\|} \\
&= \sup_{W_N \tilde{x} \neq 0} \frac{\|\tilde{M}_{ij}^{l_i} W_N^{-1} W_N \tilde{x}\|}{\|W_N \tilde{x}\|} \\
&= \|\tilde{M}_{ij}^{l_i} W_N^{-1}\| \\
&= \sum_{k=0}^{\infty} \sum_{h=0}^{N-1} |\tilde{M}_{ij}^{l_i}(k, h)|
\end{aligned} \tag{5.17}$$

Let $\hat{l} = [l_0, l_1, \dots, l_n] \in [0, N-1]^{n+1}$. $\tilde{e}_i^{l_0}$ and $\tilde{y}_j^{l_j}$, $j \in \{1, 2, \dots, n\}$ are defined as above by (5.14). Define the corresponding lifted system $\tilde{M}^{(\hat{l}, i)}(l_\infty^{n+1} \rightarrow l_\infty^{n+1})$ maps $[\tilde{r}, \tilde{\xi}_1, \dots, \tilde{\xi}_n]^T$ to $[\tilde{e}_i^{l_0}, \tilde{y}_1^{l_1}, \dots, \tilde{y}_n^{l_n}]^T$ as follows:

$$\begin{pmatrix} \tilde{e}_i^{l_0} \\ \tilde{y}_1^{l_1} \\ \vdots \\ \tilde{y}_n^{l_n} \end{pmatrix} = \begin{pmatrix} \tilde{M}_{i1}^{l_0} & \cdots & \tilde{M}_{i,p}^{l_0} & \tilde{M}_{i,p+1}^{l_0} & \cdots & \tilde{M}_{i,p+n}^{l_0} \\ \tilde{M}_{q+1,1}^{l_1} & \cdots & \tilde{M}_{q+1,p}^{l_1} & \tilde{M}_{q+1,p+1}^{l_1} & \cdots & \tilde{M}_{q+1,p+n}^{l_1} \\ \vdots & \ddots & \vdots & \vdots & \ddots & \vdots \\ \tilde{M}_{q+n,1}^{l_n} & \cdots & \tilde{M}_{q+n,p}^{l_n} & \tilde{M}_{q+n,p+1}^{l_n} & \cdots & \tilde{M}_{q+n,p+n}^{l_n} \end{pmatrix} \begin{pmatrix} \tilde{r}_1 \\ \vdots \\ \tilde{r}_p \\ \tilde{\xi}_1 \\ \vdots \\ \tilde{\xi}_n \end{pmatrix}. \tag{5.18}$$

The induced norm for the element in (5.18) can be computed using (5.17). Finally, we can define the *steady-state norm matrix* (periodic discrete-time) as follows:

$$\tilde{M}_{ss}^{(\hat{l}, i)} := \begin{pmatrix} \|\sum_{k=1}^p \tilde{M}_{i,k}^{l_0} \tilde{r}_k\|_{ss} & \|\tilde{M}_{i,p+1}^{l_0}\| & \cdots & \|\tilde{M}_{i,p+n}^{l_0}\| \\ \|\sum_{k=1}^p \tilde{M}_{q+1,k}^{l_1} \tilde{r}_k\|_{ss} & \|\tilde{M}_{q+1,p+1}^{l_1}\| & \cdots & \|\tilde{M}_{q+1,p+n}^{l_1}\| \\ \vdots & \vdots & \ddots & \vdots \\ \|\sum_{k=1}^p \tilde{M}_{q+n,k}^{l_n} \tilde{r}_k\|_{ss} & \|\tilde{M}_{q+n,p+1}^{l_n}\| & \cdots & \|\tilde{M}_{q+n,p+n}^{l_n}\| \end{pmatrix}. \tag{5.19}$$

5.3.2 Robust Steady-State Tracking

Similar to the LSI case, the robust tracking condition for periodic systems is given in the form of the above-defined matrix, which is stated in the following theorem:

Theorem 5 *The linear periodic discrete-time system $\tilde{\mathbf{M}}$ in Figure 5.6 achieves robust steady-state tracking iff*

$$\max_{1 \leq i \leq q} \sup_{\hat{i} \in [0, N-1]^{n+i}} \rho(\tilde{\mathbf{M}}_{ss}^{(\hat{i}, i)}) < 1. \quad (5.20)$$

Proof: Sufficiency: Define the lower part in (5.19) as $\hat{\mathbf{M}}_{\Delta}^{\hat{l}_{\Delta}}$

$$\hat{\mathbf{M}}_{\Delta}^{\hat{l}_{\Delta}} = \begin{pmatrix} \|\tilde{M}_{q+1, p+1}^{l_1}\| & \cdots & \|\tilde{M}_{q+1, p+n}^{l_1}\| \\ \vdots & \ddots & \vdots \\ \|\tilde{M}_{q+n, p+1}^{l_n}\| & \cdots & \|\tilde{M}_{q+n, p+n}^{l_n}\| \end{pmatrix}.$$

where $\hat{l}_{\Delta} = [l_1, l_2, \dots, l_n] \in [0, N-1]^n$.

The necessary and sufficient condition of robust stability for system $\tilde{\mathbf{M}}$ in Figure 5.6 is $\max_{\hat{l}_{\Delta}} \rho(\hat{\mathbf{M}}_{\Delta}^{\hat{l}_{\Delta}}) < 1$ (see [24]). According to the hypothesis, it is easy to see that $\rho(\tilde{\mathbf{M}}_{ss}^{(\hat{i}, i)}) < 1$ implies $\rho(\hat{\mathbf{M}}_{\Delta}^{\hat{l}_{\Delta}}) < 1$ if one applies Lemma 2. Therefore, robust stability is obtained.

Robust tracking will be proven by contradiction, i.e., contraposition will be introduced in the following if one claims robust tracking cannot be achieved even when

$$\max_{1 \leq i \leq q} \sup_{\hat{i} \in [0, N-1]^{n+i}} \rho(\tilde{\mathbf{M}}_{ss}^{(\hat{i}, i)}) < 1.$$

No robust tracking for the system in Figure 5.6 means there exists some $i, 1 \leq i \leq q$ and $\tilde{\Delta} \in \tilde{\mathcal{D}}(n)$ such that $\|\tilde{e}_i\|_{ss} \geq 1$. Clearly, this implies that there exists $l_0 \in [0, N-1]$ such that

$$\|\tilde{e}_i^{l_0}\|_{ss} \geq 1.$$

Define $\tilde{\xi}$ and \tilde{y} as in Figure 5.6, then $\tilde{e}_i^{l_0}$ and $\tilde{y}_j^{l_j}$ are given by (5.18). By Lemma 1 and the triangle inequality, we have the following inequality,

$$1 \leq \|\tilde{e}_i^{l_0}\|_{ss} \leq \left\| \sum_{k=1}^p \tilde{M}_{i,k}^{l_0} \tilde{r}_k \right\|_{ss} + \|\tilde{M}_{i,p+1}^{l_0}\| \|\tilde{\xi}_1\|_{ss} + \cdots + \|\tilde{M}_{i,p+n}^{l_0}\| \|\tilde{\xi}_n\|_{ss}. \quad (5.21)$$

Using the fact that $\|\tilde{\Delta}\| \leq 1$, we have

$$\|\tilde{\xi}_j\|_{ss} \leq \|\tilde{y}_j\|_{ss}.$$

As we mentioned before, there always exists a $l_j \in [0, N-1]$ such that

$$\|\tilde{y}_j^{l_j}\|_{ss} = \|\tilde{y}_j\|_{ss}.$$

Therefore, we have $\|\tilde{\xi}_j\|_{ss} \leq \|\tilde{y}_j^{l_j}\|_{ss}$ and the following inequalities for $1 \leq j \leq n$:

$$\begin{aligned} \|\tilde{\xi}_j\|_{ss} \leq \|\tilde{y}_j^{l_j}\|_{ss} &\leq \left\| \sum_{k=1}^p \tilde{M}_{q+j,k}^{l_j} \tilde{r}_k \right\|_{ss} + \|\tilde{M}_{q+j,p+1}^{l_j}\| \|\tilde{\xi}_1\|_{ss} + \cdots + \\ &+ \|\tilde{M}_{q+j,p+n}^{l_j}\| \|\tilde{\xi}_n\|_{ss}. \end{aligned} \quad (5.22)$$

Inequalities (5.21) and (5.22) imply that

$$x = (1, \|\tilde{\xi}_1\|_{ss}, \cdots, \|\tilde{\xi}_n\|_{ss})'$$

is a solution to $x \leq \tilde{M}_{ss}^{(\hat{l},i)} x$. By Lemma 2, this implies $\rho(\tilde{M}_{ss}^{(\hat{l},i)}) \geq 1$ for certain i and \hat{l} .

Necessity: Again we use contradiction to prove this.

Suppose $\rho(\tilde{M}_{ss}^{(\hat{l},i)}) \geq 1$ for some integer i and $\hat{l} = [l_0, l_1, \cdots, l_n]$. By Lemma 2, this implies that $x \leq \tilde{M}_{ss}^{(\hat{l},i)} x$ has a nonzero solution, $x \geq 0$. Suppose $x = (x_1, x_2, \cdots, x_{n+1})'$. First, if $x_1 = 0$, then it is clear that the inequality $y \leq \hat{M}_{\Delta}^{i,\hat{l}} y$, where $\hat{l}_{\Delta} = [l_1, l_2, \cdots, l_n]$, has a nonzero solution, $y, y = (x_2, x_3, \cdots, x_{n+1})'$. Again by Lemma 2, we have $\rho(\hat{M}_{\Delta}^{i,\hat{l}}) \geq 1$, which implies that the system is not robustly stable, a contradiction.

On the other hand, if $x_1 \neq 0$, we will show in the following that there exists some perturbation, $\tilde{\Delta} \in \tilde{\mathcal{D}}(n)$ such that $\|\tilde{e}_i^{l_0}\|_{ss} \geq 1$, also a contradiction, completing this proof.

Without loss of generality, assume $x_1 = 1$. Therefore,

$$\begin{pmatrix} 1 \\ x_2 \\ \vdots \\ x_{n+1} \end{pmatrix} \leq \tilde{M}_{ss}^{(i,i)} \begin{pmatrix} 1 \\ x_2 \\ \vdots \\ x_{n+1} \end{pmatrix}. \quad (5.23)$$

Let $\tilde{e}_i^{l_0}$, $\tilde{\xi}$, $\tilde{y}^{i\Delta}$, and $\tilde{d}^{i\Delta}$ be the corresponding lifted signals (shown in Figure 5.11) defined in the same way as in (5.14), where $\tilde{d}^{i\Delta} \in c_o^n$.

According to Lemma 3, the steady-state error will not be changed $\forall \tilde{d}^{i\Delta} \in c_o^n$. We will construct $\tilde{\xi}$, $\tilde{\Delta}^{i\Delta} \in \tilde{\mathcal{D}}(n)$ and $\tilde{d}^{i\Delta} \in c_o^n$ such that

$$\tilde{\xi} = \tilde{\Delta}^{i\Delta}(\tilde{y}^{i\Delta} + \tilde{d}^{i\Delta}), \quad (5.24)$$

and

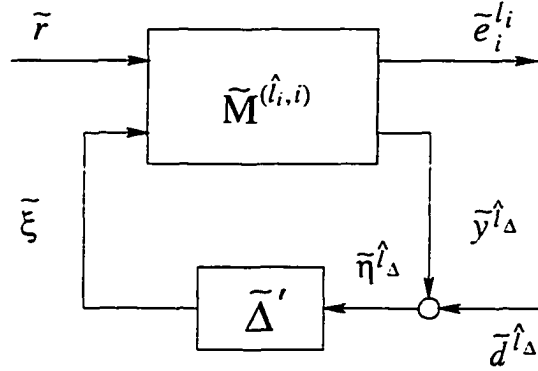


Figure 5.11 The auxiliary lifted system

an admissible $\tilde{\Delta} \in \tilde{\mathcal{D}}(n)$ can be obtained from $\tilde{\Delta}^{i\Delta}$, resulting in $\|\tilde{e}_i^{l_0}\|_{ss} \geq 1$.

Given a sequence of positive numbers $\{\epsilon_1, \epsilon_2, \dots\} \in c_o$, we can choose an integer $N_0 > 0$ and construct $\tilde{\xi}_j(k)$ for $0 \leq k \leq N_0$ and $1 \leq j \leq n$ such that $|\tilde{\xi}_j(k)| = x_{j+1}$ and

$$|\tilde{e}_i^{l_0}(N_0)| = |(\sum_{k=1}^p \tilde{M}_{i,k}^{l_0} \tilde{r}_k + \tilde{M}_{i,p+1}^{l_0} \tilde{\xi}_1 + \dots + \tilde{M}_{i,p+n}^{l_0} \tilde{\xi}_n)(N_0)|$$

$$\begin{aligned} &\geq \left\| \sum_{k=1}^p \tilde{M}_{i,k}^{l_0} \tilde{r}_k \right\|_{ss} + \|\tilde{M}_{i,p+1}^{l_0}\| x_2 + \cdots + \\ &\quad + \|\tilde{M}_{i,p+n}^{l_0}\| x_{n+1} - \epsilon_1. \end{aligned}$$

From inequality (5.23), it follows that $|\tilde{e}_i^{l_0}(N_0)| \geq x_1 - \epsilon_1$. Then we can choose $N_1 > N_0$ and construct $\tilde{\xi}_j(k)$ for $N_0 + 1 \leq k \leq N_1$ and $1 \leq j \leq n$ such that $|\tilde{\xi}_j(k)| = x_{j+1}$ and

$$\begin{aligned} |\tilde{y}_1^{l_1}(N_1)| &= \left| \left(\sum_{k=1}^p \tilde{M}_{q+1,k}^{l_1} \tilde{r}_k + \tilde{M}_{q+1,p+1}^{l_1} \tilde{\xi}_1 + \cdots + \tilde{M}_{q+1,p+n}^{l_1} \tilde{\xi}_n \right) (N_1) \right| \\ &\geq \left\| \sum_{k=1}^p \tilde{M}_{q+1,k}^{l_1} \tilde{r}_k \right\|_{ss} + \|\tilde{M}_{q+1,p+1}^{l_1}\| x_2 + \cdots + \\ &\quad + \|\tilde{M}_{q+1,p+n}^{l_1}\| x_{n+1} - \epsilon_1. \end{aligned}$$

From inequality (5.23), it follows that $|\tilde{y}_1^{l_1}(N_1)| \geq x_2 - \epsilon_1$. Repeating this process, we come up with $N_0 < N_1 < N_2 < \cdots$ and $|\tilde{\xi}_j(k)| = x_{j+1}, \forall k$ such that

$$\begin{aligned} |\tilde{e}_i^{l_0}(N_0)| &\geq x_1 - \epsilon_1 & |\tilde{e}_i^{l_0}(N_{n+1})| &\geq x_1 - \epsilon_2 & \cdots \\ |\tilde{y}_1^{l_1}(N_1)| &\geq x_2 - \epsilon_1 & |\tilde{y}_1^{l_1}(N_{n+2})| &\geq x_2 - \epsilon_2 & \cdots \\ &\vdots & &\vdots & \vdots \\ |\tilde{y}_n^{l_n}(N_n)| &\geq x_{n+1} - \epsilon_1 & |\tilde{y}_n^{l_n}(N_{2n+1})| &\geq x_{n+1} - \epsilon_2 & \cdots \end{aligned}$$

Now we can construct $\tilde{d}^{i\Delta} \in c_0^n$ by specifying its j th component.

$$\tilde{d}_j^{l_j}(k) := \begin{cases} \|\tilde{\xi}_j\|_\infty \operatorname{sgn}(\tilde{y}_j^{l_j}(0)) & k = 0 \\ \epsilon_1 \operatorname{sgn}(\tilde{y}_j^{l_j}(k)) & 1 \leq k \leq N_n \\ \epsilon_2 \operatorname{sgn}(\tilde{y}_j^{l_j}(k)) & N_n + 1 \leq k \leq N_{2n+1} \\ \vdots & \vdots \end{cases}$$

It follows that

$$\|P_k \tilde{\xi}_j\|_\infty \leq \|P_k(\tilde{y}_j^{l_j} + \tilde{d}_j^{l_j})\|_\infty \quad \forall k,$$

and $\forall m \in \mathcal{Z}^+, \exists \tilde{m} \in \mathcal{Z}^+$ such that

$$\|P_k L_{\tilde{m}} \tilde{\xi}_j\|_\infty \leq \|P_k L_m(\tilde{y}_j^{l_j} + \tilde{d}_j^{l_j})\|_\infty \quad \forall k.$$

By Lemma 4, there exists $\tilde{\Delta}^{i_\Delta} \in \tilde{\mathcal{D}}(n)$ such that $\tilde{\xi} = \tilde{\Delta}^{i_\Delta}(\tilde{y}^{i_\Delta} + \tilde{d}^{i_\Delta})$, while $\|\tilde{e}_i^{i_\Delta}\|_{ss} \geq x_1 = 1$. It is not difficult to construct an admissible $\tilde{\Delta} \in \tilde{\mathcal{D}}(n)$ such that $\|\tilde{\Delta}\| = \|\tilde{\Delta}^{i_\Delta}\|$ and $\tilde{\xi} = \tilde{\Delta}(\tilde{y} + \tilde{d})$, where \tilde{y} and \tilde{d} are constructed from \tilde{y}^{i_Δ} and \tilde{d}^{i_Δ} , respectively, completing the proof. \square

CHAPTER 6 ROBUST STEADY-STATE TRACKING OF SAMPLED-DATA SYSTEMS

6.1 Sampled-Data Systems

A sampled-data system arises when a discrete-time feedback controller is introduced to control a continuous-time plant with connection by the sampler and the hold. Such feedback control can be found naturally in numerous control applications. The resulting closed-loop system dynamics, known as the hybrid system, consists of both continuous-time and discrete-time dynamics. Though a hybrid system, from the input-output point of view, a sampled-data system is considered as a continuous-time system.

Consider the following sampled-data system shown in Figure 6.1, where G , the nom-

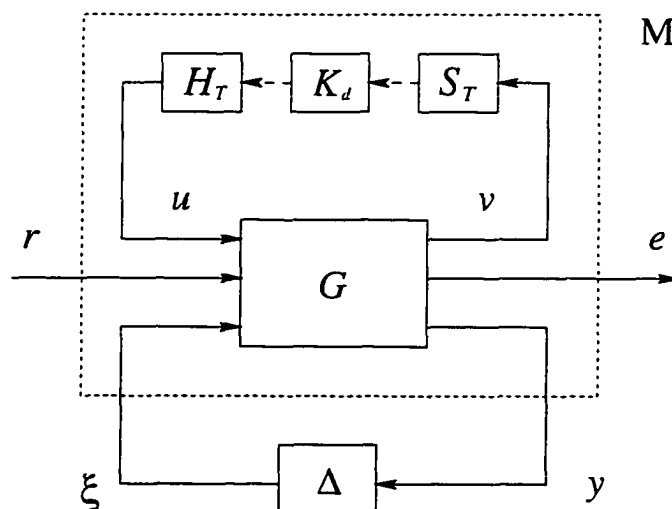


Figure 6.1 The sampled-data system

inal plant, is a linear time-invariant continuous-time system having the following state-space representation:

$$G = \left(\begin{array}{c|ccc} A & B_1 & B_2 & B_3 \\ \hline C_1 & \mathbf{0} & D_{12} & D_{13} \\ C_2 & D_{21} & D_{22} & D_{23} \\ C_3 & D_{31} & D_{32} & D_{33} \end{array} \right). \quad (6.1)$$

Without loss of generality, we may assume that $D_{11} = \mathbf{0}$ to ensure well-posedness of the feedback system. K_d is a stabilizing linear shift-invariant discrete-time controller, which stabilizes the nominal plant. The plant and controller are interfaced using sampler and hold. \mathcal{S}_T represents the sampling operator with time period T , while \mathcal{H}_T a zero-order hold with the same period. r is a known reference input, a continuous-time signal. e is the tracking error, also in continuous-time. y and ξ are the input and output of the system uncertainty respectively. u , the output of the hold \mathcal{H}_T , is the control input. v is the measured output. Strictly speaking, \mathcal{S}_T is not an operator on \mathcal{L}_∞ but on the subspace of $\mathcal{L}_\infty \cap \mathcal{RC}$ signals. To ensure that the sampling operator acting on v makes sense, we assume that r and ξ are continuous signals (or at least $\in \mathcal{L}_\infty \cap \mathcal{RC}$), which is reasonable in practice. This also ensures that we can sample e and y . We will analyze sampled-data systems with bounded signals where the signal norm is the \mathcal{L}_∞ norm. \mathcal{L}_∞ denotes the space of real valued measurable functions on $[0, \infty)$ with the norm defined as $\|x\|_{\mathcal{L}_\infty} := \text{ess sup}_t |x(t)| < \infty$. Δ belongs to the class of causal norm-bounded structured uncertainty with finite memory $\mathcal{D}(n)$. All results obtained will equally hold when Δ is fading-memory operator mapping decline signals into decline signals.

$$\mathcal{D}(n) = \{\text{diag}(\Delta_1, \dots, \Delta_n) : \Delta_i \in \Delta_F\},$$

where $\Delta_i: \mathcal{L}_\infty \cap \mathcal{RC} \rightarrow \mathcal{L}_\infty \cap \mathcal{RC}$. Δ_i belongs to the class Δ_F of linear causal norm-

bounded finite memory perturbations, and

$$\|\Delta_i\| := \sup_{x \neq 0} \frac{\|\Delta_i x\|_{\mathcal{L}_\infty}}{\|x\|_{\mathcal{L}_\infty}} \leq 1,$$

where $\|\Delta_i\|$ is the induced norm.

The difficulty in considering the continuous-time behavior of sampled-data systems is that it is time varying. A sampled-data system in this configuration, considered as a system in continuous-time, is not time-invariant even when the plant G and the controller K_d are LTI and LSI respectively. Instead, it is periodic with the time period T determined by the time period of the sampler \mathcal{S}_T and the hold \mathcal{H}_T .

In general, r and e may have dimension more than 1, i.e. the system is a MIMO system. In order to simplify the notation, only the single-reference single-tracking-error system will be discussed in the following. It can be shown that the necessary and sufficient conditions for the MIMO robust tracking can be easily obtained from those for the single-reference single-tracking-error system. Also even though only sampled-data systems will be studied in the rest of this research, the obtained corresponding results can be applied to general periodic systems.

The system in Figure 6.1 can be rearranged into the following general setting (see Figure 6.2), where \mathbf{M} , a hybrid stabilized system, includes the nominal plant G and the discrete-time controller K_d . It is clear that \mathbf{M} is a periodic linear stable time-varying

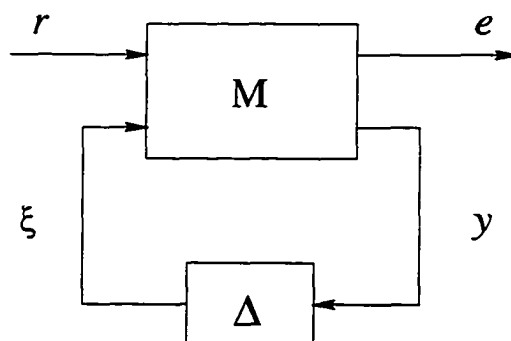


Figure 6.2 The generalized system

system with period T . With the system setting described above, both input and output signals of system \mathbf{M} are at least right (or left) continuous signals. Therefore, we can apply operator \mathcal{S}_T on these signals for sampling purpose.

A conventional approach to the sampled-data system problems is to utilize the isomorphic lifting technique due to the periodicity (see [4]).

6.2 Approximation of the Sampled-Data System

Although the lifting technique can handle the periodic system nicely, the resulting lifted system is infinite-dimensional. One such lifting technique will be discussed in the next section. To deal with the infinite-dimensional system, we introduce fast sampling. Figure 6.3 shows the approximate discrete-time system $\tilde{\mathbf{M}}$ obtained by fast sampling the input and output of the sampled-data system \mathbf{M} in Figure 6.2. \mathcal{S}_{T_N} and \mathcal{H}_{T_N} are the fast sampler and hold respectively with the same period $T_N = T/N$, where N is an integer. \tilde{r} , \tilde{e} , $\tilde{\xi}$ and \tilde{y} are the corresponding sampled signals by sampler \mathcal{S}_{T_N} .

After fast sampling both the input and output sides, we obtain an approximate discrete-time system $\tilde{\mathbf{M}} = \mathcal{S}_{T_N} \mathbf{M} \mathcal{H}_{T_N}$. This resulting discrete-time system is a linear periodic multi-rate system with period N . Since $\tilde{\mathbf{M}}$ is linear periodic, the robust tracking conditions stated in Theorem 5 in last chapter apply. That is $\tilde{\mathbf{M}}$ achieves robust steady-state tracking if and only if $\sup_i \rho(\tilde{\mathbf{M}}_{ss}^i) < 1$, where $\tilde{\mathbf{M}}_{ss}^i = \tilde{\mathbf{M}}_{ss}^{(i,1)}$ is defined by (5.19) when $p = q = 1$, the single-input single-output case.

The approximation depends on the choice of N . It can be expected that the exact robust steady-state tracking conditions for the original sampled-data system can be derived from the conditions for the approximate system as $N \rightarrow \infty$. After this approximate system is related to the original sampled-data system in the following sections, exact steady-state tracking conditions for the sampled-data system will be obtained.

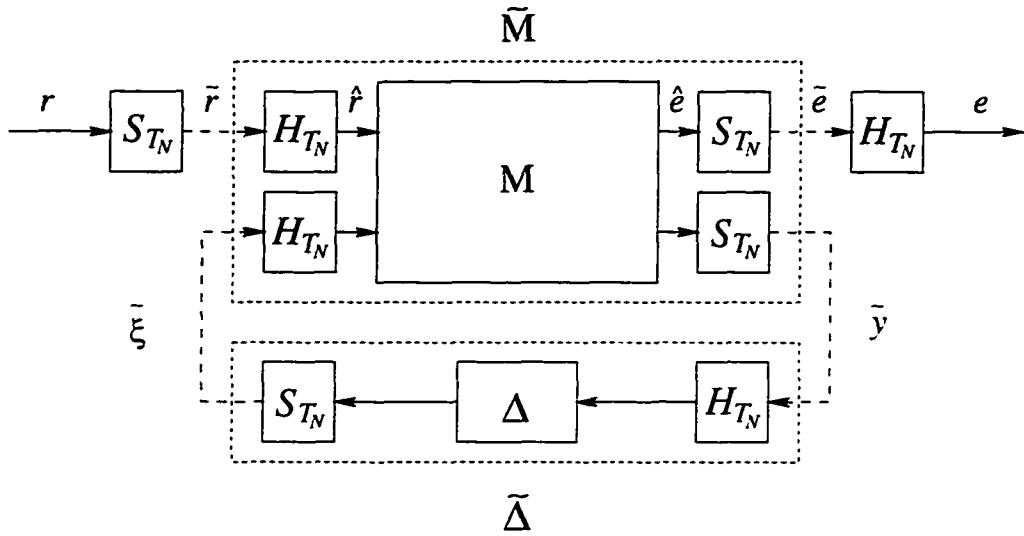


Figure 6.3 The approximate system

6.3 Steady-State Norm $\|\cdot\|_{ss}$ as Performance Measure

Sampled-data systems are considered as periodic time-varying systems in continuous-time from the input-output point of view. The performance measure is related to the measure of continuous-time signals.

6.3.1 Steady-State Norm: $\|\cdot\|_{ss}$

For continuous-time signals, we consider the usual $\mathcal{L}_\infty[0, \infty)$ space of essentially bounded signals. Let \mathcal{L}_∞ be defined as the space of real valued measurable functions on $[0, \infty)$ with the norm defined as

$$\|x\|_{\mathcal{L}_\infty} := \text{ess sup}_t |x(t)| < \infty.$$

Let L_T denote the “tail” operator on continuous-time signal

$$L_T : (L_T x)(t) := \begin{cases} x(t) & t > T. \\ 0 & \text{otherwise.} \end{cases}$$

Analogous to the steady-state performance measure for discrete-time systems, a steady-state semi-norm, or limit superior, of continuous-time signals can be defined as follows and adopted as the performance measure for continuous-time case.

Definition 5 (The Steady-State Semi-Norm $\|\cdot\|_{ss}$: Continuous-time) For a continuous-time signal $x \in \mathcal{L}_\infty$, the steady-state semi-norm, namely $\|x\|_{ss}$, is given as follows:

$$\|x\|_{ss} := \lim_{T \rightarrow \infty} \sup_{t > T} |x(t)| = \lim_{T \rightarrow \infty} \|L_T x\|_{\mathcal{L}_\infty}.$$

which is finite as long as $x \in \mathcal{L}_\infty$.

Now, the robust steady-state tracking for the system in Figure 6.2 can be defined in the following:

Definition 6 (Robust Steady-State Tracking: Continuous-Time) The periodic linear time-varying continuous-time system \mathbf{M} in Figure 6.2 is said to achieve robust steady-state tracking if

1. The interconnection of \mathbf{M} and Δ is \mathcal{L}_∞ -stable for all $\Delta \in \mathcal{D}(n)$.
2. $\sup_{\Delta \in \mathcal{D}(n)} \|e\|_{ss} < 1$.

6.3.2 System Set-Up and Lifting Technique

Partition \mathbf{M} as the following, where each element M_{ij} is again periodic with the same time period T

$$\begin{pmatrix} e \\ y_1 \\ \vdots \\ y_n \end{pmatrix} = \begin{pmatrix} M_{11} & M_{12} & \cdots & M_{1,n+1} \\ M_{21} & M_{22} & \cdots & M_{2,n+1} \\ \vdots & \vdots & \ddots & \vdots \\ M_{n+1,1} & M_{n+1,2} & \cdots & M_{n+1,n+1} \end{pmatrix} \begin{pmatrix} r \\ \xi_1 \\ \vdots \\ \xi_n \end{pmatrix}. \quad (6.2)$$

As discussed previously, we will deal with sampled-data systems by using the lifting technique due to periodicity. The lifting operator W_T for the continuous-time case can be visualized as cutting the continuous-time signal on $[0, \infty)$ into a sequence of pieces, each is a real valued function on the interval of $[0, T]$ (see Figure 6.4). Let $l_{\mathcal{L}_\infty[0, T]}^\infty$ denote the space of $\mathcal{L}_\infty[0, T]$ -valued sequences. Suppose $v \in \mathcal{L}_\infty[0, \infty)$, the lifting operator

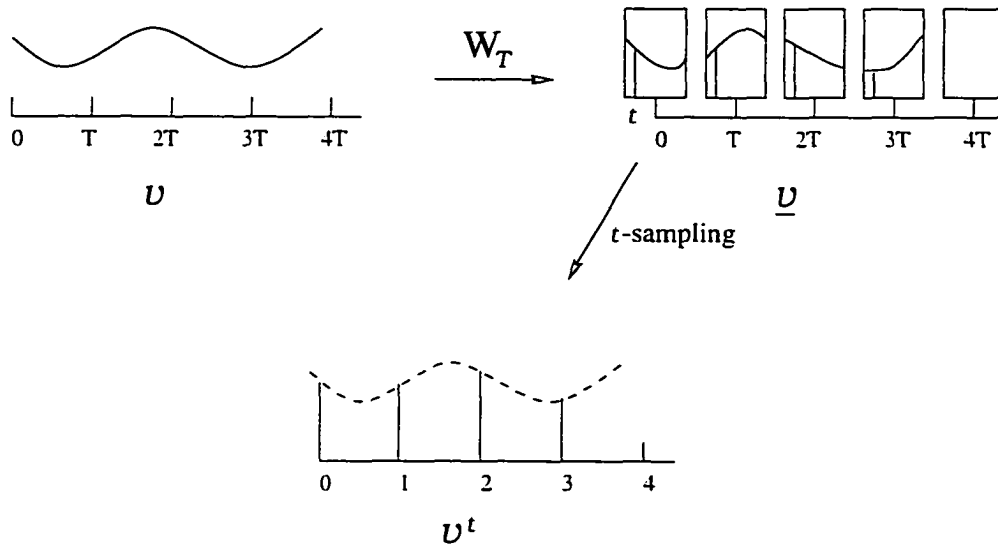


Figure 6.4 The lifting and t -sampling operator

$W_T: \mathcal{L}_\infty[0, \infty) \rightarrow l_{\mathcal{L}_\infty[0, T]}^\infty$ assigns to the signal v its lifting $\underline{v} = \{\underline{v}_k\}$, which is given by: for each k , $\underline{v}_k \in \mathcal{L}_\infty[0, T]$.

$$\underline{v}_k(t) := v(t+kT), \quad 0 \leq t \leq T. \quad (6.3)$$

The norm is defined as

$$\|\underline{v}\|_{l_{\mathcal{L}_\infty[0, T]}^\infty} := \sup_k \|\underline{v}_k\|_{\mathcal{L}_\infty[0, T]} < \infty.$$

W_T is a linear isomorphic operator, its inverse operator W_T^{-1} is well defined, and $v = W_T^{-1} \underline{v}$. Notice that the lifting operator (and its inverse operator) preserves system and signal norms. Also notice that the lifted signal $\{\underline{v}_k\}$ is a sequence of real-valued

functions over the interval of $[0, T]$. Each \underline{v}_k belongs to the infinite-dimensional space. To deal with the infinite dimensional problem, we introduce the t -sampled version (shown in Figure 6.4) of the infinite-dimensional signals. For a signal $v \in \mathcal{L}_\infty \cap \mathcal{RC}$, the t -sampled version of the lifted signal \underline{v}_k is given by an l_∞ signal, $v^t = \{v_k^t\}$ and

$$v_k^t := \underline{v}_k(t) = v(t+kT), \quad (6.4)$$

where t is fixed $\in [0, T]$. It is clear that $v_k^t \in l_\infty$ is a discrete-time signal which has the same dimension as v . Since it is a discrete-time signal, the steady-state semi-norm for this lifted signal is defined as $\|v^t\|_{ss} = \lim_{K \rightarrow \infty} \|L_K v^t\|_{l_\infty}$.

Based on the definition of the lifted and t -sampled version of signals, one can define the corresponding one side (output side) lifted and t -sampled version for systems (see Figure 6.5). Given a linear bounded continuous-time system M mapping $\mathcal{L}_\infty \cap \mathcal{RC}$ signals into $\mathcal{L}_\infty \cap \mathcal{RC}$ signals, $M: w \mapsto v$, with period T , the lifted and t -sampled system $M^t: w \mapsto v^t$ is defined as follows:

$$M^t: (M^t w)(k) := v_k^t = (Mw)(t+kT), \quad t \text{ is fixed } \in [0, T]. \quad (6.5)$$

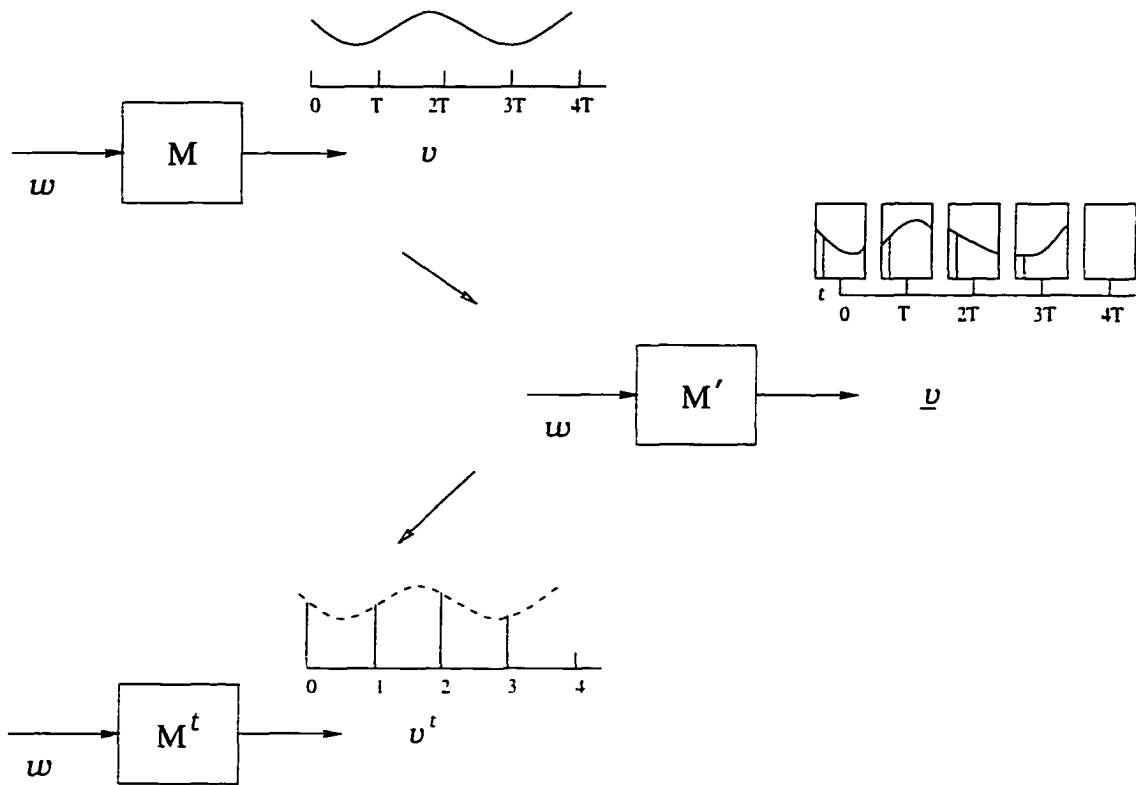
Clearly, M^t maps $\mathcal{L}_\infty \cap \mathcal{RC}$ signals into l_∞ signals. Following the similar argument we used for the discrete-time case, the above defined system M^t is related to a linear time-invariant system, namely $M^t W_T^{-1}$ by the operator W_T^{-1} . Therefore, given the kernel representation $M(t, \tau)$, a function on $\mathcal{R} \times \mathcal{R}$, of the system M , the kernel representation $M^t(k, \tau)$, a function on $\mathcal{Z}^+ \times \mathcal{R}$, for the newly defined system M^t is as follows,

$$M^t(k, \tau) := M(t+kT, \tau).$$

Also the induced norm is given by

$$\|M^t\| := \sum_{k=0}^{\infty} \int_0^T |M^t(k, \tau)| d\tau. \quad (6.6)$$

Now using the definition (6.5) of lifted and t -sampled version of systems, for each element M_{ij} of the system \mathbf{M} given by (6.2), we lift and then sample the output of

Figure 6.5 The lifted and t -sampled system

M_{ij} at $t_i \in [0, T]$. Similarly, the resulting system $M_{ij}^{t_i}$ maps $\mathcal{L}_\infty \cap \mathcal{RC}$ signals into l_∞ signals. Let $\hat{t} = [t_1, t_2, \dots, t_{n+1}] \in [0, T]^{n+1}$, a real valued vector. After defining $M_{ij}^{t_i}$ for each element of the system \mathbf{M} , we define the corresponding lifted system $\mathbf{M}^{\hat{t}}$ mapping $[r, \xi_1, \dots, \xi_n]^T$ to $[e^{t_1}, y_1^{t_2}, \dots, y_n^{t_{n+1}}]^T$ as follows,

$$\begin{pmatrix} e^{t_1} \\ y_1^{t_2} \\ \vdots \\ y_n^{t_{n+1}} \end{pmatrix} = \begin{pmatrix} M_{11}^{t_1} & M_{12}^{t_1} & \dots & M_{1,n+1}^{t_1} \\ M_{21}^{t_2} & M_{22}^{t_2} & \dots & M_{2,n+1}^{t_2} \\ \vdots & \vdots & \ddots & \vdots \\ M_{n+1,1}^{t_{n+1}} & M_{n+1,2}^{t_{n+1}} & \dots & M_{n+1,n+1}^{t_{n+1}} \end{pmatrix} \begin{pmatrix} r \\ \xi_1 \\ \vdots \\ \xi_n \end{pmatrix}. \quad (6.7)$$

Given the induced norm defined by (6.6), the continuous-time *steady-state norm*

matrix can be defined as follows:

$$\mathbf{M}_{ss}^i := \left(\begin{array}{c|ccc} \|M_{11}^{t_1} r\|_{ss} & \|M_{12}^{t_1}\| & \dots & \|M_{1,n+1}^{t_1}\| \\ \hline \|M_{21}^{t_2} r\|_{ss} & \|M_{22}^{t_2}\| & \dots & \|M_{2,n+1}^{t_2}\| \\ \vdots & \vdots & \ddots & \vdots \\ \|M_{n+1,1}^{t_{n+1}} r\|_{ss} & \|M_{n+1,2}^{t_{n+1}}\| & \dots & \|M_{n+1,n+1}^{t_{n+1}}\| \end{array} \right). \quad (6.8)$$

This matrix will play an important role in the conditions for robustness. From the robust tracking definition, it can be seen that the robust tracking problem consists of two parts: robust stability and robust tracking. The stability robustness of the system in the presence of structured norm-bounded perturbation has been addressed in [24, 25], which will be stated in the following. The solution for the tracking component will be presented in the next section.

Define the following nonnegative matrix:

$$\mathbf{M}_{\Delta}^{i_{\Delta}} := \begin{pmatrix} \|M_{22}^{t_2}\| & \dots & \|M_{2,n+1}^{t_2}\| \\ \vdots & \ddots & \vdots \\ \|M_{n+1,2}^{t_{n+1}}\| & \dots & \|M_{n+1,n+1}^{t_{n+1}}\| \end{pmatrix}.$$

where $\hat{t}_{\Delta} = [t_2, \dots, t_{n+1}] \in [0, T]^n$. $\mathbf{M}_{\Delta}^{i_{\Delta}}$ is the lower $n \times n$ matrix of \mathbf{M}_{ss}^i .

A necessary and sufficient condition for robust stability of the system in Figure 6.2 is given by the following theorem.

Theorem 6 (Robust Stability) *The interconnection of the periodic continuous-time system \mathbf{M} in Figure 6.2 and Δ is \mathcal{L}_{∞} -stable for all $\Delta \in \mathcal{D}(n)$ iff*

$$\sup_{i_{\Delta} \in [0, T]^n} \rho(\mathbf{M}_{\Delta}^{i_{\Delta}}) < 1.$$

6.3.3 Robust Steady-State Tracking ($\|\cdot\|_{ss}$ Case)

In this section, it will be shown that the exact robust steady-state tracking conditions for the sampled-data system can be derived based the continuous-time *steady-state norm matrix* defined above.

Lemma 5 *Let $H: \mathcal{L}_\infty \rightarrow l_\infty$ be any norm-bounded linear finite memory operator. Let $x \in \mathcal{L}_\infty$. Then*

$$\|Hx\|_{ss} \leq \|H\| \|x\|_{ss}, \quad (6.9)$$

where $\|H\|$ is the induced norm.

Proof: The proof is similar to that for the discrete-time case. □

Before addressing the exact necessary and sufficient robust tracking conditions, we give the following two lemmas. The first lemma shows that the steady-state semi-norm $\|\cdot\|_{ss}$ defined for the lifted signals is a continuous function with the sampling point t as its variable, provided the original reference signal satisfies a certain condition. The second lemma states that the value of the steady-state semi-norm for certain signals is achievable by the steady-state semi-norm value for the corresponding lifted signals.

Lemma 6 *Suppose $f(x)$ is uniformly continuous on $[0, \infty)$. Let $f^t = \{f^t(k)\}$ be defined by (6.4). Then $g(t) := \|f^t\|_{ss}$ is continuous on $[0, T]$.*

Proof: By hypothesis, $f(x)$ is uniformly continuous on $[0, \infty)$. It follows that for all $\epsilon > 0$, there exists a $\delta > 0$ such that

$$\forall x, y > 0, \quad |y - x| < \delta \quad \Rightarrow \quad |f(y) - f(x)| < \epsilon.$$

By definition (6.4), for all t_x and $t_y \in [0, T]$, $|t_y - t_x| < \delta$, implies

$$|f^{t_y}(k) - f^{t_x}(k)| < \epsilon, \quad \forall k,$$

$$\begin{aligned}
&\Rightarrow |f^{t_y}(k)| < |f^{t_x}(k)| + \epsilon, \quad \forall k. \\
&\Rightarrow \sup_{k > \bar{K}} |f^{t_y}(k)| \leq \sup_{k > \bar{K}} |f^{t_x}(k)| + \epsilon. \\
&\Rightarrow \lim_{K \rightarrow \infty} \sup_{k > \bar{K}} |f^{t_y}(k)| \leq \lim_{K \rightarrow \infty} \sup_{k > \bar{K}} |f^{t_x}(k)| + \epsilon. \\
&\Rightarrow g(t_y) - g(t_x) \leq \epsilon.
\end{aligned}$$

Similarly, $|t_y - t_x| < \delta$ also implies $g(t_x) - g(t_y) \leq \epsilon$. Thus $|g(t_y) - g(t_x)| \leq \epsilon$. $\forall |t_y - t_x| < \delta$.
i.e. $g(t)$ is continuous. \square

Lemma 7 Suppose $f(x)$ is uniformly continuous on $[0, \infty)$. Let $f^t(k) := f(t + kT)$, $t \in [0, T]$. Then

$$\|f\|_{ss} = \max_{0 \leq t \leq T} \|f^t\|_{ss}. \quad (6.10)$$

Proof: As in Lemma 6. let $g(t) := \|f^t\|_{ss}$. Then, $g(t)$ is continuous on $[0, T]$, which implies $\max_t g(t)$ exists. Let $L := \max_t g(t)$. It is clear that $\|f\|_{ss} \geq \|f^t\|_{ss}$ for all $t \in [0, T]$. i.e. $\|f\|_{ss} \geq L$.

By uniform continuity, for all $\epsilon > 0$, there exists a $\delta > 0$. $\forall \delta = T$ for some integer N such that

$$|x - y| < \delta \Rightarrow |f(x) - f(y)| < \frac{\epsilon}{2}.$$

Now we divide $[0, T]$ by δ and get N points. Let $L_i := g(i) < L$, $i = 0, \delta, \dots, (N-1)\delta$.

For each i , there exists a K_i , such that

$$\begin{aligned}
&\sup_{k > \bar{K}_i} |f^i(k)| - L_i < \frac{\epsilon}{2}, \\
&\Rightarrow \sup_{k > \bar{K}_i} |f^i(k)| < L_i + \frac{\epsilon}{2} < L + \frac{\epsilon}{2}.
\end{aligned}$$

Let $\bar{K} := \max_i \{K_i\}$. Then

$$\sup_{k > \bar{K}} |f^i(k)| < L + \frac{\epsilon}{2}, \quad \forall i = 0, \delta, \dots, (N-1)\delta. \quad (6.11)$$

Again by uniform continuity and (6.11), for each i and $t_i \in (i, i + \delta)$, the following is true.

$$\begin{aligned} |f^{t_i}(k) - f^i(k)| &< \frac{\epsilon}{2}, \quad \forall k, \\ \Rightarrow |f^{t_i}(k)| &< |f^i(k)| + \frac{\epsilon}{2} < L + \epsilon, \quad k > \bar{K} \end{aligned}$$

Therefore, it follows $|f^t(k)| < L + \epsilon$, for all $k > \bar{K}$, and $t \in [0, T]$, which implies $|f(x)| < L + \epsilon$, for all $x > \bar{K}T$, i.e. $L \leq \|f\|_{ss} < L + \epsilon$. Since ϵ can be chosen to be arbitrarily small, the proof is completed. \square

Notice that the requirement of uniform continuity is relative “strong”. For example, the output signals of the hold are piece-wise constant for each time period and so they are not even continuous. Obviously the equality (6.10) still holds for such right continuous signals. In this case, however, there is a bound on the rate of change of the signal except for some discontinuous points. For such kind of signals, it can be shown that Lemma 7 still holds.

Assume the matrices D_{22}, D_{23}, D_{32} and D_{33} of G in Figure 6.1 are zero matrices. Since the system is a norm-bounded linear system, we conclude that signals e and y have the property shown by Lemma 7.

Now we are ready to state our main results.

Theorem 7 *Suppose M is a norm-bounded linear system shown in Figure 6.2. Let M_{ss}^i be the matrix defined by (6.8). If*

$$\sup_{i \in [0, T]^{n+1}} \rho(M_{ss}^i) < 1, \quad (6.12)$$

then the system in Figure 6.2 achieves robust steady-state tracking.

Proof: Again define the following matrices:

$$M_{\Delta}^{i_{\Delta}} := \begin{pmatrix} \|M_{22}^{t_2}\| & \cdots & \|M_{2,n+1}^{t_2}\| \\ \vdots & \ddots & \vdots \\ \|M_{n+1,2}^{t_{n+1}}\| & \cdots & \|M_{n+1,n+1}^{t_{n+1}}\| \end{pmatrix}. \quad (6.13)$$

as before. where $\hat{t}_\Delta = [t_2, \dots, t_{n+1}] \in [0, T]^n$. By Lemma 2, $\sup_{\hat{t}} \rho(\mathbf{M}_{ss}^{\hat{t}}) < 1$ implies $\sup_{\hat{t}_\Delta} \rho(\mathbf{M}_{\Delta}^{\hat{t}_\Delta}) < 1$. This is exactly the same necessary and sufficient condition for robust stability of the system stated by Theorem 6.

The tracking part of this theorem can be proved by contradiction. As discussed above, in this system setting, signals e and y satisfy Equation (6.10). Suppose $\|e\|_{ss} \geq 1$, for some $\Delta \in \mathcal{D}(n)$. By Lemma 7, $\|e\|_{ss} \geq 1$ implies that there exists a $t_1^* \in [0, T]$ such that $\|e^{t_1^*}\|_{ss} = \|e\|_{ss} \geq 1$. According to the Equation (6.7) and the triangular inequality property, it follows that

$$\begin{aligned} 1 \leq \|e^{t_1^*}\|_{ss} &\leq \|M_{11}^{t_1^*} r\|_{ss} + \|M_{1,2}^{t_1^*}\| \|\xi_1\|_{ss} + \dots \\ &+ \|M_{1,n+1}^{t_1^*}\| \|\xi_n\|_{ss}. \end{aligned} \quad (6.14)$$

By the fact that $\|\Delta\| \leq 1$, then $\|\xi_j\|_{ss} \leq \|y_j\|_{ss}, \forall j \in [1, n]$. Again, Lemma 7 implies that for each j , there exists a $t_{j+1}^* \in [0, T]$, such that

$$\begin{aligned} \|\xi_j\|_{ss} &\leq \|y_j\|_{ss} = \|y_j^{t_{j+1}^*}\|_{ss} \\ &\leq \|M_{j+1,1}^{t_{j+1}^*} r\|_{ss} + \|M_{j+1,2}^{t_{j+1}^*}\| \|\xi_1\|_{ss} + \dots \\ &+ \|M_{j+1,n+1}^{t_{j+1}^*}\| \|\xi_n\|_{ss}. \end{aligned} \quad (6.15)$$

Equations (6.14) and (6.15) together imply that $x = (1, \|\xi_1\|_{ss}, \dots, \|\xi_n\|_{ss})^T \geq 0$ is a solution to $x \leq \mathbf{M}_{ss}^{\hat{t}^*} x$, where $\hat{t}^* = [t_1^*, t_2^*, \dots, t_{n+1}^*] \in [0, T]^{n+1}$. This implies that $\rho(\mathbf{M}_{ss}^{\hat{t}^*}) \geq 1$ for some \hat{t}^* , in contradiction to the hypothesis. This completes the proof. \square

Lemma 8 *Let M be the sampled-data system in Figure 6.2, which includes the LTI plant G and controller K_d . M is a bounded operator on the subspace of $\mathcal{L}_\infty \cap \mathcal{RC}$ signals. Let $\tilde{M} = \mathcal{S}_{T_N} M \mathcal{H}_{T_N}$, $\tilde{r} = \mathcal{S}_{T_N} r$, where $T_N = T/N$, $N > 0$ is an integer. Then, for r , a uniformly continuous signal, $\in \mathcal{L}_\infty$,*

$$\lim_{N \rightarrow \infty} \|\tilde{M} \tilde{r}\|_{ss} = \|Mr\|_{ss}. \quad (6.16)$$

where $\tilde{r} = \mathcal{S}_{T_N} r$ is the sampled signal of r .

Proof: See the approximate system in Figure 6.3. Let $\tilde{r} := \mathcal{S}_{T_N} r$, $\hat{r} := \mathcal{H}_{T_N} \tilde{r}$. Since r is uniformly continuous, we have

$$\lim_{N \rightarrow \infty} \|\hat{r} - r\|_{ss} = 0. \quad (6.17)$$

It follows that

$$\begin{aligned} & \left| \|\mathcal{S}_{T_N} M \hat{r}\|_{ss} - \|\mathcal{S}_{T_N} M r\|_{ss} \right| \\ & \leq \|\mathcal{S}_{T_N} M(\hat{r} - r)\|_{ss} \\ & \leq \|\mathcal{S}_{T_N} M\| \|(\hat{r} - r)\|_{ss}. \end{aligned}$$

which implies that

$$\lim_{N \rightarrow \infty} \|\mathcal{S}_{T_N} M \hat{r}\|_{ss} = \lim_{N \rightarrow \infty} \|\mathcal{S}_{T_N} M r\|_{ss}. \quad (6.18)$$

By the setting of M , it is clear that $M r$ is uniformly continuous, if r is. Therefore, the following is true

$$\begin{aligned} \lim_{N \rightarrow \infty} \|\tilde{M} \tilde{r}\|_{ss} &= \lim_{N \rightarrow \infty} \|\mathcal{S}_{T_N} M \hat{r}\|_{ss} \\ &= \lim_{N \rightarrow \infty} \|\mathcal{S}_{T_N} M r\|_{ss} \\ &= \|M r\|_{ss}. \end{aligned}$$

□

In the following, we will discuss an approximation procedure of sampled-data system. Let $\hat{t} = [t_1, t_2, \dots, t_{n+1}] \in [0, T]^{n+1}$. For a given periodic system \mathbf{M} and its partition representation shown in (6.2), the corresponding lifted system is as follows:

$$\mathbf{M}^{\hat{t}} := \begin{pmatrix} M_{11}^{t_1} & M_{12}^{t_1} & \dots & M_{1,n+1}^{t_1} \\ M_{21}^{t_2} & M_{22}^{t_2} & \dots & M_{2,n+1}^{t_2} \\ \vdots & \vdots & \ddots & \vdots \\ M_{n+1,1}^{t_{n+1}} & M_{n+1,2}^{t_{n+1}} & \dots & M_{n+1,n+1}^{t_{n+1}} \end{pmatrix}. \quad (6.19)$$

and its steady-state norm matrix is given by,

$$\mathbf{M}_{ss}^i := \left(\begin{array}{c|ccc} \|\tilde{M}_{11}^{t_1} r\|_{ss} & \|M_{12}^{t_1}\| & \dots & \|M_{1,n+1}^{t_1}\| \\ \hline \|\tilde{M}_{21}^{t_2} r\|_{ss} & \|M_{22}^{t_2}\| & \dots & \|M_{2,n+1}^{t_2}\| \\ \vdots & \vdots & \ddots & \vdots \\ \|\tilde{M}_{n+1,1}^{t_{n+1}} r\|_{ss} & \|M_{n+1,2}^{t_{n+1}}\| & \dots & \|M_{n+1,n+1}^{t_{n+1}}\| \end{array} \right). \quad (6.20)$$

Let fast sampling period $T_N = T/N$. Consider the approximated system given in Figure 6.3. The resulting discrete-time system is periodic with period N . Theorem 5 applies to this approximated system.

Now, let $k_{i,N}$ be the closest approximation of $t_i \in [0, T]$, $k_{i,N} = l_{i,N} * (T/N)$ for some integer $l_{i,N} \in [0, N-1]$. The choice of $l_{i,N}$ depends on the point t_i as well as the value of N . Obviously, we have $k_{i,N} \rightarrow t_i$ as $N \rightarrow \infty$. Similarly, we define $\tilde{M}_{ij}^{l_{i,N}}$ as the corresponding lifted discrete-time system of \tilde{M}_{ij} . $\tilde{M}_{ij}^{l_{i,N}}$ denotes the approximation of the system $M_{ij}^{t_i}$.

Now, the overall approximate system $\tilde{\mathbf{M}}^{i,N}$ of \mathbf{M}^i in (6.19) is given by

$$\left(\begin{array}{cccc} \tilde{M}_{11}^{l_{1,N}} & \tilde{M}_{12}^{l_{1,N}} & \dots & \tilde{M}_{1,n+1}^{l_{1,N}} \\ \tilde{M}_{21}^{l_{2,N}} & \tilde{M}_{22}^{l_{2,N}} & \dots & \tilde{M}_{2,n+1}^{l_{2,N}} \\ \vdots & \vdots & \ddots & \vdots \\ \tilde{M}_{n+1,1}^{l_{n+1,N}} & \tilde{M}_{n+1,2}^{l_{n+1,N}} & \dots & \tilde{M}_{n+1,n+1}^{l_{n+1,N}} \end{array} \right), \quad (6.21)$$

and the corresponding *steady-state norm matrix* $\tilde{\mathbf{M}}_{ss}^{i,N}$ is as follows:

$$\left(\begin{array}{c|ccc} \|\tilde{M}_{11}^{l_{1,N}} \tilde{r}\|_{ss} & \|\tilde{M}_{12}^{l_{1,N}}\| & \dots & \|\tilde{M}_{1,n+1}^{l_{1,N}}\| \\ \hline \|\tilde{M}_{21}^{l_{2,N}} \tilde{r}\|_{ss} & \|\tilde{M}_{22}^{l_{2,N}}\| & \dots & \|\tilde{M}_{2,n+1}^{l_{2,N}}\| \\ \vdots & \vdots & \ddots & \vdots \\ \|\tilde{M}_{n+1,1}^{l_{n+1,N}} \tilde{r}\|_{ss} & \|\tilde{M}_{n+1,2}^{l_{n+1,N}}\| & \dots & \|\tilde{M}_{n+1,n+1}^{l_{n+1,N}}\| \end{array} \right) := \begin{pmatrix} \hat{M}_{11} & \hat{M}_{12} \\ \hat{M}_{21} & \hat{M}_{22} \end{pmatrix}, \quad (6.22)$$

where $\hat{l}_N = [l_{1,N}, l_{2,N}, \dots, l_{n+1,N}] \in [0, N-1]^{n+1}$ is the closest approximation of $\hat{t} = [t_1, t_2, \dots, t_{n+1}] \in [0, T]^{n+1}$.

A convergent approximate procedure to the system norm has been discussed in [3].

Lemma 9 *Suppose M is a norm-bounded linear system, which maps $\mathcal{L}_\infty \cap \mathcal{RC}$ signals into $\mathcal{L}_\infty \cap \mathcal{RC}$ signals. Let M^t and \tilde{M}^{l_N} be defined similarly as above. Then the following statements are true:*

$$\lim_{N \rightarrow \infty} \|\tilde{M}^{l_N}\| = \|M^t\|, \quad (6.23)$$

$$\|\tilde{M}^{l_N}\| \leq \|M^t\| \leq \frac{K_1}{N} + (1 + \frac{K_0}{N}) \|\tilde{M}^{l_N}\|, \quad (6.24)$$

where K_0 and K_1 are constant depends on the dynamics of the plant G .

Now, we are ready to present the following theorem.

Theorem 8 *If $\rho(\mathbf{M}_{ss}^i) > 1$ for some $\hat{t} \in [0, T]^{n+1}$, then the system in Figure 6.2 does not achieve robust steady-state tracking.*

Proof: We will prove it by using the approximate system (Figure 6.3) by fast sampling of the sampled-data system discussed above. According to Theorem 5, the approximate system $\tilde{\mathbf{M}}$ achieves robust tracking if and only if $\sup_{i_N} \rho(\tilde{\mathbf{M}}_{ss}^{i_N}) < 1$.

By Lemma 8 and Lemma 9, the steady state norm matrix $\tilde{\mathbf{M}}_{ss}^{i_N}$ converges to \mathbf{M}_{ss}^i component-wisely when N goes to ∞ . Since each component in $\tilde{\mathbf{M}}_{ss}^{i_N}$ converges to and bounded from above by the corresponding component in \mathbf{M}_{ss}^i , we can choose a sequence of N such that the convergent sequence of the each component is a nondecreasing sequence.

By the discussion above and the continuity of spectral radius function, the hypothesis $\rho(\mathbf{M}_{ss}^i) > 1$ implies there exists a K such that for all $N > K$, $\rho(\tilde{\mathbf{M}}_{ss}^{i_N}) > 1$. Similar to Equation (6.13), define $\tilde{\mathbf{M}}_{\Delta}^{i_{\Delta}, N}$, which is the lower $n \times n$ matrix of $\tilde{\mathbf{M}}_{ss}^{i_N}$, where $\hat{l}_{\Delta, N} = [l_{2N}, \dots, l_{n+1, N}] \in [0, N-1]^n$.

By the proof of Theorem 5 in last chapter for periodic discrete-time systems. $\rho(\tilde{\mathbf{M}}_{ss}^{i_N}) > 1$ implies either.

1. $\rho(\tilde{\mathbf{M}}_{\tilde{\Delta}}^{i_{\Delta N}}) > 1$. therefore we have $\rho(\mathbf{M}_{\tilde{\Delta}}^{i_{\Delta}}) > 1$ by (6.24) and monotonicity of the spectral function of nonnegative matrix, where $\hat{t}_{\Delta} = [t_2, \dots, t_{n+1}] \in [0, T]^n$. This means that the interconnection of Δ and \mathbf{M} is not robustly stable.
2. Or, there exists a $\tilde{\Delta} \in \tilde{\mathcal{D}}(n)$ such that $\|\tilde{e}\|_{ss} > 1$. i.e., no robust tracking. According to the system setting in Figure 6.3. this implies $\|\hat{e}\|_{ss} > 1$ with input \hat{r} .

The approximate input signal \hat{r} can be arbitrarily close to the input signal r of the sampled-data system in the sense of the steady-state semi-norm. From the proof of Lemma 8, we have $\lim_{N \rightarrow \infty} \|\hat{r} - r\|_{ss} = 0 \Rightarrow \lim_{N \rightarrow \infty} \|\hat{e} - e\|_{ss} = 0$. where e is the tracking error of the sampled-data system with r as the input reference. By a similar proof in [26], the worst-case steady-state tracking error of the sampled-data system is given as following provided that $\rho(\hat{\mathbf{M}}_{22}) < 1$:

$$\sup_{\tilde{\mathcal{D}}(n)} \|\tilde{e}\|_{ss} = \hat{\mathbf{M}}_{11} + \hat{\mathbf{M}}_{12}(I - \hat{\mathbf{M}}_{22})^{-1}\hat{\mathbf{M}}_{21}. \quad (6.25)$$

It follows that $\sup_{\tilde{\mathcal{D}}(n)} \|\tilde{e}\|_{ss}$ is nondecreasing since the sequence of each component of $\tilde{\mathbf{M}}_{ss}^{i_N}$ is nondecreasing. Therefore, for the second situation discussed above, there exists an integer N large enough such that $\|\hat{e}\|_{ss} > 1$ implies $\|e\|_{ss} > 1$. A continuous-time uncertainty, Δ , can be constructed from $\tilde{\Delta}$ by letting $\Delta := \mathcal{H}_{T_N} \tilde{\Delta} \mathcal{S}_{T_N}$ (see Figure 6.6). It follows that there exists a Δ defined as above such that the system in Figure 6.2 does

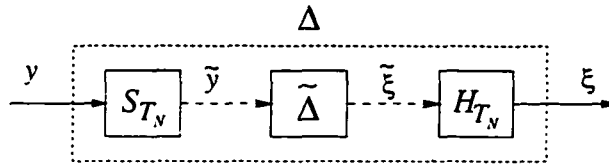


Figure 6.6 An equivalent uncertainty

not achieve robust tracking when r is the tracking input.

Now, we complete this proof by showing that Δ constructed above belongs to $\mathcal{D}(n)$. By the assumption of the system, $y \in \mathcal{L}_\infty \cap \mathcal{RC}$. Then, $\|y\|_\infty \geq \|\tilde{y}\|_\infty$ and $\|\tilde{\xi}\|_\infty = \|\xi\|_\infty$, which implies $\|\Delta\| \leq 1$ as long as $\|\tilde{\Delta}\| \leq 1$. This completes the proof. \square

6.4 Steady-State Norm $\|\cdot\|_{cs}$ as Performance Measure

Robust steady-state tracking conditions are derived in last section by using the steady-state norm, $\|\cdot\|_{ss}$ as the performance measure. However, the results are restricted to certain systems as described above. The reason is that in general we do not have $\|e\|_{ss} = \sup_t \|e^t\|_{ss}$ though the equality holds when e is a uniformly continuous signal. The assumption in the system setting of D_{22} , D_{23} , D_{32} and D_{33} to be zero matrices is relatively strong. This assumption simply ensures that the output signals of the system have the property described by Lemma 7. In order to drop this requirement posed on the system, another steady-state norm is introduced in the following section.

6.4.1 Steady-State Norm: $\|\cdot\|_{cs}$

Notice that the lifted signal e^t is a discrete-time signal. The steady-state norm, $\|\cdot\|_{ss}$, for e^t is given as,

$$\|e^t\|_{ss} := \lim_{K \rightarrow \infty} \|L_K e^t\|_{l^\infty}. \quad (6.26)$$

However, with the steady-state norm defined by (6.26), the signals $\{e^t: t \in [0, T]\}$ may not capture the property the original continuous-time signal e has in the sense of steady-state norm. Consider the following example. e is a continuous-time signal as shown in Figure 6.7. $e(t) = 0$ except for the triangles with peak value of 1. The width of the triangle base, $1/k$, goes to 0 as k goes to ∞ . It is clear that $\|e\|_{ss} = 1$ while $\|e^t\|_{ss} = 0$, for all $t \in [0, T]$ because $\lim_{K \rightarrow \infty} \|L_K e^t\|_{l^\infty} = 0$ for all $t \in [0, T]$.

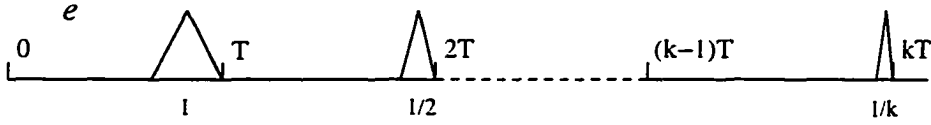


Figure 6.7 An example: $\|\cdot\|_{ss}$ vs. $\|\cdot\|_{cs}$

To retain the steady-state norm property of the continuous-time signal, a new definition of the steady-state norm for lifted signals is introduced in the following. Instead of defining the steady-state norm of the discrete-time signal e^t by only investigating its discrete-time values, this new steady-state norm is defined for e^t by studying its behavior in the original continuous-time signal.

First define the following intervals. For $t \in [0, T]$, $0 < \delta < T/2$, let

$$I[t, \delta] = \begin{cases} [t - \delta, t + \delta] & \text{if } [t - \delta, t + \delta] \subset [0, T], \\ [0, t + \delta] & \text{if } t - \delta < 0, \\ [t - \delta, T] & \text{if } t + \delta > T. \end{cases} \quad (6.27)$$

Let $\mathcal{L}_\infty I[t, \delta]$ denote the space of \mathcal{L}_∞ functions on interval $I[t, \delta]$, and $l_{\mathcal{L}_\infty I[t, \delta]}^\infty$ the space of $\mathcal{L}_\infty I[t, \delta]$ valued sequences. Define the lifting operator $\mathcal{W}_{t, \delta}: \mathcal{L}_\infty[0, \infty) \rightarrow l_{\mathcal{L}_\infty I[t, \delta]}^\infty$ as follows. For $e \in \mathcal{L}_\infty[0, \infty)$, $\mathcal{W}_{t, \delta} e := \{e_k^{t, \delta}\}_{k=0}^\infty$, where

$$e_k^{t, \delta}(\tau) := e(\tau + kT), \quad \tau \in I[t, \delta]. \quad (6.28)$$

The norm of $\{e_k^{t, \delta}\} =: e^{t, \delta}$ is defined by

$$\|e^{t, \delta}\|_I = \sup_k \sup_{\tau \in I[t, \delta]} |e(\tau + kT)|.$$

Note that $e_k^{t, \delta} \in \mathcal{L}_\infty I[t, \delta]$ takes values over the interval $I[t, \delta]$. Each $e_k^{t, \delta}$ contains information of e in the interval $I[t, \delta]$. The signal $e^{t, \delta} = \{e_k^{t, \delta}\}$ will be studied in the rest of this research instead of the discrete-time signal $e^t = \{e_k^t\}$. Similarly, the semi-norm:

$\|e^{t,\delta}\|_{ss} := \lim_{K \rightarrow \infty} \|L_K e^{t,\delta}\|_I$ is well defined. It can be considered as a positively valued function of δ and decreases as δ does. Therefore the limit exists as $\delta \rightarrow 0$, and this limit is defined as the new steady-state norm.

Definition 7 (Steady-State Semi-Norm $\|\cdot\|_{cs}$) Suppose $e \in \mathcal{L}_\infty$ is a continuous-time signal. Let $e^t = \{e_k^t\}$, $I[t, \delta]$ and $e^{t,\delta} = \{e_k^{t,\delta}\}$ be defined by (6.4), (6.27) and (6.28) respectively. Then the steady-state semi-norm $\|\cdot\|_{cs}$ is defined as follows:

$$\|e^t\|_{cs} := \lim_{\delta \rightarrow 0} \lim_{K \rightarrow \infty} \|L_K e^{t,\delta}\|_I. \quad (6.29)$$

The difference between the above two definitions of steady-state norms, $\|e^t\|_{cs}$ and $\|e^t\|_{ss}$, bears analogy to the difference between the limit value $\lim_{t \rightarrow t_0} e(t)$ and the value $e(t_0)$ of the function e at the point t_0 . The $\|\cdot\|_{cs}$ norm is defined by the continuous-time signal's behavior at the neighborhood of the point of interest rather than just by the value at the single point itself. The single point value is not relevant in this definition.

Notice that for a uniformly continuous signal e , $\|e^t\|_{cs} = \|e^t\|_{ss}$. Now, let us use the new steady-state norm $\|\cdot\|_{cs}$ to measure the signal in Figure 6.7. At $t = T$, $I[t, \delta] = [T - \delta, T]$ as defined above, then $\forall \delta > 0$, $\lim_{K \rightarrow \infty} \|L_K e^{t,\delta}\|_I = 1$. It follows that $\|e^T\|_{cs} = 1 = \|e\|_{ss}$ while $\|e^T\|_{ss} = 0$ because $c^T(k) = c(kT) = 0$.

Lemma 10 Suppose e is a continuous-time signal $\in \mathcal{L}_\infty$. Let steady-state semi-norms, $\|\cdot\|_{ss}$ and $\|\cdot\|_{cs}$, be defined as above for the original continuous-time signal e and the lifted signal e^t respectively, there exists $t^* \in [0, T]$ such that

$$\|e\|_{ss} = \|e^{t^*}\|_{cs}. \quad (6.30)$$

Proof: As shown in Figure 6.8, we start with the interval $I_0 = [0, T]$. Let $e^{I_0} := \{e_k^{I_0}\}$, where $e_k^{I_0}(\tau) = e(\tau + kT)$, $\tau \in I_0$. The norm is given by $\|L_K e^{I_0}\|_{I_0} = \sup_k \sup_{t \in I_0} |e(\tau + kT)|$. It is obvious that $\lim_{K \rightarrow \infty} \|L_K e^{I_0}\|_{I_0} = \|e\|_{ss}$. Then divide each of the intervals of length T into n subintervals of length T/n , where n is an integer. It is clear that

there exists a subinterval, namely I_1 , such that $\lim_{K \rightarrow \infty} \|L_K e^{I_1}\|_{I_1} = \|e\|_{ss}$, where e^{I_1} is similarly defined as above. Once again, we can divide the subintervals I_1 further into n sub-subintervals of length T/n^2 , and there exists a sub-subinterval, say I_2 , with the following equality $\lim_{K \rightarrow \infty} \|L_K e^{I_2}\|_{I_2} = \|e\|_{ss}$.

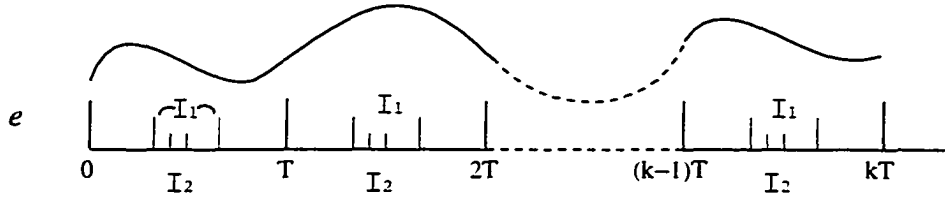


Figure 6.8 The new steady-state norm: $\|\cdot\|_{cs}$

Repeating this process, we obtain a sequence of intervals with $I_0 \supset I_1 \supset I_2 \supset \dots \supset I_j \supset \dots$, and the corresponding sequence of real numbers with $T/n > T/n^2 > \dots > T/n^j > \dots$. These intervals are nested and the length of these intervals $T/n^j \rightarrow 0$. Since each I_j is closed and bounded, then

$$I := \bigcap_{j=0}^{\infty} I_j \neq \emptyset.$$

Since $I \subset I_j$ for each j , $\lim_{j \rightarrow \infty} I_j \neq \emptyset$. However, the limit, $\lim_{j \rightarrow \infty} I_j$, can not be an interval because the length (T/n^j) of the the interval, I_j , converges to 0. Therefore I_j converges to a unique point $t^* \in [0, T]$ as $j \rightarrow \infty$ (see a complete proof in [7]). Since $\lim_{K \rightarrow \infty} \|L_K e^{I_j}\|_{I_j} = \|e\|_{ss}$ holds for each j , the limit, $\lim_{j \rightarrow \infty} \lim_{K \rightarrow \infty} \|L_K e^{I_j}\|_{I_j}$, exists and equals the constant $\|e\|_{ss}$. Since $I_j \rightarrow t^*$ as $j \rightarrow \infty$, we have $\|e^{t^*}\|_{cs} = \lim_{j \rightarrow \infty} \lim_{K \rightarrow \infty} \|L_K e^{I_j}\|_{I_j} = \|e\|_{ss}$. This completes the proof. \square

6.4.2 Robust Steady-State Tracking ($\|\cdot\|_{cs}$ Case)

Let M be a linear norm-bounded system mapping $\mathcal{L}_{\infty} \cap \mathcal{RC}$ signals into $\mathcal{L}_{\infty} \cap \mathcal{RC}$ signals. With the lifted signals y^t and $y^{t,\delta}$ defined by Equation (6.4) and (6.28) respectively, one can define the following systems:

1. M^t : mapping $\mathcal{L}_\infty \cap \mathcal{RC}$ signal x into $y^t \in l_\infty$. $M^t x = (Mx)^t = y^t$.
2. $M^{t,\delta}$: mapping $\mathcal{L}_\infty \cap \mathcal{RC}$ signal x into $y^{t,\delta} \in l_{\mathcal{L}_\infty I[t,\delta]}^\infty$. $M^{t,\delta} x = (Mx)^{t,\delta} = y^{t,\delta}$.

In order to derive the robust steady-state tracking condition, we need the following two lemmas. The first lemma shows that $\|M^t\|$ is a continuous function of t over the interval $[0, T]$. Using this property, we will show in the second lemma that the triangular inequality holds for the steady-state semi-norm. $\|\cdot\|_{cs}$.

Lemma 11 *Let M be the sampled-data system in Figure 6.2, which includes the LTI plant G and controller K_d . M is a norm-bounded operator on the subspace of $\mathcal{L}_\infty \cap \mathcal{RC}$ signals. M^t is the lifted operator defined as above. Then $f(t) := \|M^t\|$ is a right continuous function on $[0, T]$*

Proof: Suppose t_1 and $t_2 \in [0, T]$ and $t_1 < t_2$. We need to prove that $t_2 \rightarrow t_1 \Rightarrow \|M^{t_2}\| \rightarrow \|M^{t_1}\|$. Since it is linear time-invariant system, the plant G maps right continuous signals into right continuous signals. Suppose $x \in \mathcal{L}_\infty \cap \mathcal{RC}$, then Mx is right continuous as well. By definition of $M^t x$, we have $\|M^{t_2} x - M^{t_1} x\|_\infty \rightarrow 0$ as $t_2 \rightarrow t_1$. It follows that when $t_2 \rightarrow t_1$,

$$\|M^{t_2} - M^{t_1}\| = \sup_{x \neq 0} \frac{\|M^{t_2} x - M^{t_1} x\|_\infty}{\|x\|_\infty} \rightarrow 0.$$

This implies that $\|M^{t_2}\| \rightarrow \|M^{t_1}\|$ as $t_2 \rightarrow t_1$. □

Lemma 12 *Let M be the sampled-data system in Figure 6.2, which includes the LTI plant G and controller K_d . M is a norm-bounded operator on the subspace of $\mathcal{L}_\infty \cap \mathcal{RC}$ signals. M^t is the lifted operator defined as above. Let $x \in \mathcal{L}_\infty \cap \mathcal{RC}$. Then*

$$\|M^t x\|_{cs} \leq \|M^t\| \cdot \|x\|_{ss}, \quad (6.31)$$

where $\|M^t\|$ is the induced norm.

Proof: Let $I[t, \delta]$ be the interval defined by (6.27). For $\tau \in I[t, \delta]$, consider the lifted signals $M^\tau x \in l_\infty$ of Mx as defined above. Because of the linearity of the operator M^τ , for all $\tau \in I[t, \delta]$,

$$\begin{aligned} \|L_m M^\tau x\|_{l_\infty} &\leq \|L_m M^\tau L_n x\|_{l_\infty} + \|L_m M^\tau P_n x\|_{l_\infty} \\ &\leq \|M^\tau\| \cdot \|L_n x\|_{\mathcal{L}^\infty} + \|L_m M^\tau P_n x\|_{l_\infty}. \end{aligned}$$

Now take sup on both side over $I[t, \delta]$,

$$\sup_{\tau \in I[t, \delta]} \|L_m M^\tau x\|_{l_\infty} \leq \max_{\tau \in I[t, \delta]} \|M^\tau\| \cdot \|L_n x\|_{\mathcal{L}^\infty} + \sup_{\tau \in I[t, \delta]} \|L_m M^\tau P_n x\|_{l_\infty}.$$

The maximum exists because of right (or left) continuity of $\|M^\tau\|$ on $[0, T]$ by Lemma 11. Then, first let m go to ∞ , the term $\|L_m M^\tau P_n x\|_{l_\infty}$ goes to 0 since M^τ is a finite memory operator. And finally, take the limit as n and δ go to ∞ and 0 respectively, by definition of the steady-state semi-norm in (6.29)

$$\|M^t x\|_{cs} \leq \|M^t\| \cdot \|x\|_{ss}.$$

Notice that $\lim_{\delta \rightarrow 0} \max_{\tau \in I[t, \delta]} \|M^\tau\| = \|M^t\|$ because of right (or left) continuity of $\|M^\tau\|$.

□

With the new steady-state semi-norm given by (6.29), we define the following *steady-state norm matrix*:

$$\hat{M}_{cs}^t := \begin{pmatrix} \hat{M}_{11} & \hat{M}_{12} \\ \hat{M}_{21} & \hat{M}_{22} \end{pmatrix} := \left(\begin{array}{c|ccc} \|M_{11}^{t_1} r\|_{cs} & \|M_{12}^{t_1}\| & \dots & \|M_{1, n+1}^{t_1}\| \\ \|M_{21}^{t_2} r\|_{cs} & \|M_{22}^{t_2}\| & \dots & \|M_{2, n+1}^{t_2}\| \\ \vdots & \vdots & \ddots & \vdots \\ \|M_{n+1, 1}^{t_{n+1}} r\|_{cs} & \|M_{n+1, 2}^{t_{n+1}}\| & \dots & \|M_{n+1, n+1}^{t_{n+1}}\| \end{array} \right). \quad (6.32)$$

Now the main results are ready to be presented. In the last section, there are assumptions on signals and the D matrix of the system. However, as the following theorems show by using the new steady-state norm defined above, similar results hold without these restriction on the system setting.

Theorem 9 *The system in Figure 6.2 achieves robust steady-state tracking if*

$$\sup_{\hat{t}} \rho(\hat{\mathbf{M}}_{cs}^{\hat{t}}) < 1, \quad (6.33)$$

where $\hat{t} \in [0, T]^{n+1}$.

Proof: The proof will go through similarly as in the proof of Theorem 7 if the following is noticed. Suppose $\|\epsilon\|_{ss} \geq 1$. By Lemma 10 this implies that there exists a t_1^* such that $\|e^{t_1^*}\|_{cs} \geq 1$. According to Lemma 12 it follows that

$$1 \leq \|e^{t_1^*}\|_{cs} \leq \|M_{11}^{t_1^*} r\|_{cs} + \|M_{1,2}^{t_1^*}\| \|\xi_1\|_{ss} + \cdots + \|M_{1,n+1}^{t_1^*}\| \|\xi_n\|_{ss}. \quad (6.34)$$

By the fact that $\|\Delta\| \leq 1$, $\|\xi_j\|_{ss} \leq \|y_j\|_{ss}$, $j \in [1, n]$. Again by Lemma 10 and Lemma 12, for each j , there exists a t_{j+1}^* , such that

$$\|\xi_j\|_{ss} \leq \|y_j^{t_{j+1}^*}\|_{cs} \leq \|M_{j+1,1}^{t_{j+1}^*} r\|_{cs} + \|M_{j+1,2}^{t_{j+1}^*}\| \|\xi_1\|_{ss} + \cdots + \|M_{j+1,n+1}^{t_{j+1}^*}\| \|\xi_n\|_{ss}. \quad (6.35)$$

Equations (6.34) and (6.35) imply that there exists $\hat{t}^* = [t_1^*, t_2^*, \dots, t_{n+1}^*]$ such that $(1, \|\xi_1\|_{ss}, \dots, \|\xi_n\|_{ss})^T$ is a solution to $x \leq \hat{\mathbf{M}}_{cs}^{\hat{t}^*} x$, $x \geq 0$. Therefore, $\rho(\hat{\mathbf{M}}_{cs}^{\hat{t}^*}) \geq 1$. \square

Following the similar modification and using the same argument in the corresponding proof of Theorem 8, one can similarly prove the following theorem. The proof will be omitted here.

Theorem 10 *If $\rho(\hat{\mathbf{M}}_{cs}^{\hat{t}}) > 1$ for some \hat{t} , then the system in Figure 6.2 does not achieve robust steady-state tracking.*

CHAPTER 7 COMPUTATIONAL ALGORITHM AND SIMULATIONS

7.1 Computation Algorithm

The original sampled-data system is a linear periodic time-varying hybrid system with period T . The robust tracking problem is solved in the last chapter by using the lifting technique. However, the result is based on the following so-called steady-state norm matrix

$$\hat{\mathbf{M}}_{cs}^i := \begin{pmatrix} \hat{\mathbf{M}}_{11} & \hat{\mathbf{M}}_{12} \\ \hat{\mathbf{M}}_{21} & \hat{\mathbf{M}}_{22} \end{pmatrix} := \left(\begin{array}{c|ccc} \|M_{11}^{t_1} r\|_{cs} & \|M_{12}^{t_1}\| & \cdots & \|M_{L,n+1}^{t_1}\| \\ \|M_{21}^{t_2} r\|_{cs} & \|M_{22}^{t_2}\| & \cdots & \|M_{2,n+1}^{t_2}\| \\ \vdots & \vdots & \ddots & \vdots \\ \|M_{n+1,1}^{t_{n+1}} r\|_{cs} & \|M_{n+1,2}^{t_{n+1}}\| & \cdots & \|M_{n+1,n+1}^{t_{n+1}}\| \end{array} \right). \quad (7.1)$$

and the obtained robust tracking conditions in Theorem 9 and 10 are “infinite dimensional conditions,”

$$\sup_{\hat{t}} \rho(\hat{\mathbf{M}}_{cs}^{\hat{t}}) \leq 1,$$

where $\hat{t} = [t_1, t_2, \dots, t_{n+1}] \in [0, T]^{n+1}$. The supremum is taken over the interval $[0, T]$ for each t_i . The system induced norms in $\hat{\mathbf{M}}_{cs}^{\hat{t}}$ is not readily computable, and neither is the robust tracking conditions due to this infinite dimensional property.

As discussed in [35], this problem can be solved by approximation rather than an exact procedure. The infinite dimensional system can be approximated by fast sampling,

say with period T/N . $N > 0$ is an integer. Therefore, the robust tracking problem of the original sampled-data system is solved by the approximation of the robust tracking problem of the approximate discrete-time system. As shown in Figure 7.1, the resulting approximate system is a multi-rate periodic discrete-time system with period N from the input-output point view. The exact robust tracking conditions are proven after being

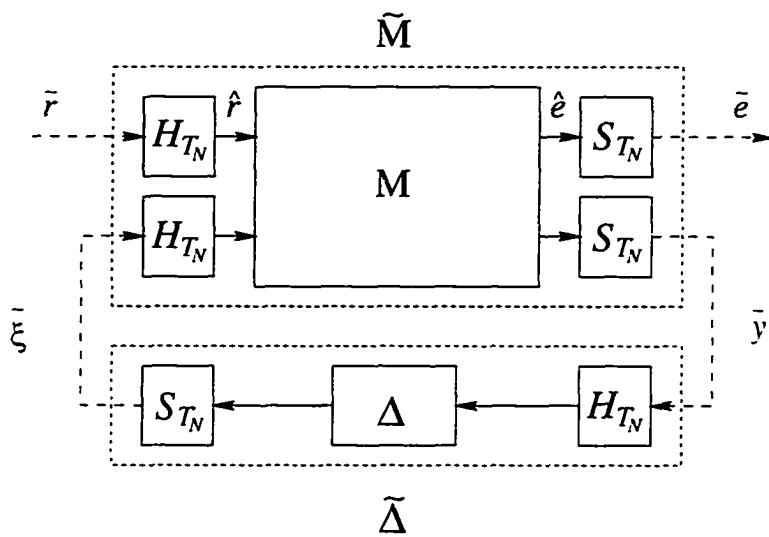


Figure 7.1 The approximate system

compared to the robust tracking conditions of the approximate discrete-time system. As in Section 6.3.3, let $\hat{l}_N = [l_{1N}, l_{2N}, \dots, l_{n+1,N}] \in [0, N-1]^{n+1}$ be the closest approximation of $\hat{l} = [l_1, l_2, \dots, l_{n+1}] \in [0, T]^{n+1}$. Define the steady-state norm matrix $\tilde{M}_{cs}^{i_N}$ of the approximate discrete-time system as follows:

$$\tilde{M}_{cs}^{i_N} := \left(\begin{array}{c|ccc} \|\tilde{M}_{11}^{l_{1N}} \tilde{r}\|_{cs} & \|\tilde{M}_{12}^{l_{1N}}\| & \dots & \|\tilde{M}_{1,n+1}^{l_{1N}}\| \\ \hline \|\tilde{M}_{21}^{l_{2N}} \tilde{r}\|_{cs} & \|\tilde{M}_{22}^{l_{2N}}\| & \dots & \|\tilde{M}_{2,n+1}^{l_{2N}}\| \\ \vdots & \vdots & \ddots & \vdots \\ \|\tilde{M}_{n+1,1}^{l_{n+1,N}} \tilde{r}\|_{cs} & \|\tilde{M}_{n+1,2}^{l_{n+1,N}}\| & \dots & \|\tilde{M}_{n+1,n+1}^{l_{n+1,N}}\| \end{array} \right). \quad (7.2)$$

Obviously, $\tilde{M}_{cs}^{i_N}$ is computable since each element of this matrix is. The computation

algorithm for sampled-data systems is given in the following by showing the convergent upper bound and lower bound from the approximation.

By Lemma 9, each element of the induced norm in the steady-state norm matrix \hat{M}_{cs}^i is bounded by the corresponding induced norm of the approximate system, i.e.,

$$\|\tilde{M}_{ij}^{t,N}\| \leq \|M_{ij}^t\| \leq \frac{K_1}{N} + (1 + \frac{K_0}{N})\|\tilde{M}_{ij}^{t,N}\|. \quad (7.3)$$

K_0 and K_1 only depend on the dynamics of the nominal plant not the discrete-time controller. This is because the discrete-time controller only effects the hybrid system at the sampling instants, while the interstate is governed by the nominal plant. By Equation (7.3), we have lower bound and upper bound for $\|M_{ij}^t\|$ and clearly both bounds converge.

The elements of induced norm in (7.1) are computed by the convergence discussed above. Obviously, the steady-state norm term $\|\cdot\|_{cs}$ in (7.1), is not readily computable either. However, if we only impose the requirement of uniform continuity on the input signal r , which is reasonable in practice, without changing the setting of the system, we have $\|\cdot\|_{cs} = \|\cdot\|_{ss}$ and the latter can be computed by approximation. Even though r is required to be uniformly continuous in this case, steady-state matrices (6.8) and (6.32) for the $\|\cdot\|_{ss}$ and $\|\cdot\|_{cs}$ semi-norm cases respectively still remain fundamental different. In (6.8), not only does r need to be uniformly continuous but also the corresponding D matrices of the system are required to be zero matrices. However, for (6.32), when we discuss computation, the only requirement is imposed on r , the input reference. Actually, as discussed in last chapter, we can relax this requirement on r a little.

In the following, we will show the convergent process of computing the semi-norm, $\|\cdot\|_{ss}$. Lemma 9 was prove in [3] by giving bounds of the following induced norm:

$$\|(I - (\mathcal{H}_{T_N}\mathcal{S}_{T_N})^{-L})|_{\mathcal{R}(\mathcal{H}_{T_N}\mathcal{S}_{T_N}M)}\| \leq \frac{K_a}{N}, \quad (7.4)$$

where $(\mathcal{H}_{T_N}\mathcal{S}_{T_N})^{-L}$ denotes the left inverse of $(\mathcal{H}_{T_N}\mathcal{S}_{T_N})$ on the range of $\mathcal{R}(M)$. K_a is a

constant determined by the plant G . It is clear that we have

$$\begin{aligned} \|Mr - \mathcal{H}_{T_N} \mathcal{S}_{T_N} M \mathcal{H}_{T_N} \mathcal{S}_{T_N} r\|_{ss} &\leq \| \mathcal{H}_{T_N} \mathcal{S}_{T_N} Mr - Mr \|_{ss} + \\ &\quad + \| \mathcal{H}_{T_N} \mathcal{S}_{T_N} Mr - \mathcal{H}_{T_N} \mathcal{S}_{T_N} M \mathcal{H}_{T_N} \mathcal{S}_{T_N} r \|_{ss}. \end{aligned}$$

By inequality (7.4), it follows that

$$\begin{aligned} \| \mathcal{H}_{T_N} \mathcal{S}_{T_N} Mr - Mr \|_{ss} &\leq \| (I - (\mathcal{H}_{T_N} \mathcal{S}_{T_N})^{-L}) |_{\mathcal{R}(\mathcal{H}_{T_N} \mathcal{S}_{T_N} M)} \| \| \mathcal{H}_{T_N} \mathcal{S}_{T_N} Mr \|_{ss} \\ &\leq \frac{K_a}{N} \| \mathcal{H}_{T_N} \mathcal{S}_{T_N} Mr \|_{ss}. \end{aligned} \quad (7.5)$$

Since r is assumed to be uniformly continuous, then

$$\|r - \mathcal{H}_{T_N} \mathcal{S}_{T_N} r\|_{ss} \leq K \frac{T}{N} \|r\|_{ss},$$

where K , a constant, is the bound of the derivative of r . Therefore,

$$\begin{aligned} \| \mathcal{H}_{T_N} \mathcal{S}_{T_N} Mr - \mathcal{H}_{T_N} \mathcal{S}_{T_N} M \mathcal{H}_{T_N} \mathcal{S}_{T_N} r \|_{ss} &\leq \| \mathcal{H}_{T_N} \mathcal{S}_{T_N} M \| \|r - \mathcal{H}_{T_N} \mathcal{S}_{T_N} r\|_{ss} \\ &\leq K \frac{T}{N} \|M\| \|r\|_{ss} \\ &\leq K \frac{T}{N} \left[\frac{K_1}{N} + \left(1 + \frac{K_0}{N}\right) \| \mathcal{S}_{T_N} M \mathcal{H}_{T_N} \| \right] \|r\|_{ss} \end{aligned} \quad (7.6)$$

where the last step is from Lemma 9. Let $\tilde{M} := \mathcal{S}_{T_N} M \mathcal{H}_{T_N}$. It follows that

$$\begin{aligned} \| \mathcal{H}_{T_N} \mathcal{S}_{T_N} Mr \|_{ss} &\leq K \frac{T}{N} \left[\frac{K_1}{N} + \left(1 + \frac{K_0}{N}\right) \| \tilde{M} \| \right] \|r\|_{ss} + \\ &\quad + \| \mathcal{H}_{T_N} \mathcal{S}_{T_N} M \mathcal{H}_{T_N} \mathcal{S}_{T_N} r \|_{ss} \end{aligned} \quad (7.7)$$

Combining inequalities (7.5), (7.6) and (7.7), we obtain,

$$\begin{aligned} \| Mr - \mathcal{H}_{T_N} \mathcal{S}_{T_N} M \mathcal{H}_{T_N} \mathcal{S}_{T_N} r \|_{ss} &\leq K \frac{T}{N} \left[\frac{K_1}{N} + \left(1 + \frac{K_2}{N}\right) \| \tilde{M} \| \right] \|r\|_{ss} + \frac{K_a}{N} \| \mathcal{H}_{T_N} \mathcal{S}_{T_N} Mr \|_{ss} \\ &\leq \left(1 + \frac{K_a}{N}\right) K \frac{T}{N} \left[\frac{K_1}{N} + \left(1 + \frac{K_2}{N}\right) \| \tilde{M} \| \right] \|r\|_{ss} + \end{aligned}$$

$$\begin{aligned}
& + \frac{K_a}{N} \|\mathcal{H}_{T_N} \mathcal{S}_{T_N} M \mathcal{H}_{T_N} \mathcal{S}_{T_N} r\|_{ss} \\
\Rightarrow \|Mr\|_{ss} & \leq \left(1 + \frac{K_a}{N}\right) K \frac{T}{N} \left[\frac{K_1}{N} + \left(1 + \frac{K_2}{N}\right) \|\tilde{M}\|\right] \|r\|_{ss} + \\
& + \left(1 + \frac{K_a}{N}\right) \|\mathcal{H}_{T_N} \mathcal{S}_{T_N} M \mathcal{H}_{T_N} \mathcal{S}_{T_N} r\|_{ss} \\
& \leq \left(1 + \frac{K_a}{N}\right) K \frac{T}{N} \left[\frac{K_1}{N} + \left(1 + \frac{K_2}{N}\right) \|\tilde{M}\|\right] \|r\|_{ss} + \\
& + \left(1 + \frac{K_a}{N}\right) \|\tilde{M} \tilde{r}\|_{ss}, \tag{7.8}
\end{aligned}$$

where $\tilde{r} := \mathcal{S}_{T_N} r$. The last step follows by using the fact, $\|\mathcal{H}_{T_N}\| = 1$.

By the convergence as shown in (7.3) and (7.8), all the elements of \tilde{M}_{cs}^{iN} are convergent to the corresponding elements of \hat{M}_{cs}^i as N goes to ∞ . Therefore, the spectral $\rho(\tilde{M}_{cs}^{iN})$ will converge to $\rho(\hat{M}_{cs}^i)$ as N goes to ∞ because of the continuity of the spectral radius function.

Furthermore, applying Equations (7.3) and (7.8) to the steady-state norm matrix \hat{M}_{cs}^i , we obtain a lower bound and an upper bound for each element in \hat{M}_{cs}^i , and both lower and upper bounds converge as the fast sampling period goes to 0. This means that the robust steady-state tracking condition, $\rho(\hat{M}_{cs}^i)$, can be approximated and computed by the discrete-time case, $\rho(\tilde{M}_{cs}^{iN})$, at the convergence rate of $1/N$, where $\rho(\tilde{M}_{cs}^{iN})$ is a finite dimension problem and is computable.

For the sake of the simulation algorithm, besides the convergence issue, we are also interested in how we can choose a sequence for N to make the convergence more efficient. Of course, one can let N be any monotone increasing sequence to get the convergence. However, some improvement can be made to make the convergence process faster. Let's see the following example. Let G_N denote the discretized and lifted nominal system with fast sampling period of T/N , M_N the corresponding close loop system which is a LSI system (see Figure 7.2).

Let $(A_{fN}, [B_{1fN}, B_{2f1}])$ be the corresponding system matrices of the discretized system.

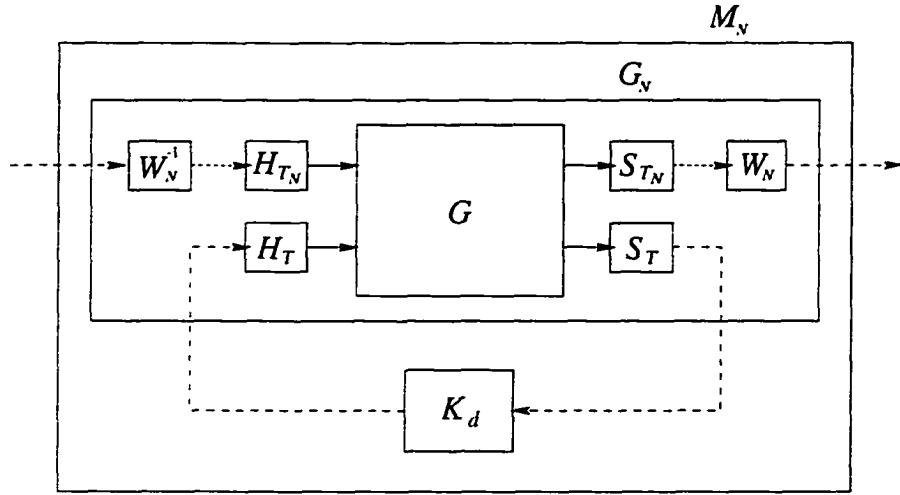


Figure 7.2 Discretization and lifting of the sampled-data system

$$A_{f_N} = e^{AT/N},$$

$$B_{1f_N} = \int_0^{T/N} e^{\tau A} d\tau B_1, \quad B_{2f_1} = \int_0^T e^{\tau A} d\tau B_2,$$

where $(A, [B_1, B_2])$ are the system matrices of G . Notice that matrices B_{1f_N} and B_{2f_1} act on different rate signals, say f_N and f_1 respectively, if $N \neq 1$. When $N = 1$, no lifting needed. We have G_1 and M_1 in the following forms respectively:

$$G_1 = \left[\begin{array}{c|cc} A_{f_1} & B_{1f_1} & B_{2f_1} \\ \hline C_{g1} & D_{g11} & D_{g12} \\ C_{g2} & D_{g21} & D_{g22} \end{array} \right], \quad M_1 = \left[\begin{array}{c|c} A & \begin{bmatrix} B_{11} + B_{1f_1} \\ B_{21} \end{bmatrix} \\ \hline C_1 & D_{11} \end{array} \right],$$

where A, B_{11}, B_{21}, C_1 and D_{11} are certain matrices obtained for the closed-loop system.

Then the impulse response is

$$\left\{ D_{11}, \quad C_1 \begin{bmatrix} B_{11} + B_{1f_1} \\ B_{21} \end{bmatrix}, \quad C_1 A \begin{bmatrix} B_{11} + B_{1f_1} \\ B_{21} \end{bmatrix}, \quad \dots \right\}. \quad (7.9)$$

Now when $N = 2$, lifting is needed, and the systems become

$$G_2 = \left[\begin{array}{c|cc} A_{f_1} & [A_{f_2} B_{1f_2} \quad B_{1f_2}] & B_{2f_1} \\ \hline \begin{bmatrix} C_{g1} \\ C_{g1} A_{f_2} \end{bmatrix} & \begin{bmatrix} D_{g11} & 0 \\ C_{g1} B_{1f_2} & D_{g11} \end{bmatrix} & \begin{bmatrix} D_{g12} \\ C_{g1} B_{2f_2} + D_{g12} \end{bmatrix} \\ C_{g2} & [D_{g21} \quad 0] & D_{g22} \end{array} \right],$$

$$M_2 = \left[\begin{array}{c|cc} A & \begin{bmatrix} B_{11} + A_{f_2} B_{1f_2} & B_{1f_2} \\ B_{21} & 0 \end{bmatrix} \\ \hline \begin{bmatrix} C_1 \\ * \end{bmatrix} & \begin{bmatrix} D_{11} & 0 \\ * & * \end{bmatrix} \end{array} \right] := \begin{bmatrix} M_2^1 \\ M_2^2 \end{bmatrix}.$$

Notice that $[A_{f_2} B_{1f_2} \quad B_{1f_2}]$ and B_{1f_2} act on the same rate of signals now. The impulse response is

$$\left\{ \begin{bmatrix} D_{11} & 0 \\ * & * \end{bmatrix}, \begin{bmatrix} C_1 \\ * \end{bmatrix} \begin{bmatrix} B_{11} + A_{f_2} B_{1f_2} & B_{1f_2} \\ B_{21} & 0 \end{bmatrix}, \right. \\ \left. \begin{bmatrix} C_1 \\ * \end{bmatrix} A \begin{bmatrix} B_{11} + A_{f_2} B_{1f_2} & B_{1f_2} \\ B_{21} & 0 \end{bmatrix}, \dots \right\}. \quad (7.10)$$

Notice that

$$\begin{aligned} B_{f_{N_1}} &= \int_0^{\frac{T}{N_1}} e^{\tau A} d\tau B \\ &= \int_0^{\frac{T}{N_2}} e^{\tau A} d\tau B + \dots + \int_{\frac{(m-1)T}{N_2}}^{\frac{T}{N_2}} e^{\tau A} d\tau B \\ &= (I + e^{\frac{T}{N_2} A} + \dots + e^{\frac{(m-1)T}{N_2} A}) B_{f_{N_2}}. \end{aligned} \quad (7.11)$$

$$B_{f_{N_1}} = (I + A_{f_{N_2}} + \dots + A_{f_{N_2}}^{m-1}) B_{f_{N_2}}, \quad (7.12)$$

where $m = \frac{N_2}{N_1}$ is an integer. Therefore $\|M_2^1\| = \|M_1\|$ because $B_{1f_1} = (I + A_{f_2})B_{1f_2}$ by (7.12). Comparing the impulse responses (7.9) and (7.10), we can conclude that $\|M_2\| = \max_{k=1,2} \|M_2^k\| \geq \|M_1\|$. It can be shown that $\|M_{N_2}\| = \max_{1 \leq k \leq m} \|M_{N_2}^k\| \geq \|M_{N_1}\|$, where $m = \frac{N_2}{N_1}$ is an integer, since $B_{1f_{N_1}} = (I + A_{f_{N_2}} + \dots + A_{f_{N_2}}^{N_2-1})B_{1f_{N_2}}$.

Therefore we can choose a sequence for N , $\{N_1, N_2, \dots, N_i, \dots, N_j, \dots\}$ such that $N_i < N_j$ if $i < j$ and $\frac{N_j}{N_i}$ is an integer. In this case, the resulting sequence of the approximate induced norm is a monotonically increasing sequence, meaning this sequence converges to the exact induced norm for the sampled-data system from below and converges more efficient than if we just arbitrarily pick N .

7.2 An Example and Simulation

In this section, we will give an example of a tracking problem of a sampled-data system to compute the steady-state tracking error subject to system uncertainty.

As shown in Figure 7.3, the nominal plant P_0 is given by

$$P_0(s) = \frac{1}{s+1}.$$

The system uncertainty is given as multiplicative uncertainty of the form

$$P(s) = P_0(s)(1 + W_t(s)\Delta).$$

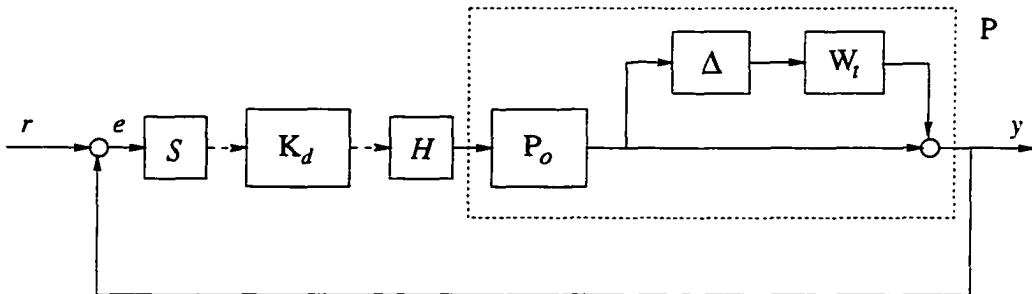


Figure 7.3 An example: Robust steady-state tracking

where the uncertainty is norm bounded with $\|\Delta\| \leq 0.25$. The weighting function $W_t = 1$. The discrete-time controller K_d is designed for the nominal plant P_0 to force the plant to track the reference input r , a unit step input.

$$K_d(z) = \frac{10}{6} \frac{z - 0.3}{z - 1}.$$

The discrete-time controller works well for the nominal plant (see simulation in Figure 7.4). The steady-state tracking error is zero due to the integrator in the controller.

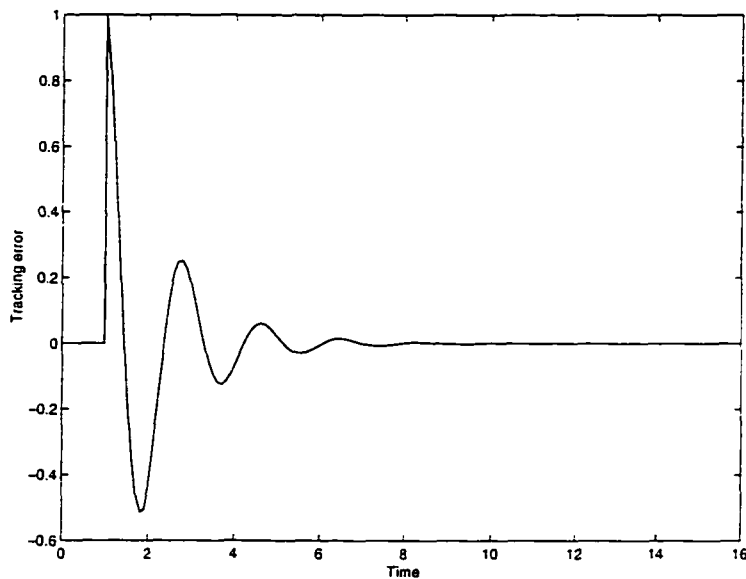


Figure 7.4 Steady-state tracking error: Nominal case

In the following, we will show how this sampled-data system performs when system uncertainty is considered. First, the steady-state tracking error is computed. Table 7.1 shows the lower bound (*BdLow*) and upper bound (*BdUp*) of the tracking errors obtained by computing the corresponding approximate system at the fast sampling rate of T/N , when $N = 8, 16, 32$ and 64 , respectively.

One can see from the computation results in Table 7.1, the computation process is converging, and the tracking error lies somewhere between .7935 and .8141. This means

that this is not a good design for robust tracking since the system will result in an error of about 80%.

Secondly, we do simulation for this system. The uncertainty is given as a gain slider in SIMULINK taking values between -0.25 and 0.25 (dash in Figure 7.5). The simulation result is shown in Figure 7.5. One can see that the system under this uncertainty at least has the tracking error of 66.72%, which is below and close to the result obtained by computation.

Table 7.1: Steady-state tracking error

	$N = 8$	$N = 16$	$N = 32$	$N = 64$
BdLow	.7771	.7863	.7911	.7935
BdUp	.9506	.8704	.8325	.8141

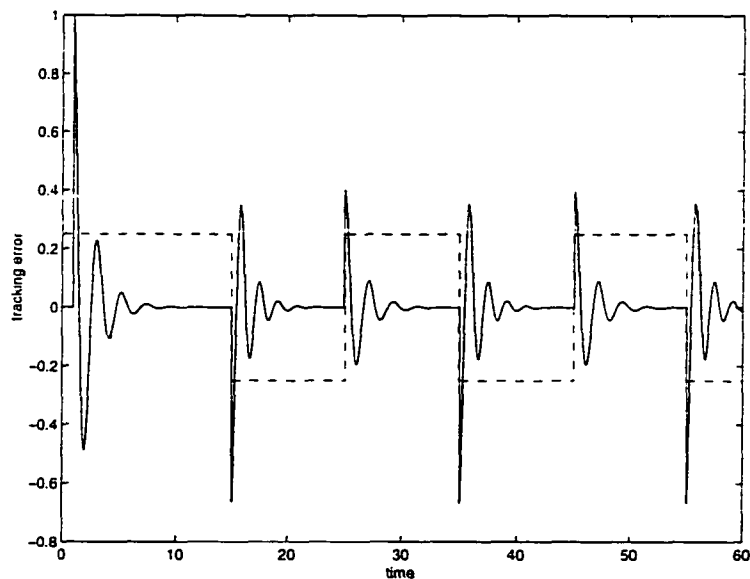


Figure 7.5 Steady-state tracking error: with uncertainty

CHAPTER 8 CONCLUSIONS

In this part, robust tracking for both discrete-time systems and sampled-data systems has been addressed with the presence of structured norm bounded finite memory uncertainty. Appropriate steady-state norms, $\|\cdot\|_{ss}$ for discrete-time and $\|\cdot\|_{cs}$ for lifted continuous-time signals, have been defined and adopted as steady-state tracking measures. Based on those steady-state norms, the so-called steady-state norm matrices, $\tilde{\mathbf{M}}_{ss}^i$ and $\hat{\mathbf{M}}_{cs}^i$, have been constructed and then robust steady-state tracking conditions are derived in terms of the spectral radius of those matrices. Similar conditions can be obtained for general periodic systems and MIMO systems, or multi-tracking systems. A convergent approximate approach and computation algorithm are given to solve the steady-state tracking problem, and an example and simulation are shown as well.

PART II

ROBUST AIRCRAFT PITCH CONTROL

CHAPTER 9 INTRODUCTION

Robust control techniques are applied to the aircraft control. Due to different flight conditions, the flight model varies accordingly with certain parameters, such as weight, center of gravity, etc. For the purpose of applying robust control techniques, the aircraft dynamics is modeled as a linear time-invariant system plus uncertainty due to the variations.

\mathcal{H}_∞ and μ techniques have been developed as powerful tools in analysis and synthesis for system robustness. \mathcal{H}_∞ control is a frequency-domain synthesis theory that was developed to deal with plant uncertainty and unknown system disturbances. The \mathcal{H}_∞ norm captures the induced operator norm when \mathcal{L}_2 signals, or bounded energy signals, affect the system. The \mathcal{H}_∞ norm, as a measure of the system energy gain, is given by the peak value of the transfer function in the frequency domain. Indeed for a stable transfer function $G(s)$, the \mathcal{H}_∞ norm is given by $\|G\|_\infty = \sup_\omega |G(j\omega)|$. Dolye [14] presented an earlier state-space solution to the \mathcal{H}_∞ problem. Glover and Dolye [20] treated the detailed derivation of the \mathcal{H}_∞ solution for general cases. The results and techniques developed in Dolye, Francis, and Tannenbaum [15] have generated more interest in applications of \mathcal{H}_∞ methods.

Based on the \mathcal{H}_∞ control theory, singular values have been developed as μ -analysis and synthesis tools for the robustness and performance of feedback systems (see [2]). μ is defined as a measure of the smallest structured uncertainty that causes instability of the closed-loop system. μ -analysis gives the level of robustness of the system that can be assessed, while μ -synthesis determines a controller such that the singular value (μ) is

minimized.

The objective of our research is to apply these robust control techniques to optimize control system performance when the aircraft model is subject to variations. The problem focuses on the longitudinal (pitch) attitude control problem when aircraft weight and center of gravity are unavailable as control inputs. The weight and center of gravity of the aircraft can vary throughout the duration of a flight as well as from one flight to another. These two parameters significantly affect the pitch moment and elevator effectiveness of the aircraft. A longitudinal attitude robust control algorithm is designed to provide consistent performance throughout the flight regime at varying weight and center of gravity locations.

CHAPTER 10 AIRCRAFT DYNAMICS AND PERFORMANCE CRITERIA

As we mentioned before, the aircraft model varies with parametric variations such as weight and center of gravity in our case.

10.1 Aircraft Dynamics

Generated from a full six degree of freedom nonlinear aircraft model, nine linear state space models are given as the dynamics of light commercial aircraft (see [1]). The nonlinear model is trimmed under level flight ($\dot{h} = 0$), zero longitudinal acceleration ($\dot{U} = 0$) and zero pitch rate ($Q = 0$) constraints. With these constraints, the nonlinear model is trimmed at three different flight conditions: low-altitude/low-airspeed, middle-altitude/high-airspeed, and high-altitude/high-airspeed. At each of these three flight conditions, three linear state space models were generated: heavy weight at forward *cg*, medium weight at middle *cg*, and light weight at aft *cg*. The flight conditions for the nine linear models are listed in Table 10.1.

The resulting nine linear models all have five states, three inputs and six outputs.

States:

- x_1 : *Theta* (θ , rad), pitch angle;
- x_2 : Q ($\dot{\theta}$, rad/sec), pitch rate;
- x_3 : U (meters/sec), component of inertial velocity along body X-axis;
- x_4 : W (meters/sec), component of inertial velocity along body Z-axis;

Table 10.1: Linearization points for linear state-space models

Case #	Alt (ft)	IAS (knots)	Weight (lbs)	CG (%chord)	Class (wt/cg)
1	5,000	114	10,000	0.300	Mid/Mid
43	5,000	98	7,464	0.384	Lt/Aft
57	5,000	123	11,800	0.228	Hvy/Fwd
7	20,000	250	10,000	0.300	Mid/Mid
49	20,000	250	7,464	0.384	Lt/Aft
63	20,000	250	11,800	0.228	Hvy/Fwd
14	41,000	245	10,000	0.300	Mid/Mid
56	41,000	245	7,464	0.384	Lt/Aft
76	41,000	245	11,800	0.228	Hvy/Fwd

x_5 : Altitude (feet).

Inputs:

u_1 : Elevator Deflection (δ , deg);

u_2 : U Disturbance (meters/sec), longitudinal wind disturbance;

u_3 : W Disturbance (meters/sec), vertical wind disturbance.

Outputs:

y_1 : θ (deg), pitch angle;

y_2 : $\dot{\theta}$ (deg/sec), pitch rate;

y_3 : N_z (g), normalized acceleration along Z-axis;

y_4 : N_x (g), normalized acceleration along X-axis;

y_5 : True Airspeed, Tas (knots);

y_6 : Altitude (feet).

The aircraft dynamics, along with the elevator actuator dynamics, are shown in Figure 10.1. The pitch command $ServoCmdD$, generated by the outer loop, applies to

the aircraft dynamics through the integrator and the servo model, which are given. An elevator deflection limit of ± 5 degrees is imposed on the output of the actuator and then applied to the aircraft model. Longitudinal and vertical wind models, the Dryden wind models (see [1]), are first-order and second-order transfer functions respectively.

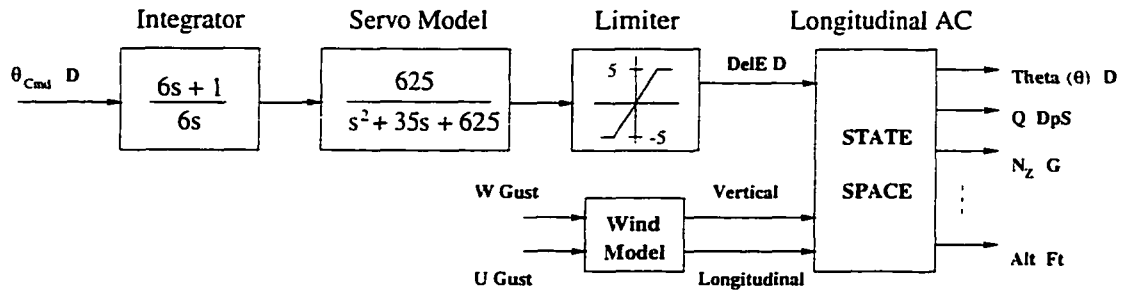


Figure 10.1 Longitudinal aircraft model with servo motor dynamics

10.2 Performance Criteria

The performance criteria are given in the time domain as well as the frequency domain. Time responses to step disturbances or commands are compared against three given transfer functions.

1. As a part of the performance criteria for this problem, a second-order model,

$$\text{Desired Model: } \frac{\theta}{\theta_{Cmd}}(s) := \frac{4}{s^2 + 4s + 4},$$

is given as the desired model from *pitch command*(θ_{Cmd}) to *theta* (θ). An upper bound and lower bound dynamics are also given as second-order systems for the performance measurement of the transient and steady-state tracking as well,

$$\text{Upper Bound: } \frac{4}{s^2 + 2.8s + 4}.$$

$$\text{Lower Bound: } \frac{1.96}{s^2 + 3.64s + 1.96}.$$

The corresponding unit step responses are shown in Figure 10.2.

2. The normal acceleration, the third output N_z , shall not exceed 0.4 g for a standard pitch maneuver.
3. The frequency response of the open loop system shall not exceed 4 rad/second crossover frequency. No high frequency signal is allowed in the system because of consideration of energy consumption in the system and the mechanical linkage from the elevator to the control column.

The performance criteria are listed in Table 10.2.

Table 10.2: Performance criteria

Desired Dynamics	$\frac{4}{s^2 + 4s + 4}$
Upper Dynamics	$\frac{4}{s^2 + 2.8s + 4}$
Lower Dynamics	$\frac{1.96}{s^2 + 3.64s + 1.96}$
Normal Acceleration	$n_z \leq 0.4G$
Crossover Frequency	$\omega_c \leq 4 \text{ rad/sec}$

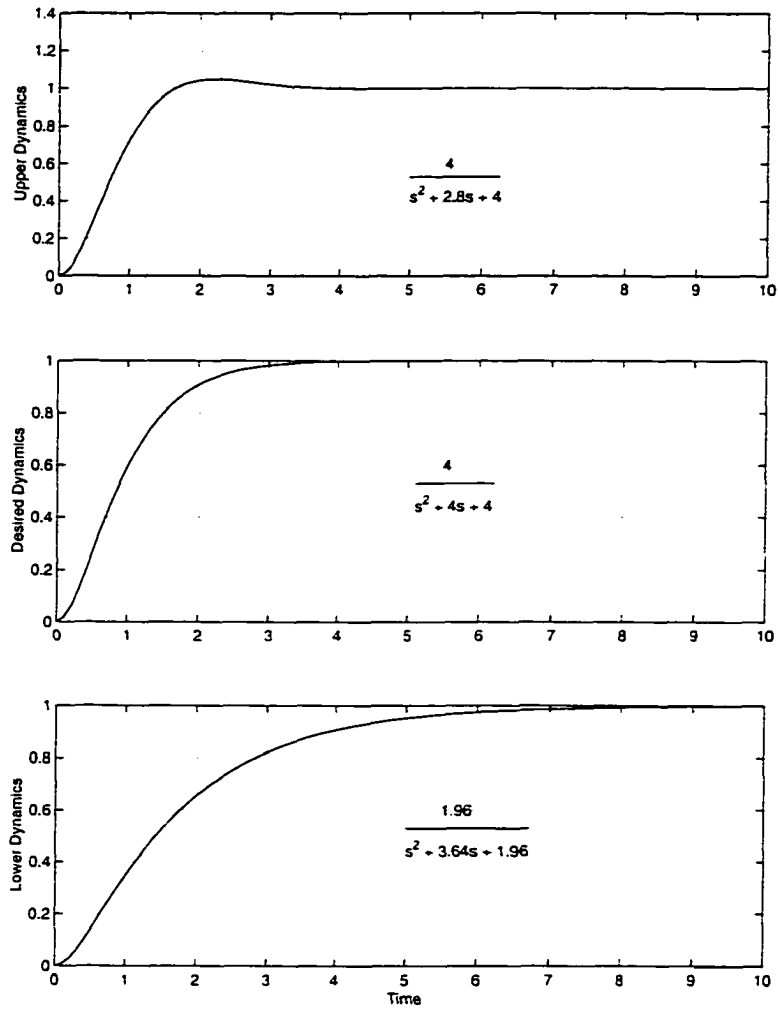


Figure 10.2 Longitudinal attitude control law dynamic thresholds

CHAPTER 11 NOMINAL PERFORMANCE

Before the design of the robust controller for the aircraft at different flight conditions and with variations of weight and center of gravity location, we start with the \mathcal{H}_∞ controller design for the nominal models. i.e., models without variations. to study the behavior of these nominal models at different conditions.

11.1 Model Matching

As stated in the objective of this project. the controlled system should behave similarly to a second-order system. referred to as the desired model. This naturally gives rise to \mathcal{H}_∞ model matching problem. The model matching problem is to find a controller such that the difference of the closed-loop system from the desired system is minimized in the \mathcal{H}_∞ norm. Let H_{DM} be the desired transfer function. $H_{r\theta}(K)$ is the closed-loop system determined by the designed controller K . The model matching problem is to design the controller K such that $\|H_{DM} - H_{r\theta}(K)\|_\infty$ is minimized. That means the maximum magnitude of the transfer function $H_{DM} - H_{r\theta}(K)$ is minimized in the frequency domain. Usually, some weighting functions are incorporated to penalize the minimization on certain frequency range of interest. For instance, the tracking performance requires the difference of the two transfer functions is small in the low frequency range. Therefore, we can use a low-pass weighting function, $W_{low}(s)$, for this purpose. Then the problem becomes minimizing the quantity of

$$\|W_{low}(H_{DM} - H_{r\theta}(K))\|_\infty.$$

11.1.1 Model Matching: Set-Up I

The set-up of the problem should be handled carefully. For example, a problem set-up for model matching is shown in Figure 11.1. In this set-up, the controller (K) takes the reference command ref and the aircraft output measurements, pitch angle θ and acceleration N_z as its inputs. Notice that the controller does not directly take the tracking error as its input. Instead, the error through a low-pass filter W_e is considered as a performance measure. A controller designed in this way has two degrees of freedom for the structure of the controller.

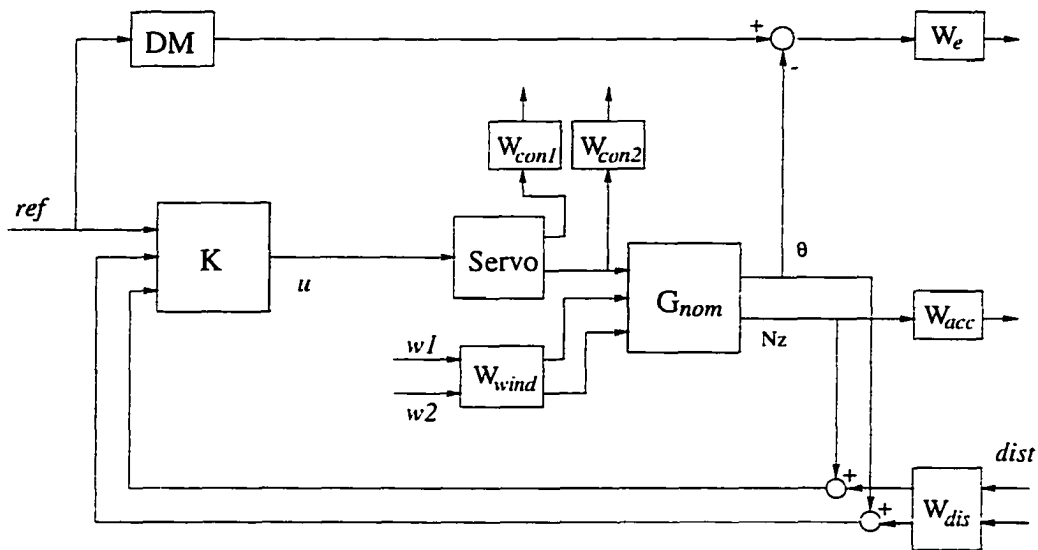


Figure 11.1 Nominal set-up I: Model matching

A controller is synthesized using this set-up for the nominal model of middle-altitude at medium weight and middle cg (case # 7). As one can see from the system responses in Figure A.1 (Appendix A), this design seems good in terms of system's tracking to the reference input and the crossover frequency. These criteria are easily achieved by the designed controller. However, after careful inspection of the controller designed in this way, one can find that the feedback part of this controller, U_2 and U_3 , has a very small gain and close to zero (see Figure A.1 in Appendix A). The only part of this controller,

which plays a role in controlling, is the feed-forward one, i.e., from reference ref to the control signal u . In fact, the obtained controller acts as an open-loop feedforward controller instead of a feedback closed-loop controller. Though the requirements can be achieved by this design for the specific model, it is not a good design. Some changes in the nominal plant will result in bad responses because this design is not robust at all. See Figure A.2 for an example in Appendix A.

11.1.2 A Modified Set-Up for Model Matching

The set-up in last section can become a useful one by adding two more weighting functions W_{del} and W_{deli} into the set-up (see Figure 11.2). In this way, the performance

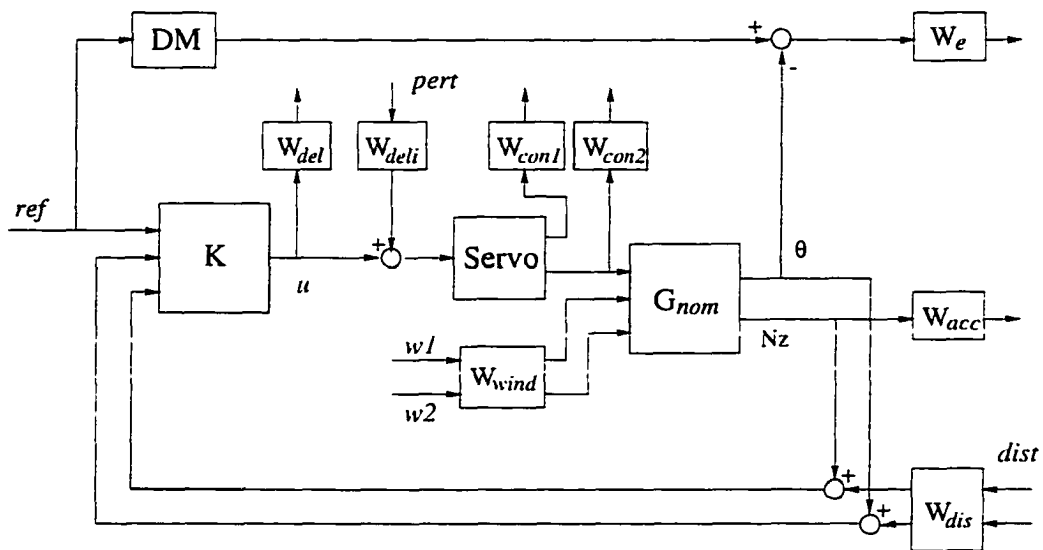


Figure 11.2 Nominal set-up I: The modified model matching

evaluation includes not only the channel from reference ref to error W_e but also the channel from $pert$ to error W_e . The latter one ensures that the controller obtained will not be of zero gain in the feedback path.

The performance measurements in this set-up include:

1. The error between the output θ , the pitch angle, of the system and the desired output from the desired model (**DM**). A low pass weight W_e ($\frac{1}{s+0.05}$) is chosen to ensure the steady-state error to be satisfied. See the bode plot of W_e in Figure 11.3:
2. The normalized acceleration, N_Z . A constant weight W_{acc} (0.001) is imposed on N_Z for the normal acceleration requirement;
3. The elevator deflection and the acceleration. Weights W_{con1} (0.1) and W_{con2} (0.1) are introduced to penalize the crossover frequency.

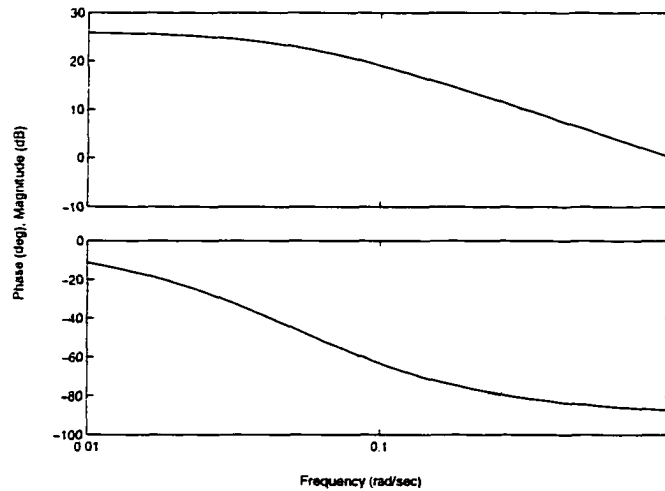


Figure 11.3 The bode plot of weight W_e for tracking error

The input *dist* is introduced as the measurement noise. The input *pert* and the measure of output of controller *u* are introduced to ensure the problem is set-up properly for the μ -synthesis.

Controllers are designed for the given nine different models (see [36]). Simulation results are shown in Appendix B (see Figures B.1 - B.3) for models of medium weight at middle cg of all three different flight altitudes.

1. Low-altitude/low-airspeed at medium weight and middle cg (Case # 1):

2. Middle-altitude/high-air-speed at medium weight and middle cg (Case # 7):
3. High-altitude/high-air-speed at medium weight and middle cg (Case # 14).

As simulation results show, the feedback parts of the controllers designed in this way are no longer zero controllers. The designed controller is evaluated for the corresponding nominal model and the performance requirement can be met.

1. The θ response falls in the envelope (dots) in the plot except for the initial stage:
2. Elevator deflection in the transient is small (< 5 deg):
3. The crossover frequency of the open-loop system frequency response is less than the 4 rad/sec restriction.

From the design experience of nominal models and simulation of the system, it is clear that robust control design should be introduced to handle the model variation.

11.1.3 Discussion and Analysis

The system should be set up very carefully for the problem. The case of set-up I should be avoided. Though the open-loop controller works well on the nominal model, the controller is not a good one since the open-loop system is not robust at all. The modified set-up avoids this problem because the performance of the transfer function from *pert* to tracking error is also evaluated.

Notice that the feedback path from the third output N_z to the control signal u has a very small gain (see Figure A.3 in Appendix A). This feedback path does not play a big role in system controlling. Therefore, the controller structure can be simplified by dropping the N_z feedback path, i.e., the controller only takes reference ref and system output θ as its inputs. Figure A.3 in Appendix A shows the bode plots of controllers designed for case # 7 (middle altitude/airspeed at Mid/Mid) with and without N_z as the feedback control signal.

The order of the resulting controller depends on the order of the nominal system and those weighting functions. The higher the order of those functions, the higher the order of the controller obtained. For the modified model matching set-up discussed in last section, one can get a controller with 10th order. Using Hankel norm model reduction, one can reduce the controller to 6th order with acceptable performance (See Figure A.4 in Appendix A).

11.2 Desired Model as Prefilter

In the modified model matching set-up, as many as eight weighting functions are involved. This makes the design procedure more complicated. Tuning any weight will affect other performance. Besides, the more the weighting functions, the higher the order of the obtained controller.

A simpler set-up of this problem is investigated. In this set-up, the desired model is not taken into account for the design stage but will be used as a prefilter for the reference command after the controller is obtained (see Figure 11.4). The tracking error can be kept small if the open-loop gain is large at low frequency range.

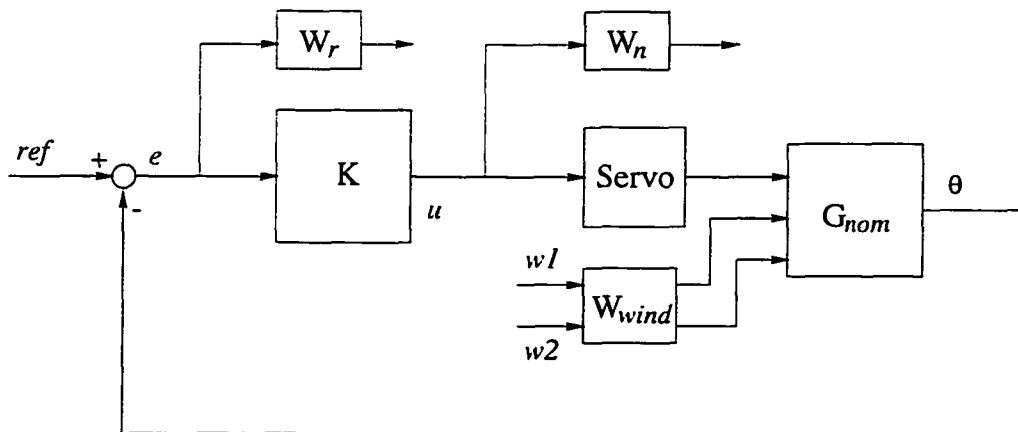


Figure 11.4 Nominal set-up II: The desired model as a prefilter

In this set-up, the controller (\mathbf{K}) takes the tracking error (ϵ) as its input. The number of weighting functions drops down to two. The performance measurement includes:

1. The error between the output θ , the pitch angle, of the system and the reference command. A low pass weight $W_r \left(\frac{3}{s+0.15} \right)$ is chosen to ensure the steady-state error to be satisfied. The bode plot of W_r is shown in Figure 11.5;
2. The controller output u . A weight $W_n \left(\frac{s}{s+10} \right)$ is introduced to penalize the crossover frequency. The bode plot is shown in Figure 11.5.

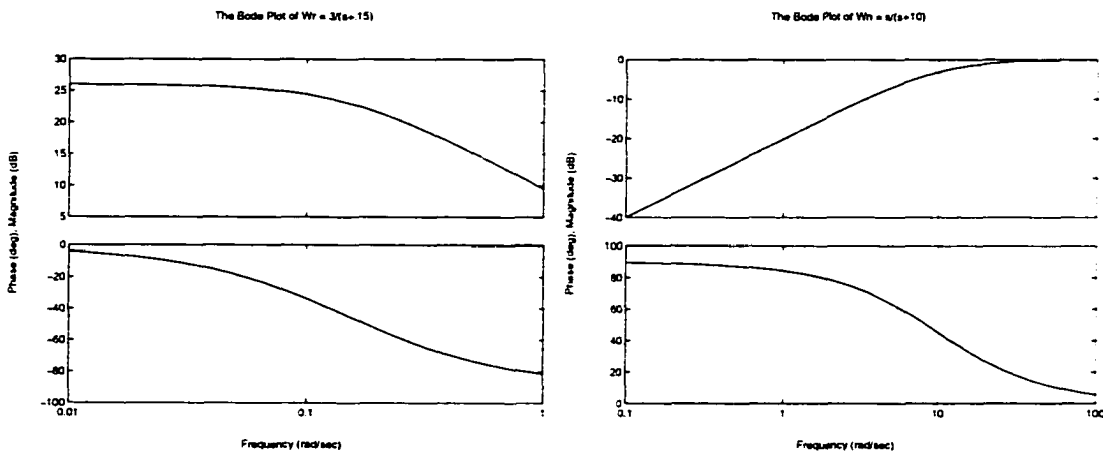


Figure 11.5 The bode plots of weights W_r and W_n

The bode plot of the integrator and servo model together is very close to 1 at the middle frequency range (see Figure 11.6). Therefore, one can even take the integrator and servo model aside at the design stage, and get a simpler system to design and obtain a simpler controller.

Controllers are designed by using this simplified set-up. Simulation results are shown in Appendix B (see Figure B.4 - B.6) for the same models as in set-up I:

1. Low-altitude/low-air-speed at medium weight and middle cg (Case # 1);
2. Middle-altitude/high-air-speed at medium weight and middle cg (Case # 7);

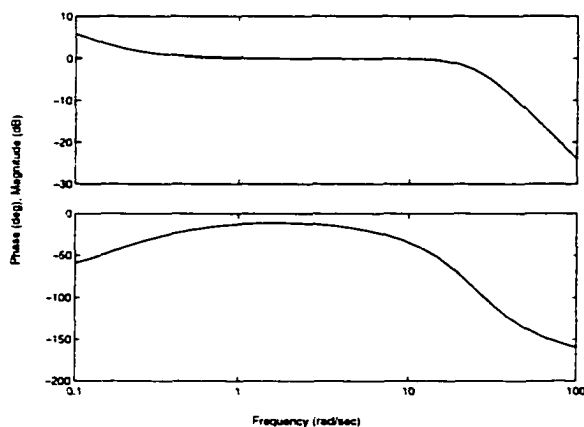


Figure 11.6 The bode plot of Integrator and Servo

3. High-altitude/high-air-speed at medium weight and middle cg (Case # 14).

The resulting controller by this set-up has the order of 6 without model reduction. All performance requirements are satisfied by the design.

11.3 Results

The design of controllers for the chosen nominal models is carried out based on two different system set-ups described as above: the modified model matching and the desired model as the prefilter set-up. From simulation results, it can be seen that the designed controllers work very well for the corresponding nominal models for which they are designed. However, these controllers are not robust and perform poorly against other models under the same flight condition. In the following example, model # 1 (low-altitude/low-air-speed at mid/mid) is chosen as the nominal model. The nominal controller is synthesized by using the modified model matching and prefilter set-ups both. As one can see from Figure 11.7, where the dot lines are the unit step responses of the upper and lower bound systems, the response (solid) for the nominal model is fairly good.

However, if the same controller designed for model #1 is applied to other two models, # 43 (dash) and # 57 (dash-dot), at the same flight condition (low-altitude/low-airspeed), the system responses are not acceptable. For other flight conditions, the situation is even worse. Systems may become unstable when the nominal controller is applied to other models.

This is reasonable because the nominal synthesis does not take model variations into account. The robustness can not be guaranteed by this synthesis. In the following section, the robust control method will be address and the robust controller will be designed against model variations.

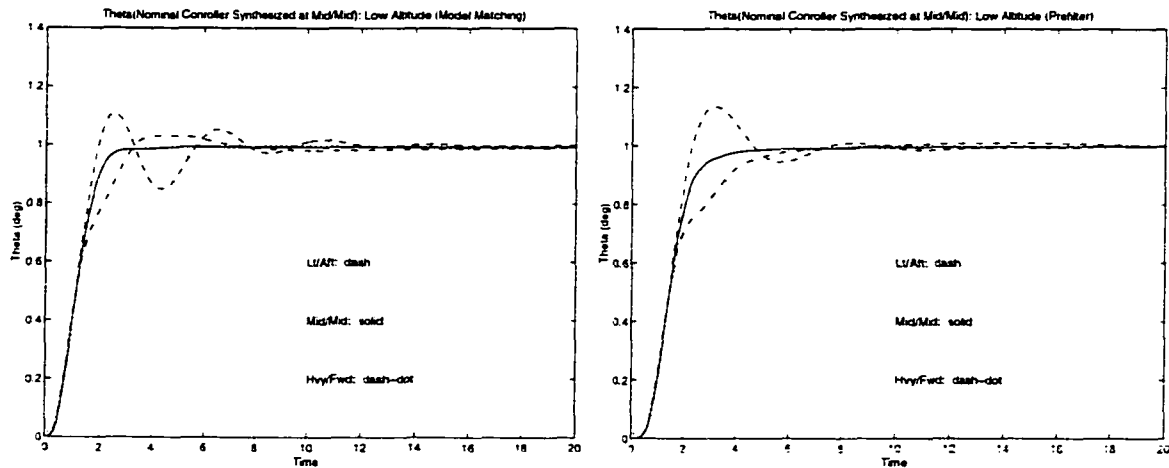


Figure 11.7 Nominal controller: Performance for different models

CHAPTER 12 ROBUST PERFORMANCE

Three different flight conditions at different altitude/airspeed are considered. At each flight condition, the robust controller is designed against the model variations of weight and center of gravity. This will provide guidelines for selecting the initial scheduling control law.

12.1 Parametric Variations of State-Space Model

Because the weight and center of gravity appear in the model as real scalars, variations are modeled as parametric uncertainty. Parameter variations consist of weight (in forms of W and $1/W$), center of gravity (X_{cg}), and moment of inertia ($1/I_{yy}$).

The derivation of the closed-form framework for robustness analysis is given as follows by using Linear Fraction Transformation (LFT). The purpose is to reconstruct the state-space model such that those parameters are considered as uncertainty blocks in the general robust problem set-up. Let ρ_i denote one of the varying parameters described above. A , B , C and D are the state-space matrices for the varying model, which is linearized in ρ_i . The varying linear model can be represented as the follows;

$$\begin{aligned} \left[\begin{array}{c|c} A & B \\ \hline C & D \end{array} \right] &= \left[\begin{array}{c|c} A_0 & B_0 \\ \hline C_0 & D_0 \end{array} \right] + \sum_i \rho_i \left[\begin{array}{c|c} A_i & B_i \\ \hline C_i & D_i \end{array} \right] \\ &= \left[\begin{array}{c|c} A_0 & B_0 \\ \hline C_0 & D_0 \end{array} \right] + W \left[\begin{array}{c|c} A_1 & B_1 \\ \hline C_1 & D_1 \end{array} \right] + 1/W \left[\begin{array}{c|c} A_2 & B_2 \\ \hline C_2 & D_2 \end{array} \right] + \end{aligned}$$

$$+ X_{cg} \begin{bmatrix} A_3 & B_3 \\ C_3 & D_3 \end{bmatrix} + 1/I_{yy} \begin{bmatrix} A_4 & B_4 \\ C_4 & D_4 \end{bmatrix}.$$

Figure 12.1 shows the system variations in A matrix of the state-space model. As one can see from the variable dependence table in Appendix C, most entries of A_i , B_i , C_i and D_i are zeros.

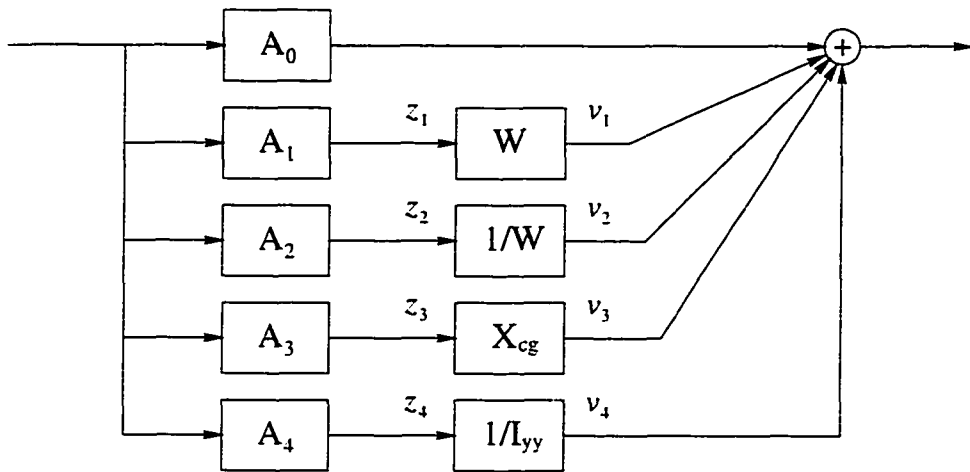


Figure 12.1 System variations (A matrix)

In order to reduce the complicity of this model, those matrices each can be written as the multiplication of two full rank matrices. For example, $[A_1 B_1]$ has rank 3 and can be represented as follows.

$$[A_1 B_1] = \begin{bmatrix} 0 & 0 & 0 & 0 & 0 & 0 \\ 0 & 0 & 0 & 0 & 0 & 0 \\ 0 & a_{32}^1 & 0 & 0 & 0 & 0 \\ a_{41}^1 & 0 & 0 & 0 & 0 & 0 \\ 0 & 0 & a_{53}^1 & 0 & 0 & 0 \end{bmatrix} = \begin{bmatrix} 0 & 0 & 0 \\ 0 & 0 & 0 \\ 1 & 0 & 0 \\ 0 & 1 & 0 \\ 0 & 0 & 1 \end{bmatrix} \begin{bmatrix} 0 & a_{32}^1 & 0 & 0 & 0 & 0 \\ a_{41}^1 & 0 & 0 & 0 & 0 & 0 \\ 0 & 0 & a_{53}^1 & 0 & 0 & 0 \end{bmatrix}$$

$$:= F_1 [G_1 H_1].$$

Therefore, we can rewrite

$$W [A_1 \ B_1] = F_1(W I_3) [G_1 \ H_1].$$

Let F_i, G_i and H_i be the corresponding resulting matrices for $[A_i, B_i]$. Similarly for $[C_i, D_i]$, let E_i be the corresponding matrix similar to F_i . Then, we have

$$\begin{pmatrix} \dot{x} \\ y \end{pmatrix} = \left[\left[\begin{array}{c|c} A_0 & B_0 \\ \hline C_0 & D_0 \end{array} \right] + \sum_i \left[\begin{array}{c} F_i \\ E_i \end{array} \right] \rho_i \left[\begin{array}{c|c} G_i & H_i \end{array} \right] \right] \begin{pmatrix} x \\ u \end{pmatrix}.$$

The purpose to do this rearrangement is to pull out the varying parameters from the system. To do this, we consider v_i and z_i to be the input and output respectively of a linear time-invariant state-space model which has variation ρ_i as the feedback block (may be a matrix) as shown in Figure 12.2. The linear time-invariant model is given by

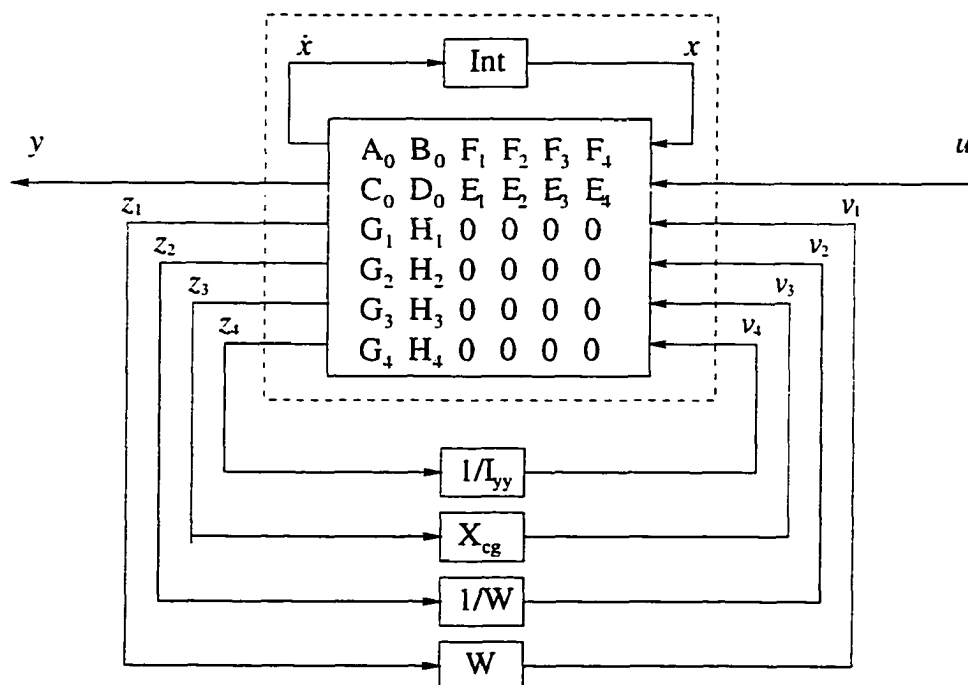


Figure 12.2 An equivalent state-space representation

$$\begin{pmatrix} \dot{x} \\ y \\ z_1 \\ z_2 \\ z_3 \\ z_4 \end{pmatrix} = \begin{bmatrix} A_0 & B_0 & F_1 & F_2 & F_3 & F_4 \\ C_0 & D_0 & E_1 & E_2 & E_3 & E_4 \\ G_1 & H_1 & 0 & 0 & 0 & 0 \\ G_2 & H_2 & 0 & 0 & 0 & 0 \\ G_3 & H_3 & 0 & 0 & 0 & 0 \\ G_4 & H_4 & 0 & 0 & 0 & 0 \end{bmatrix} \begin{pmatrix} x \\ u \\ v_1 \\ v_2 \\ v_3 \\ v_4 \end{pmatrix}$$

In the following, we will use Linear Fraction Transformation to rewrite the structure of the variation blocks. This may be done for various reasons:

1. To normalize the parameter variation:
2. To express $1/W$ in terms of δ_w ;
3. To express $1/I_{yy}$ in terms of $\delta_{I_{yy}}$.

The parameter ρ_i is considered as a variation around its nominal value ρ_{i_0} and the variation is scaled to unity δ_i by the factor K_i . Let $\rho_i = \rho_{i_0} + K_i \delta_i$, where $|\delta_i| = 1$.

In our case, parameter variations appear both in the form of ρ_i and $1/\rho_i$. As shown in Figure 12.3, using Linear Fraction Transformation, we can express the parameter ρ_i and $1/\rho_i$ in the form of unity parameter δ_i .

Figure 12.4 shows the overall rearrangement of the state-space model which combines the above two steps.

In this case, we need to rewrite our equations in terms of v'_i and z'_i . J_{nm}^i denotes the nm th block of the transfer matrix J^i in Figure 12.3.

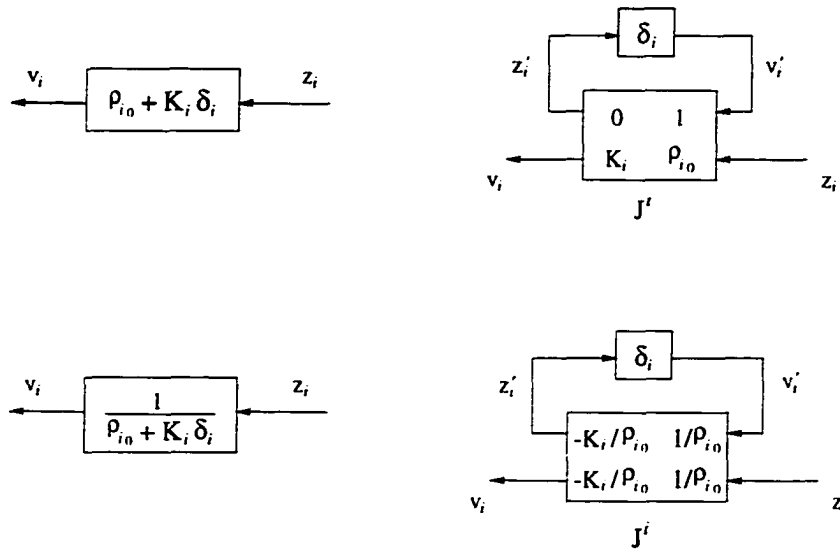


Figure 12.3 Linear fraction transformation

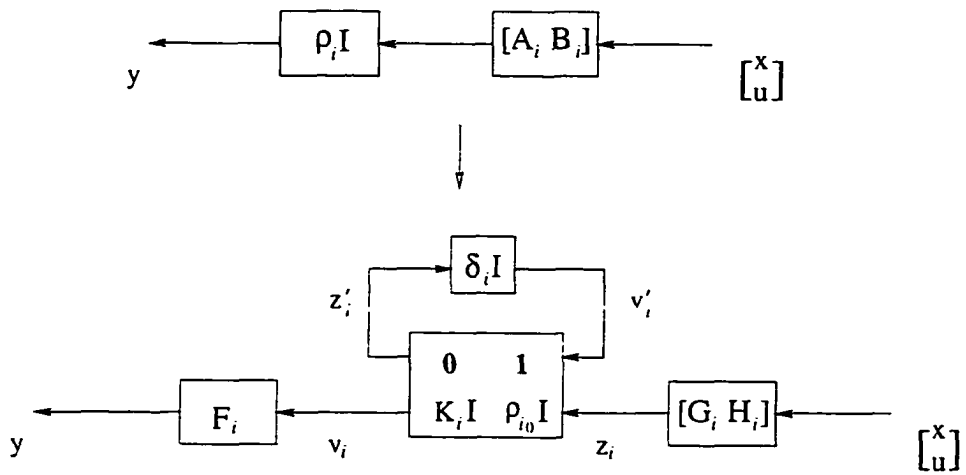


Figure 12.4 LFT modeling for parameter variations

Then the overall system is given as follows:

$$\begin{pmatrix} \dot{x} \\ y \\ z'_1 \\ z'_2 \\ z'_3 \\ z'_4 \end{pmatrix} = \begin{bmatrix} A_0 + \sum_{i=1}^4 F_i J_{22}^i H_i & B_0 + \sum_{i=1}^4 F_i J_{22}^i G_i & F_1 J_{21}^1 & F_2 J_{21}^2 & F_3 J_{21}^3 & F_4 J_{21}^4 \\ C_0 & D_0 & E_1 & E_2 & E_3 & E_4 \\ J_{12}^1 G_1 & J_{12}^1 H_1 & J_{11}^1 & 0 & 0 & 0 \\ J_{12}^2 G_2 & J_{12}^2 H_2 & 0 & J_{11}^2 & 0 & 0 \\ J_{12}^3 G_3 & J_{12}^3 H_3 & 0 & 0 & J_{11}^3 & 0 \\ J_{12}^4 G_4 & J_{12}^4 H_4 & 0 & 0 & 0 & J_{11}^4 \end{bmatrix} \begin{pmatrix} x \\ u \\ v'_1 \\ v'_2 \\ v'_3 \\ v'_4 \end{pmatrix}$$

The controller designed later using multiplicative uncertainty model will be evaluated with this parametric model in the μ -analysis. For the analysis purpose, the structure singular value is computed, where the δ_w uncertainty is treated as repeated 1×1 blocks and $\delta_{x_{cg}}$, $\delta_{I_{yy}}$ as complex scalars.

12.2 Plant Variation in Frequency Domain Set-Up

An alternative treatment of system uncertainty is the multiplicative model. In this set-up, the uncertainty is treated as a multiplicative one, i.e.,

$$G_i(s) = [I + \Delta W_{add}(s)] G_0(s), \quad (12.1)$$

where G_0 is the nominal model, G_i 's are all the possible models in the same flight condition (altitude/airspeed). In the following design, the medium weight at middle cg models, which are the middle plots (dash) in Figure 12.5, are chosen as the nominal models G_0 for each of three flight conditions.

The uncertainty Δ is set to have norm of 1. In this way, the corresponding magnitude of weight on the uncertainty can be obtained by

$$|W_{add}(j\omega)| = \max_i \left| \frac{G_i(j\omega) - G_0(j\omega)}{G_0(j\omega)} \right|, \quad (12.2)$$

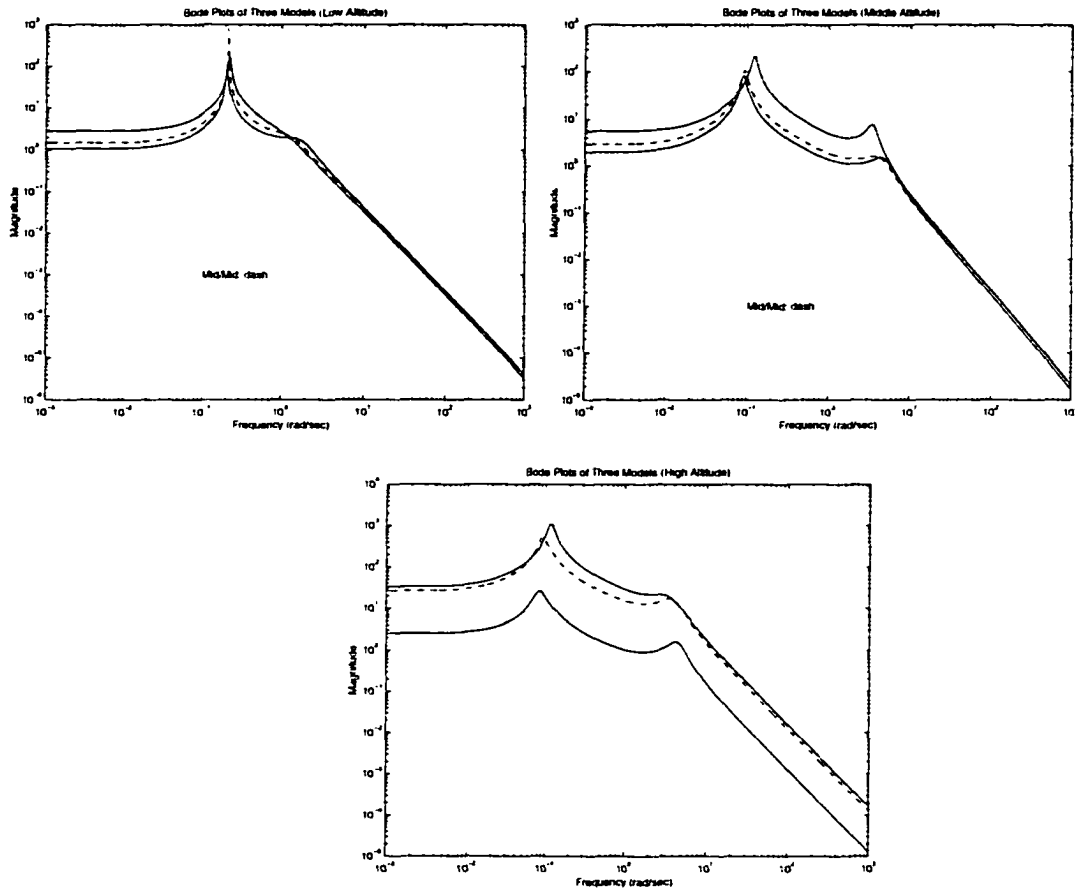


Figure 12.5 Bode plots of three models for three flight conditions

which is computed point by point in the frequency domain. Using “fitmag” routine in MATLAB, one can choose the order of the fitting function for the magnitude data and get a stable minimum phase transfer function from the obtained data. The following weighting transfer functions are obtained for the three different flight conditions. See Appendix D for bode plots.

1. Low altitude:

$$\frac{0.1713s^6 + 1.1877s^5 + 1.6825s^4 + 1.2084s^3 + 0.1471s^2 + 0.0444s + 0.0020}{s^6 + 2.4472s^5 + 3.2401s^4 + 1.4224s^3 + 0.2243s^2 + 0.0606s + 0.0022}$$

2. Middle altitude:

$$\frac{0.2786s^6 + 3.8195s^5 + 17.8112s^4 + 32.3562s^3 + 1.2459s^2 + 0.1670s + 0.0038}{s^6 + 2.6260s^5 + 13.4042s^4 + 19.2241s^3 + 0.8423s^2 + 0.2808s + 0.0042}$$

3. High altitude:

$$\frac{0.9036s^3 + 0.3521s^2 + 0.0241s + 0.0028}{s^3 + 0.2424s^2 + 0.0180s + 0.0030}$$

This uncertainty model is used in the following design set-up for robust synthesis.

The set-up for robust design follows the prefilter set-up discussed in the nominal performance case (see Figure 12.6). As in the case of the nominal design, the gain of the

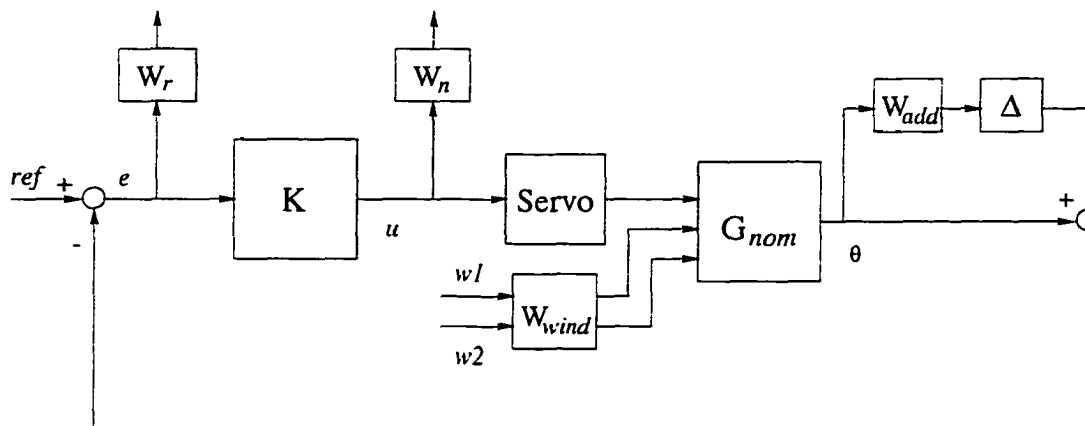


Figure 12.6 Set-up for robust synthesis: Multiplicative uncertainty

feedback control path for N_z , if it is considered as a feedback control signal, is very small. Therefore, the set-up without N_z feedback is used later for robust synthesis. The performance measurement includes:

1. The error between the output θ , the pitch angle, of the system and the reference command. A low pass weight $W_r \left(\frac{3}{s+0.15} \right)$ is chosen to ensure the steady-state error to be satisfied:

2. The controller output u . A weight $W_n \left(\frac{s}{s+10} \right)$ is introduced to penalize the crossover frequency:
3. The system output θ . The weight, W_{add} , for uncertainty is used.

Notice that the third model (Hvy/Fwd) at high altitude is relatively far away from the other two models (see Figure 12.5). Therefore, the size of the system uncertainty is relatively large in this case. As one can see from the simulation results (Figure 12.7), the robust performance at high altitude is not as good as that at other two flight conditions. The reason is that the open-loop system needs to have relatively large gain at low fre-

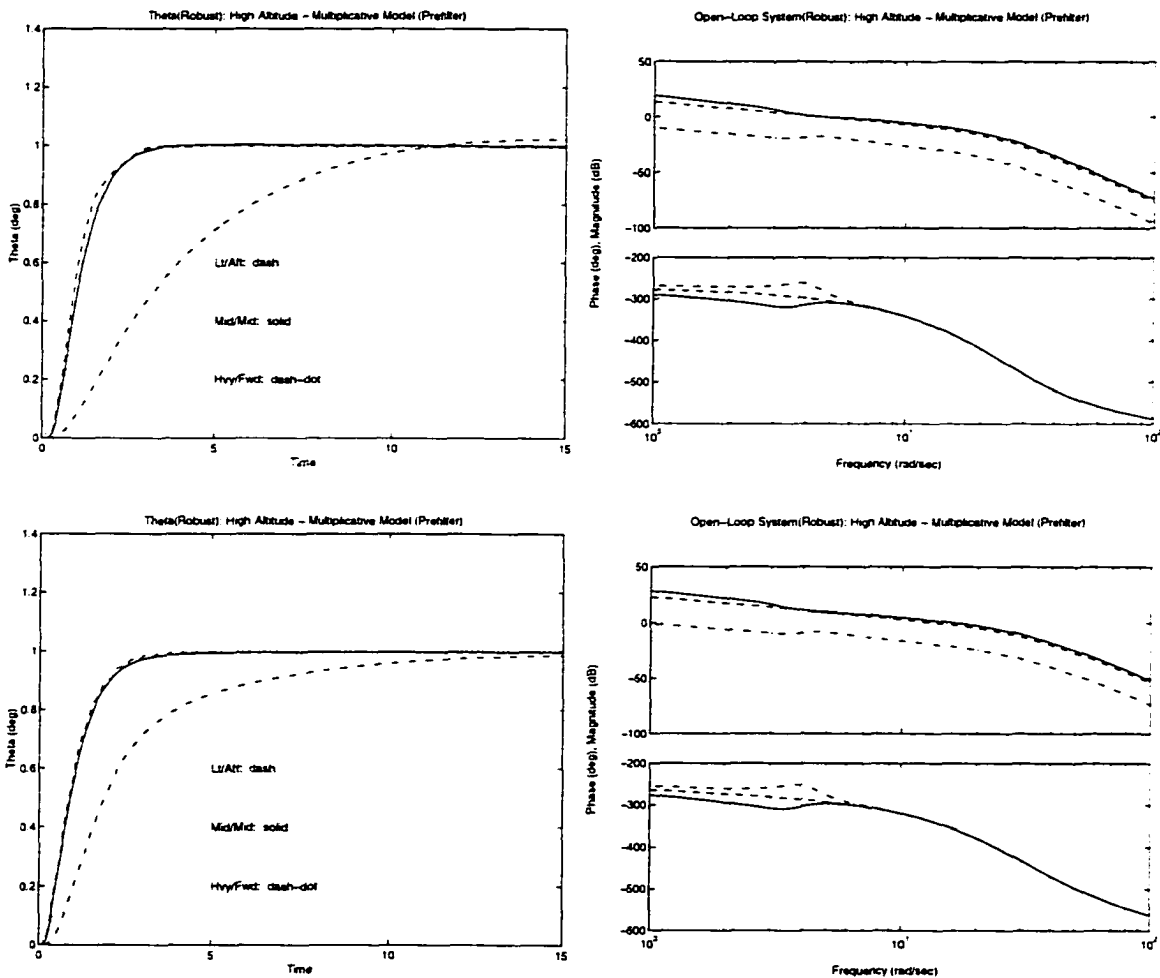


Figure 12.7 Crossover vs. performance (high-altitude/high-airspeed)

quency for the third model (Hvy/Fwd) in order to satisfy the tracking performance requirement. However, for other two models, this will result in a larger crossover frequency which exceeds the limit. See simulation results in Figure 12.7. The first two show the designed controller meets the crossover frequency requirement for all models, but the performance for the third model (Hvy/Fwd) is not as good as the second case, which allows higher crossover frequency. Any improvement in the design for the third model (Hvy/Fwd) will result in the increase of the crossover frequency. This design limitation is because the third model is far away from the other two.

See Appendix E for all simulation results. Two singular value plots are shown for each case. The left bottom one is the μ plot for the multiplicative uncertainty model (synthesis model). The right bottom one is for the parametric model with the same controller designed using multiplicative model.

As one can see from the simulation result in Figure E.4 of Appendix E, the robust controllers (higher than 10th order) can be reduced to 5th order controllers and can still work fairly well.

12.3 Robust Design vs. Nominal Design

The robust stability and performance with variations of weight and center of gravity can be achieved by robust controller design in the same flight condition, which is not true for nominal controller design. The comparison of robust controller and nominal controller is shown in Figure 12.8. For low-altitude/low-air-speed flight condition, plots of system responses are shown for robust controller, nominal controller using modified model matching set-up and controller using prefilter set-up respectively.

One can see that robust controller outperforms the nominal controller. For the middle-altitude/high-air-speed case, systems even become unstable when the designed nominal controller is applied to other two models in the same flight condition.

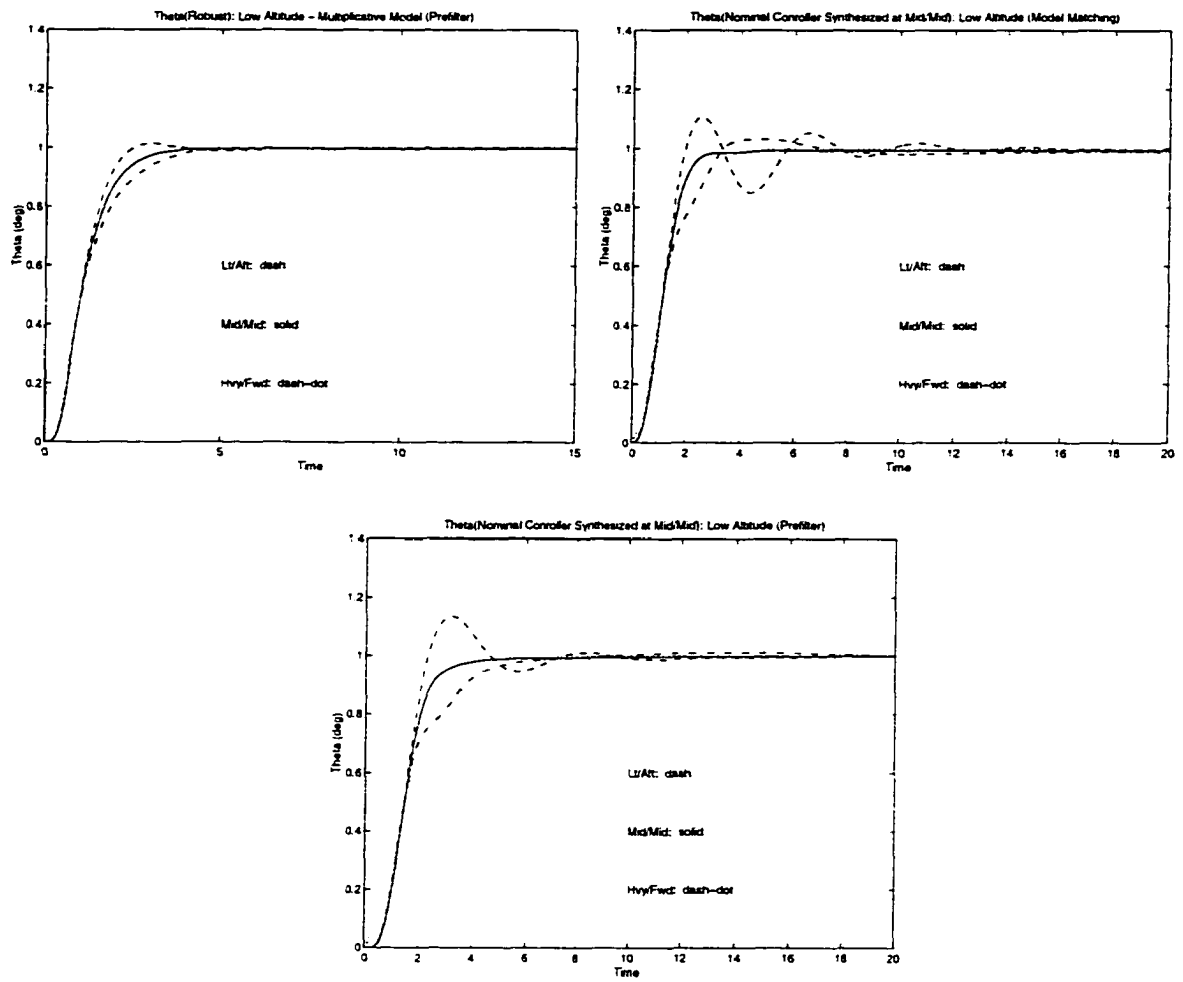


Figure 12.8 Robust controller vs. nominal controller (low-altitude/low-airspeed)

CHAPTER 13 CONCLUSIONS

The aircraft dynamics has been discussed. The nominal \mathcal{H}_∞ controller design is addressed first. Two synthesis set-ups have been compared. For the model matching approach, the problem needs to be set up properly to avoid obtaining an almost open-loop controller.

Due to variations of weight and center of gravity in the aircraft model, robust controller is needed to consider those variations. A multiplicative uncertainty model for different flight conditions (three different altitudes/airspeeds) is derived for robust synthesis. The robust controller is synthesized using MATLAB μ toolbox for each flight conditions. The resulting controller provides good robust performance against the system variations. Future work need to be done on gain scheduling to handle the variation due to different flight conditions.

CHAPTER 14 GENERAL CONCLUSIONS

Two robustness issues have been addressed in this dissertation: robust steady-state tracking for sampled-data systems and robust aircraft pitch control

Two different steady-state norms are defined as the robust performance measures for steady-state tracking. Robust steady-state tracking problem is explored by first solving robust steady-state tracking for periodic discrete-time systems. Then by using the lifting technique for periodic systems and using an approximation approach, exact conditions for sampled-data systems are found in the form of spectral radius of so-called steady-state norm matrix. This nonnegative matrix is defined on the system induced norms and the corresponding steady-state norms. A computation algorithm is given by a converging approximation procedure. As one possible future work, the tools of \mathcal{L}_1/l_1 controller design and robust steady-state tracking performance analysis can be combined as an analysis and synthesis tool for the robust steady-state tracking problem. The robust steady-state tracking conditions developed in this dissertation are given as the spectral radius of certain nonnegative matrix, which consists of system induced norms. The spectral radius of the nonnegative matrix is a monotonic function of the elements in the matrix. These elements, induced norms and steady-state semi-norms, can be minimized by the \mathcal{L}_1/l_1 controller design.

In the second part, aircraft models with parametric variations of weight and center of gravity are discussed and used for robust analysis. A multiplicative uncertainty model is derived and adopted as the synthesis set-up for the \mathcal{H}_∞ control design by using the powerful MATLAB μ -analysis and synthesis toolbox.

In general, when considering a model matching problem, we should carefully set up the problem, especially when all the zeros of the plant are stable zeros. For the nominal set-up I in Figure 11.1, the controller can simply be designed as an open-loop compensator, which consists of the desired model and the inverse of the plant. Though performance criteria can be achieved by this design for the specific model, it is not a useful design. Some changes in the nominal plant will result in bad responses because this design is not robust at all.

As part of the design criteria, an elevator deflection limit of ± 5 degrees is imposed on the output of the actuator, and the normal acceleration, the third output N_z , shall not exceed 0.4 G. These requirements can easily be achieved. The output N_z , as a feedback measurement, does not play an effective role in system controlling. Therefore, we do not need to take N_z as the feedback measurement.

In each flight condition, aircraft is controlled by one robust controller. Gain scheduling should be developed only for variations due to different flight conditions. For the high altitude case, due to the system variations and performance criteria limitation, one controller can not achieve the control task. In order to achieve better performance for the third model (Hvy/Fwd), we need to make a large gain of the open-loop system at low frequency. However, for the other two models, this will result in a larger crossover frequency which exceeds the limit. This is the tradeoff we have to deal with between system performance and system crossover frequency.

APPENDIX A SET-UP: DISCUSSION AND ANALYSIS

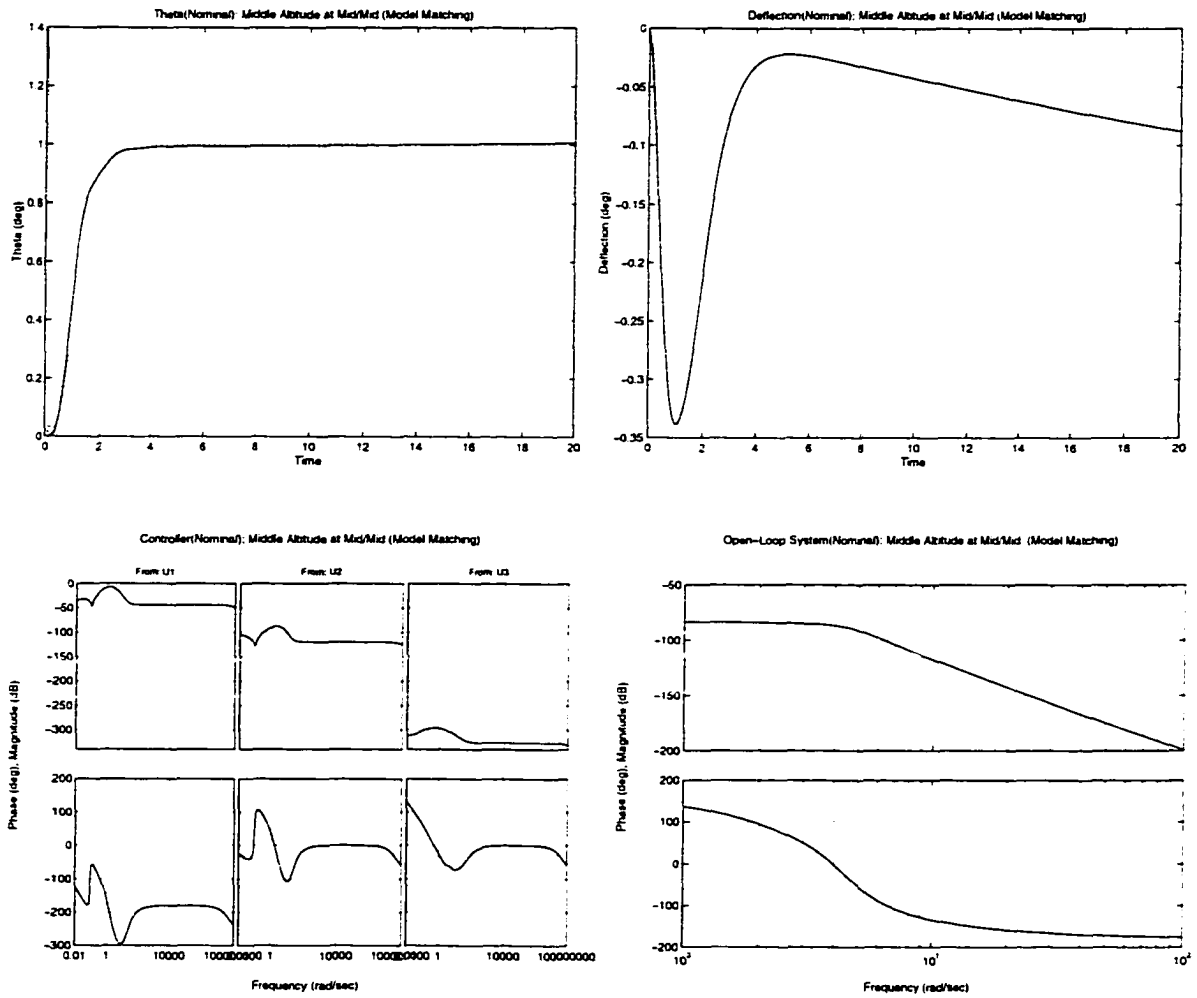


Figure A.1 Model matching I: Small controller in feedback path

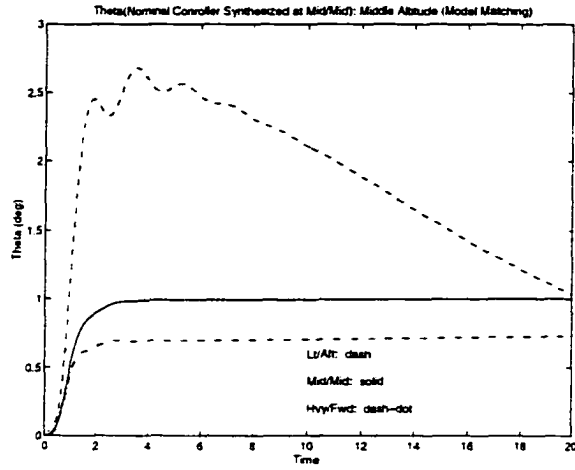


Figure A.2 Nominal controller (synthesized at Mid/Mid) vs. different models (Hvy/Fwd & Lt/Aft)

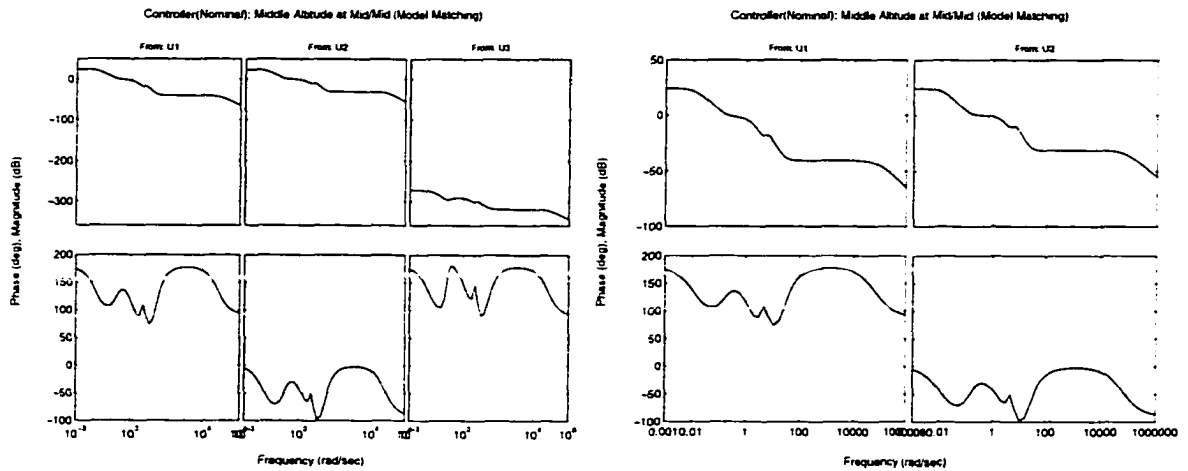


Figure A.3 Feedback control with N_2 vs. without N_2 (case #7)

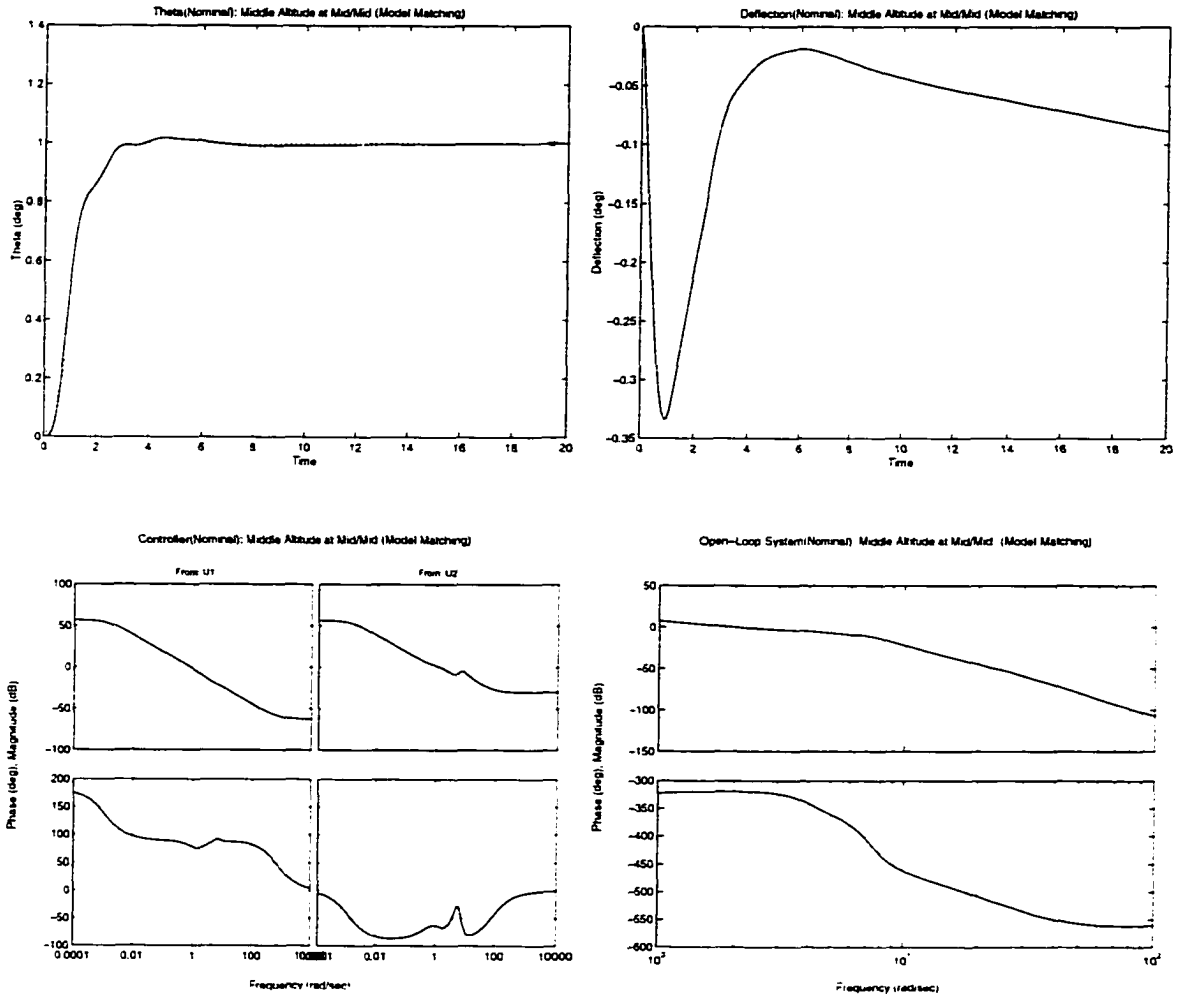


Figure A.4 Reduced 6th order controller (case #1)

APPENDIX B NOMINAL PERFORMANCE

Modified model matching set-up: low-altitude/low-airspeed at Mid/Mid (#1)

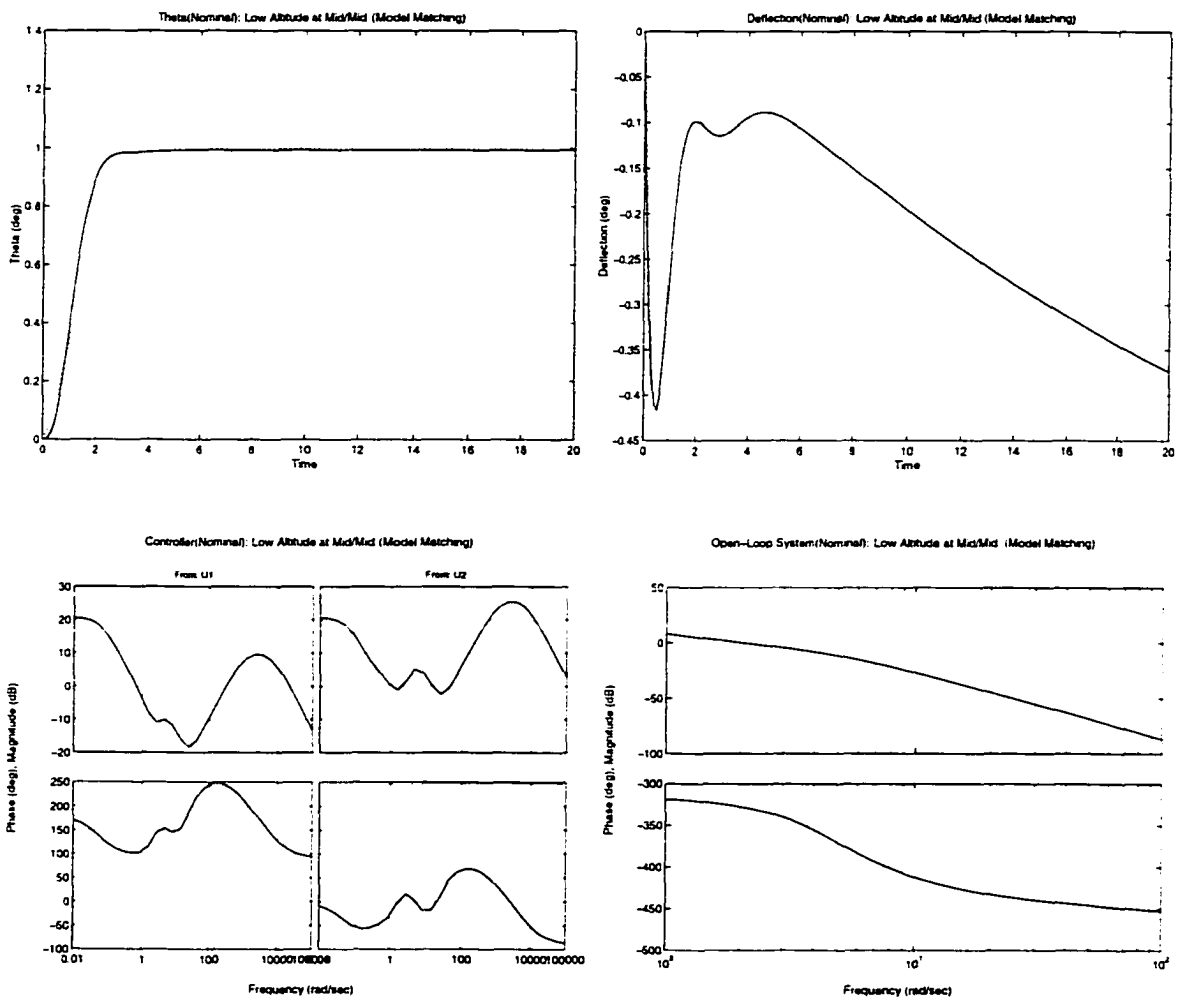


Figure B.1 Nominal case: Modified model matching (case #1)

The state-space representation (K_A, K_B, K_C, K_D) of the designed controller K at Low Altitude/Airspeed (Mid/Mid #1):

$K_A =$

Columns 1 through 6

-4.4753e-01	-2.9494e+03	-2.5804e+06	8.3018e+05	3.0491e+05	4.6724e+02
-6.8797e-01	-7.2595e+03	-6.3212e+06	2.0334e+06	7.4686e+05	1.1445e+03
0	1.0000e+00	1.9232e-04	2.5723e-02	0	0
0	3.5887e-04	-4.1243e-05	-2.1243e+00	1.0000e+00	0
0	6.6729e-03	-3.6926e+01	-2.2556e+00	-6.0158e-01	6.0802e-03
0	-3.9400e-03	2.6572e+00	1.0905e+01	-9.9291e+00	-7.1859e-03
0	2.9861e-02	-4.5622e+01	-9.2047e+01	6.0963e+01	-1.6270e-01
0	0	0	0	0	0
0	0	0	0	0	0
0	3.2139e-05	-2.6992e-03	2.9922e+00	0	0

Columns 7 through 10

-1.6253e+03	1.0822e+04	-1.9650e+02	1.5470e+04
-3.9812e+03	2.6508e+04	-4.8134e+02	3.7894e+04
0	-7.7126e-19	7.7126e-19	-6.9100e-07
0	1.5080e-17	-1.5080e-17	2.2289e-05
-2.3172e-02	1.6330e-16	-1.6330e-16	-1.8510e-06
2.0715e-01	-4.5247e-16	4.5247e-16	-2.9498e-03
-9.2092e-01	3.5291e-17	-3.5291e-17	4.9745e-04
0	-5.8579e-01	1.4142e+00	0
0	-1.4142e+00	-3.4142e+00	0
0	8.4090e-01	-8.4090e-01	-3.4004e-02

$K_B =$

0	-4.3254e+00	
0	3.3059e-02	
0	-3.7993e-03	
0	3.1375e-01	
0	3.3315e-01	
0	-3.0407e+00	
0	1.3365e+01	
-7.1160e+00		0
-7.1160e+00		0
0	8.0205e+00	

 $K_C =$

Columns 1 through 6

-1.2954e-01	-8.5373e+02	-7.4690e+05	2.4029e+05	8.8257e+04	1.3525e+02
-------------	-------------	-------------	------------	------------	------------

Columns 7 through 10

-4.7045e+02	3.1324e+03	-5.6879e+01	4.4779e+03
-------------	------------	-------------	------------

 $K_D =$

0	0
---	---

Modified model matching set-up: middle-altitude/high-airspeed at Mid/Mid (#7)

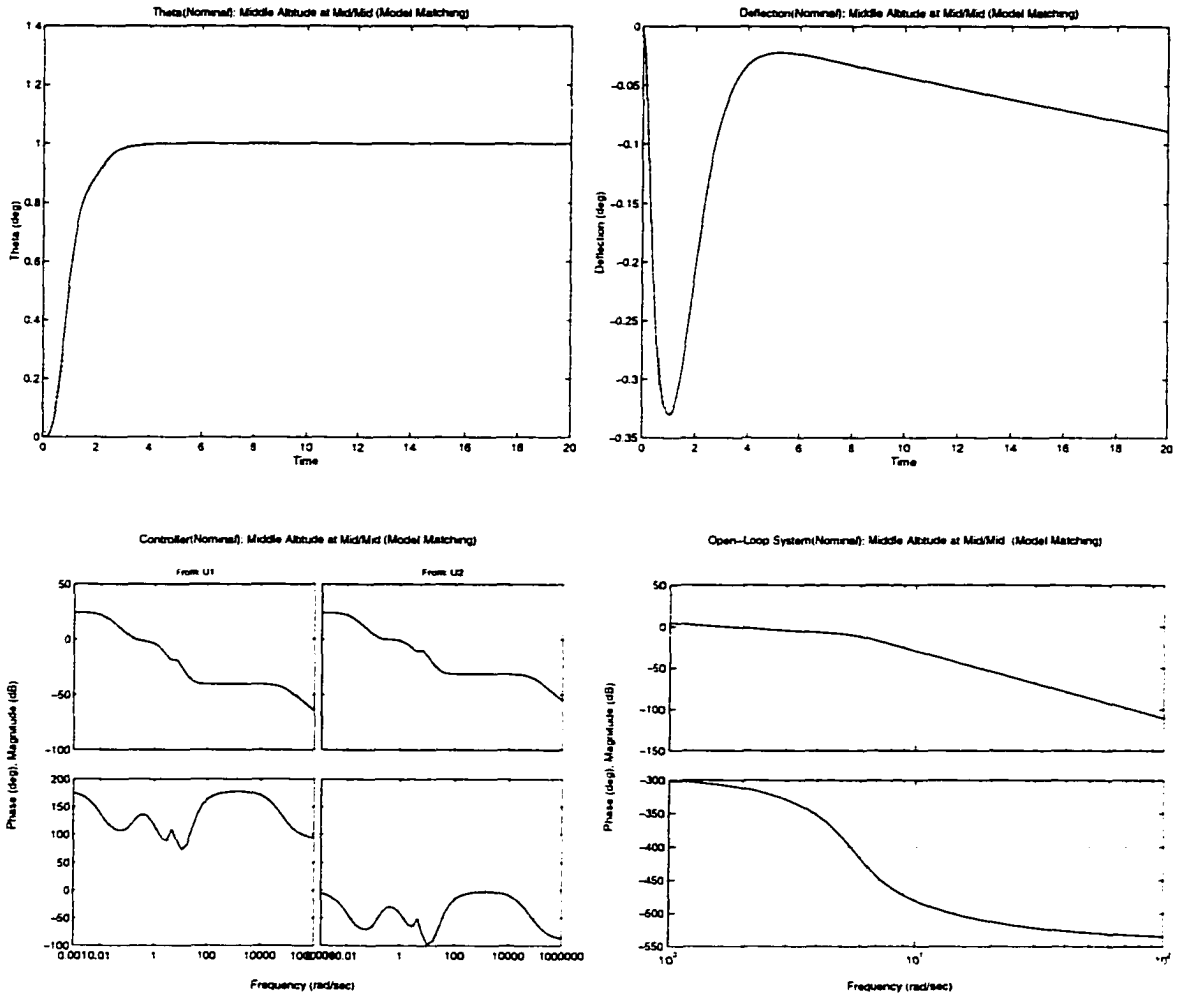


Figure B.2 Nominal case: Modified model matching (case #7)

The state-space representation (K_A, K_B, K_C, K_D) of the designed controller K at Middle Altitude/Airspeed (Mid/Mid #7):

$K_A =$

Columns 1 through 6

-1.6727e-01	-2.5407e+03	-2.0689e+04	2.3807e+03	3.7808e+02	6.0213e-01
-1.4871e-03	-6.2582e+03	-5.1303e+04	5.7586e+03	9.2610e+02	1.4749e+00
0	1.0000e+00	3.5692e-04	5.1374e-02	0	0
0	3.0360e-03	-1.5281e-04	-3.7158e+00	1.0000e+00	0
0	5.6994e-02	-1.8081e+02	-6.9008e+00	-1.0736e+00	3.8751e-03
0	-5.7454e-03	-1.9425e+00	4.3171e+00	-2.2673e+00	-1.3574e-02
0	5.9038e-01	-2.3218e+02	-4.6677e+02	1.7403e+02	-9.3563e-02
0	0	0	0	0	0
0	0	0	0	0	0
0	6.9606e-06	-5.2325e-03	5.3547e-02	0	0

Columns 7 through 10

-8.4720e+00	3.3016e+01	-3.8808e+00	5.9351e+01
-2.0752e+01	8.0871e+01	-9.5059e+00	1.4539e+02
0	4.4704e-19	-4.4704e-19	-1.3395e-06
0	-1.2925e-17	1.2925e-17	4.3586e-05
-9.2822e-02	-6.6294e-17	6.6294e-17	-1.2598e-07
4.0667e-02	-2.2074e-16	2.2074e-16	-2.5572e-02
-1.7426e+00	-4.2864e-15	4.2864e-15	1.5461e-03
0	-5.8579e-01	1.4142e+00	0
0	-1.4142e+00	-3.4142e+00	0
0	8.4090e-01	-8.4090e-01	-5.9040e-04

$K_B =$

0	-4.3325e+00
0	1.5076e-01
0	-7.5878e-03
0	5.4881e-01
0	1.0192e+00
0	-2.0860e+00
0	6.8922e+01
-7.1160e+00	0
-7.1160e+00	0
0	8.4545e+00

 $K_C =$

Columns 1 through 6

-4.8418e-02	-7.3542e+02	-5.9885e+03	6.8061e+02	1.0944e+02	1.7429e-01
-------------	-------------	-------------	------------	------------	------------

Columns 7 through 10

-2.4523e+00	9.5565e+00	-1.1233e+00	1.7180e+01
-------------	------------	-------------	------------

 $K_D =$

0	0
---	---

Modified model matching set-up: high-altitude/high-airspeed at Mid/Mid (#14)

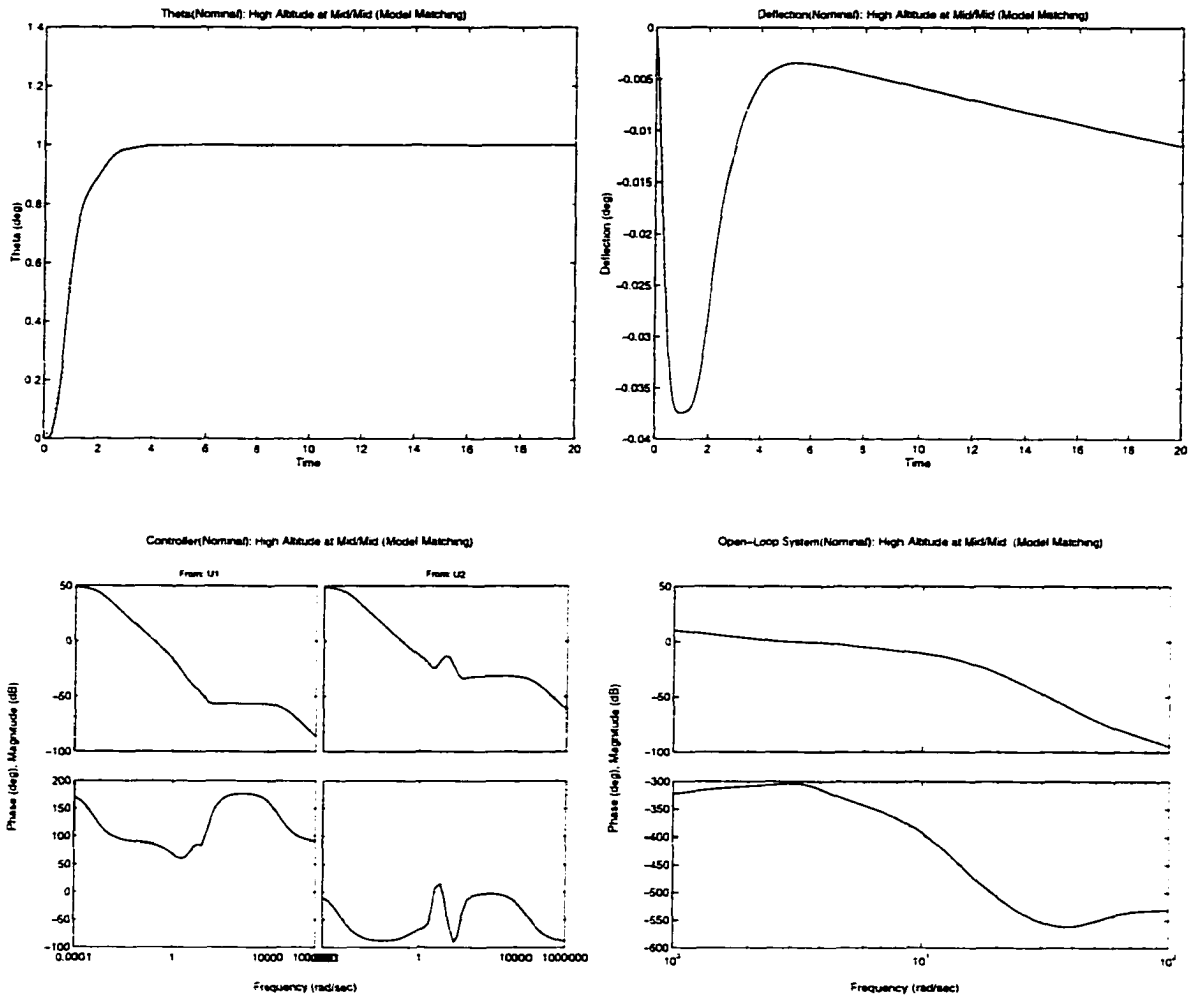


Figure B.3 Nominal case: Modified model matching (case #14)

The state-space representation (K_A, K_B, K_C, K_D) of the designed controller K at High Altitude/Airspeed (Mid/Mid #14):

$K_A =$

Columns 1 through 6

-1.6677e-01	-1.2749e+04	-1.2312e+05	1.9308e+03	3.5925e+02	4.7815e-01
-2.5463e-04	-3.1259e+04	-3.0221e+05	4.6525e+03	8.7998e+02	1.1712e+00
0	1.0013e+00	3.8648e-04	1.8435e-01	0	0
0	4.0256e-01	-5.4833e-04	-1.6370e+01	1.0000e+00	0
0	1.0627e+01	-1.3552e+03	-1.3289e+02	-6.9723e-01	4.4633e-03
0	-1.4524e+00	-3.9082e+00	5.7685e+01	-3.6938e+00	-1.8661e-02
0	9.4188e+01	-1.7455e+02	-3.4951e+03	2.3114e+02	-1.1177e-01
0	0	0	0	0	0
0	0	0	0	0	0
0	7.7726e-05	-5.6894e-04	5.8929e-03	0	0

Columns 7 through 10

-4.5674e+00	2.7295e+01	-4.5565e+00	5.4370e+01
-1.1188e+01	6.6859e+01	-1.1161e+01	1.3318e+02
0	-3.1855e-19	3.1855e-19	-1.4565e-07
0	9.4752e-19	-9.4752e-19	4.3623e-05
-5.9996e-02	-1.6663e-17	1.6663e-17	-4.7922e-08
1.0575e-02	-5.9145e-16	5.9145e-16	-2.1247e-02
-1.3938e+00	-1.5016e-15	1.5016e-15	1.7199e-03
0	-5.8579e-01	1.4142e+00	0
0	-1.4142e+00	-3.4142e+00	0
0	8.4090e-01	-8.4090e-01	-5.9442e-04

$K_B =$

0	-4.3242e+00
0	7.9960e-01
0	-2.7228e-02
0	2.4177e+00
0	1.9628e+01
0	-9.9682e+00
0	5.1619e+02
-7.1160e+00	0
-7.1160e+00	0
0	8.4616e+00

 $K_C =$

Columns 1 through 6

-4.8273e-02	-3.6905e+03	-3.5638e+04	5.5042e+02	1.0399e+02	1.3840e-01
-------------	-------------	-------------	------------	------------	------------

Columns 7 through 10

-1.3220e+00	7.9007e+00	-1.3189e+00	1.5738e+01
-------------	------------	-------------	------------

 $K_D =$

0	0
---	---

Prefilter Set-Up: low-altitude/low-airspeed Mid/Mid (#1)

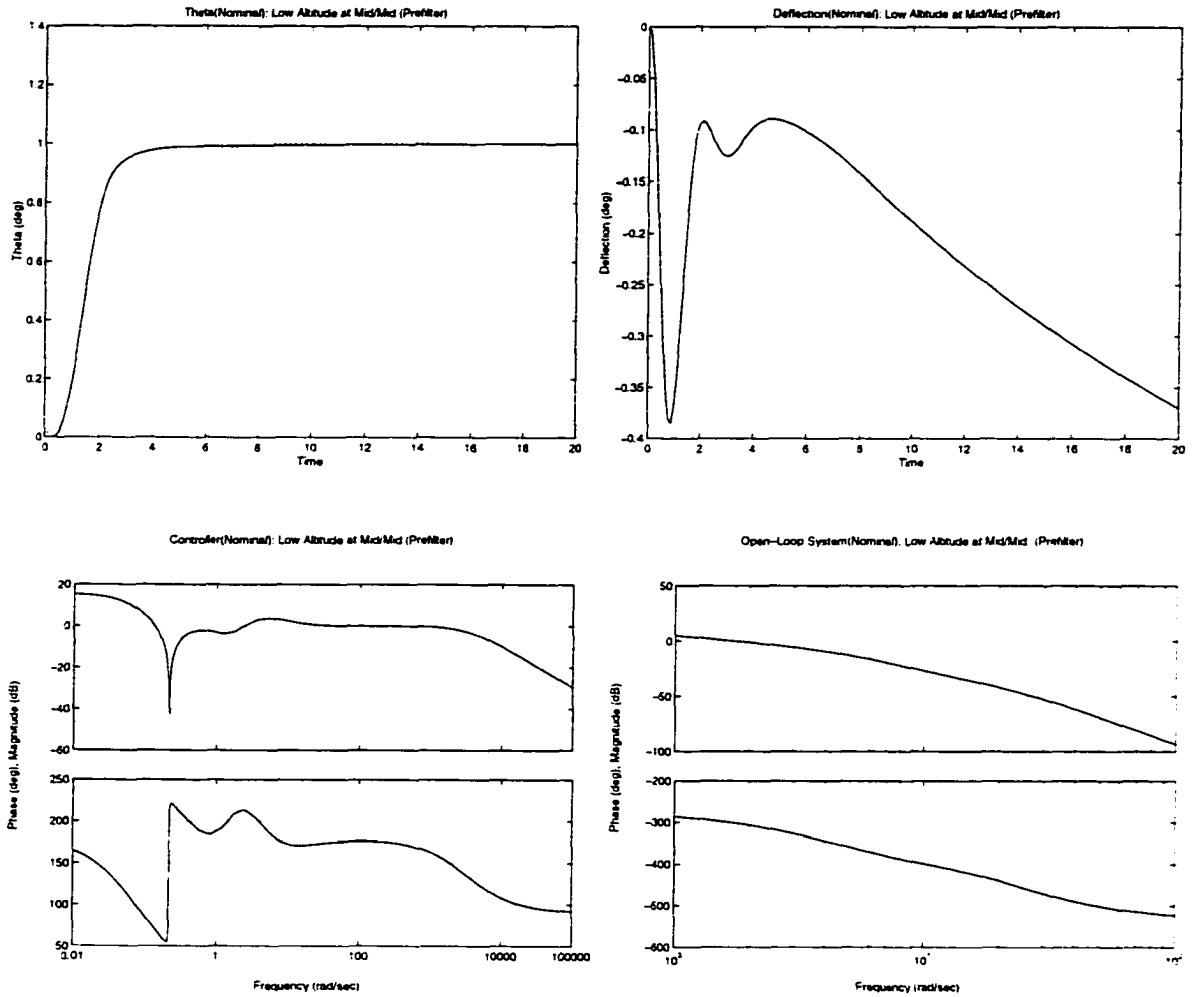


Figure B.4 Nominal case: Prefilter set-up (case #1)

The state-space representation (K_A, K_B, K_C, K_D) of the designed controller K at Low Altitude/Airspeed (Mid/Mid #1):

$K_A =$

0	1.0000e+00	0	0	0	0
-6.3101e+03	-1.5442e+03	-1.0152e+00	4.4108e+00	9.8324e+01	1.0415e+01
4.4425e+02	1.0111e+02	6.6284e-02	-1.1181e-01	-7.0731e+00	-7.4925e-01
-7.7972e+03	-1.8460e+03	-1.4244e+00	4.5569e+00	1.2147e+02	1.2867e+01
0	0	0	0	-2.0000e-01	0
1.0680e+06	2.6126e+05	1.7286e+02	-7.5048e+02	-1.6642e+04	-1.7729e+03

$K_B =$

0
0
0
0
4.7873e+00
0

$K_C =$

4.4619e+04	1.0915e+04	7.2217e+00	-3.1353e+01	-6.9526e+02	-7.3648e+01
------------	------------	------------	-------------	-------------	-------------

$K_D =$

0

Prefilter Set-Up: middle-altitude/high-airspeed Mid/Mid (#7)

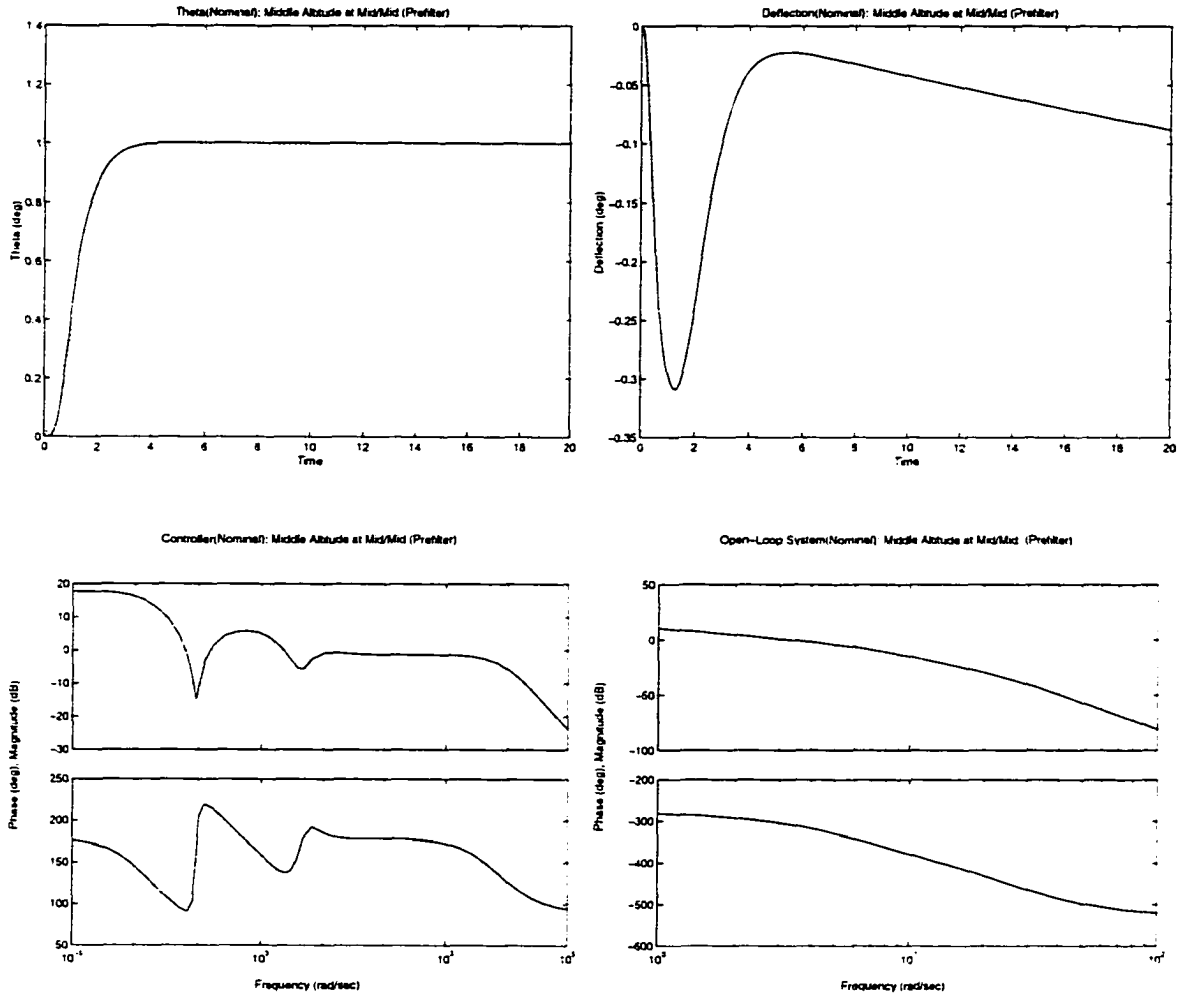


Figure B.5 Nominal case: Prefilter set-up (case #7)

The state-space representation $(\bar{K}_A, \bar{K}_B, \bar{K}_C, \bar{K}_D)$ of the designed controller \bar{K} at Middle Altitude/Airspeed (Mid/Mid #7):

$\bar{K}_A =$

0	1.0000e+00	0	0	0	0
-3.1948e+04	-4.3631e+03	-1.0197e+00	3.2349e+01	6.1935e+02	9.0668e+01
-3.5392e+02	-4.9252e+01	-2.4600e-02	3.9011e-01	6.6712e+00	9.7661e-01
-4.1021e+04	-5.4268e+03	-1.4079e+00	3.9913e+01	7.9526e+02	1.1642e+02
-2.8422e-14	0	0	0	-1.5000e-01	0
1.1044e+06	1.5079e+05	3.5383e+01	-1.1215e+03	-2.1410e+04	-3.1442e+03

$\bar{K}_B =$

0
0
0
0
7.1810e+00

0

$\bar{K}_C =$

4.6137e+04	6.2994e+03	1.4782e+00	-4.6851e+01	-8.9444e+02	-1.3094e+02
------------	------------	------------	-------------	-------------	-------------

$\bar{K}_D =$

0

Prefilter Set-Up: high-altitude/high-air-speed Mid/Mid (#14)

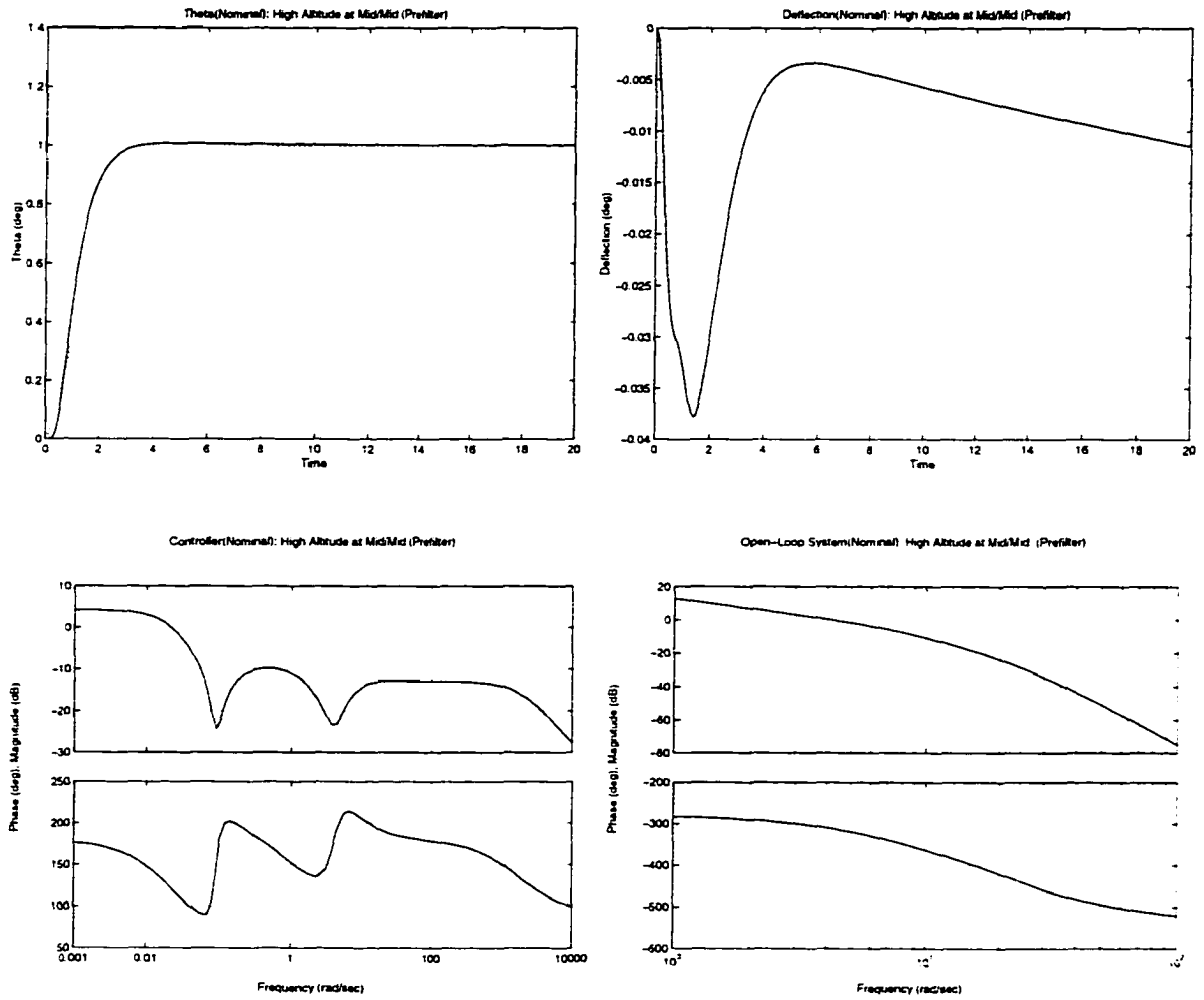


Figure B.6 Nominal case: Prefilter set-up (case #14)

The state-space representation (K_A, K_B, K_C, K_D) of the designed controller K at High Altitude/Airspeed (Mid/Mid #14):

$K_A =$

0	1.0000e+00	0	0	0	0
-1.1891e+04	-1.3016e+03	-2.0151e-01	3.5329e+00	8.9473e+02	1.1331e+02
-4.4119e+01	-7.4478e+00	-1.9256e-02	2.0943e-02	2.5819e+00	3.2697e-01
-1.5306e+03	6.3707e+01	-1.3828e-01	-9.3135e-01	1.1516e+02	1.4583e+01
0	0	0	0	-1.0000e-01	0
5.4842e+04	5.9997e+03	9.4997e-01	-1.6570e+01	-4.1265e+03	-5.3258e+02

$K_B =$

0
0
0
0
2.3937e+00
0

$K_C =$

2.2911e+03	2.5065e+02	3.9687e-02	-6.9226e-01	-1.7239e+02	-2.1832e+01
------------	------------	------------	-------------	-------------	-------------

$K_D =$

0

APPENDIX C VARIABLE DEPENDENCE TABLES

Table C.1: The variable dependence of matrices *A* and *B*

A	1	2	3	4	5	B	1	2	3
1	-	-	-	-	-	1	-	-	-
2	-	$X_{cg}, 1/I_{yy}$	$X_{cg}, 1/I_{yy}$	$X_{cg}, 1/I_{yy}$	-	2	$X_{cg}, 1/I_{yy}$	$X_{cg}, 1/I_{yy}$	$X_{cg}, 1/I_{yy}$
3	-	$W, 1/W$	$W, 1/W$	$W, 1/W$	-	3	$1/W$	$1/W$	$1/W$
4	W	$1/W$	$1/W$	$1/W$	-	4	$1/W$	$1/W$	$1/W$
5	-	-	W	-	-	5	-	-	-

Table C.2: The variable dependence of matrices *C* and *D*

C	1	2	3	4	5	D	1	2	3
1	-	-	-	-	-	1	-	-	-
2	-	-	-	-	-	2	-	-	-
3	W	-	-	-	-	3	-	-	-
4	-	W	-	-	-	4	-	-	-
5	-	-	-	W	-	5	-	-	W
6	-	-	-	-	-	6	-	-	-

APPENDIX D PLOTS OF WEIGHTING FUNCTIONS

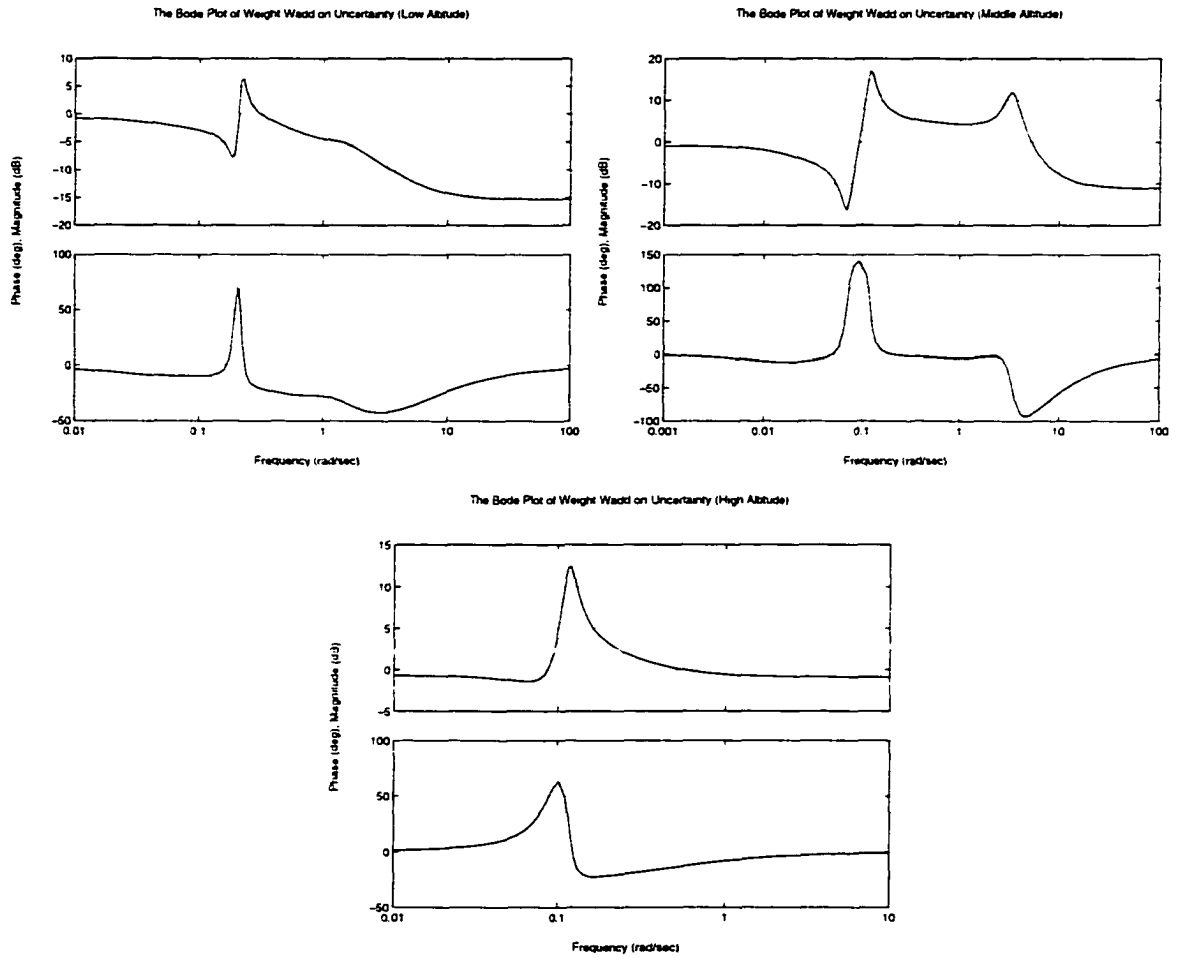


Figure D.1 Weights for multiplicative uncertainty (three flight conditions)

APPENDIX E ROBUST PERFORMANCE

Multiplicative Uncertainty: System Responses and μ Analysis (Low Altitude)

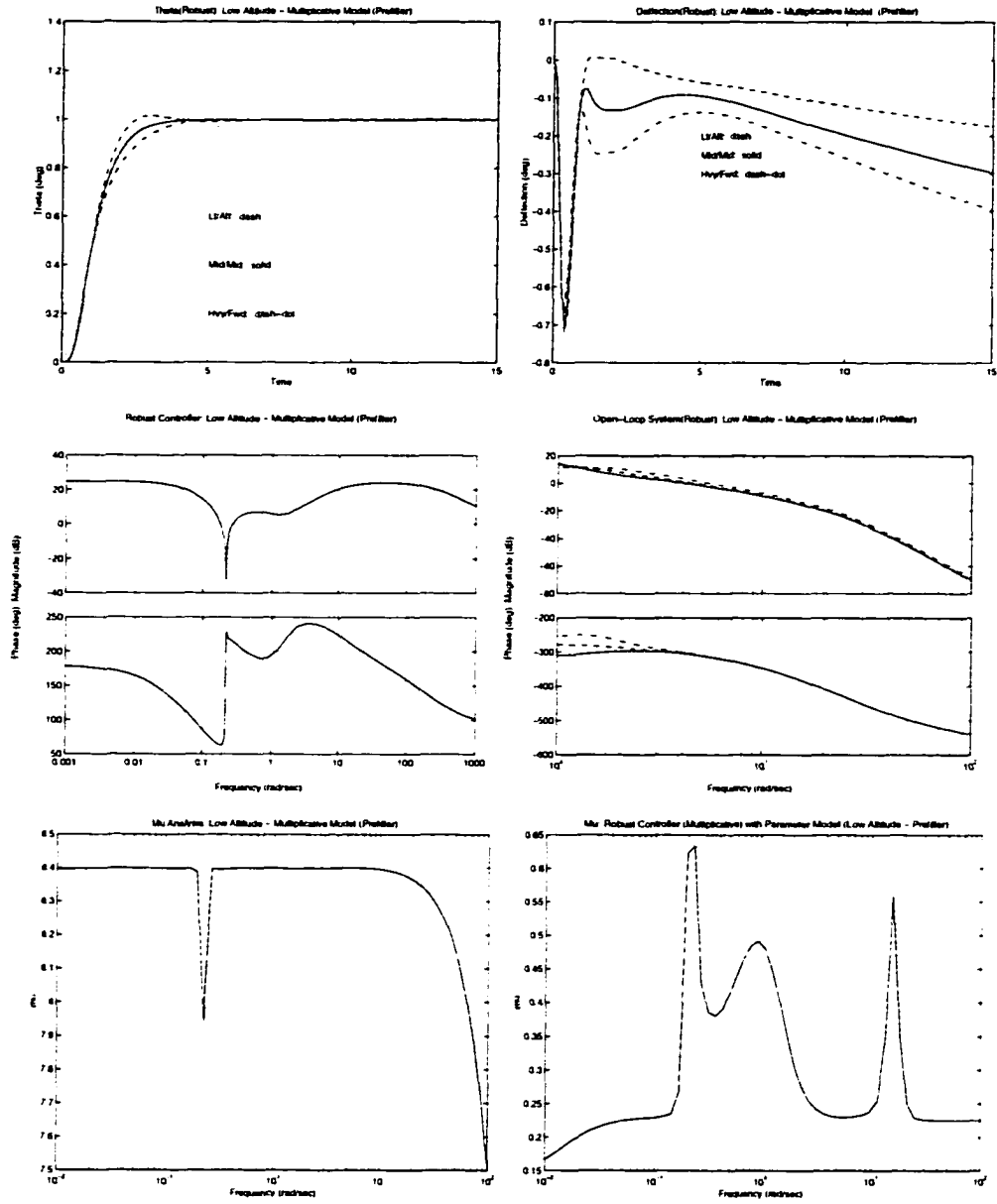


Figure E.1 Robust synthesis: Low-altitude/low-air-speed

The state-space representation (K_A, K_B, K_C, K_D) of the designed robust controller K at Low Altitude/Airspeed:

$$K_A =$$

Columns 1 through 6

-1.5256e+02	-2.3028e-01	-2.8138e-01	-1.6813e+03	0	0
2.3028e-01	-1.1105e-02	-2.1271e-01	1.2591e+00	0	0
-2.8138e-01	2.1271e-01	-1.9604e-02	-1.5609e+00	0	0
-1.9396e-34	-1.4526e-37	-1.8007e-37	4.4958e-22	1.0000e+00	0
3.8052e-02	-1.4475e-01	-4.2820e-01	-3.1211e+03	-3.4116e+02	-4.5884e-02
-2.7373e-03	1.0413e-02	3.0804e-02	2.1484e+02	1.4570e+01	-3.4477e-03
4.7010e-02	-1.7883e-01	-5.2901e-01	-3.8575e+03	-3.5977e+02	-2.2690e-01
-3.7797e-26	-2.8306e-29	-3.5091e-29	0	0	0
-3.8643e+00	1.4700e+01	4.3486e+01	3.1696e+05	3.4585e+04	5.2772e+00
7.3319e-33	5.4908e-36	6.8068e-36	1.6530e+00	0	0
4.9347e-33	3.6956e-36	4.5814e-36	1.7778e+01	0	0
-6.0118e-32	-4.5022e-35	-5.5813e-35	-4.5347e+01	0	0
-1.8251e-31	-1.3668e-34	-1.6944e-34	-1.6189e+01	0	0
-2.1625e-31	-1.6195e-34	-2.0076e-34	-3.2403e+00	0	0
2.2368e-31	1.6751e-34	2.0766e-34	-1.0919e+01	0	0
-5.3087e-18	-3.9756e-21	-4.9285e-21	-7.5079e+00	0	0
-6.9464e-18	-5.2021e-21	-6.4490e-21	-2.0630e-01	0	0
-8.5426e-19	-6.3975e-22	-7.9309e-22	4.9271e-01	0	0

Columns 7 through 12

0	5.8559e-23	0	4.9431e+00	-5.3162e+01	1.3560e+02
0	-7.3464e-26	0	-3.7019e-03	3.9813e-02	-1.0155e-01
0	1.4230e-27	0	4.5891e-03	-4.9355e-02	1.2589e-01
0	1.9965e-36	0	6.3934e-36	-6.8759e-35	1.7539e-34
2.3227e-01	5.4616e+00	5.0538e-01	-1.6129e-01	1.7443e+00	-1.2571e+00
1.8878e-01	-3.9289e-01	-3.6355e-02	1.1603e-02	-1.2548e-01	9.0429e-02
-6.0533e-01	6.7474e+00	6.2436e-01	-1.9926e-01	2.1549e+00	-1.5530e+00
0	-2.0000e-01	0	1.2459e-27	-1.3399e-26	3.4178e-26
-2.5942e+01	-5.5465e+02	-5.7324e+01	1.6380e+01	-1.7714e+02	1.2766e+02
0	-2.6916e-34	0	-4.5432e-04	2.3173e-01	-3.8001e-02
0	8.6241e-34	0	-2.3173e-01	-5.4863e-02	2.0592e-01
0	-4.1427e-33	0	3.8001e-02	2.0592e-01	-9.9373e-01
0	-1.6676e-33	0	9.8310e-03	9.0920e-02	-5.5625e-01
0	9.1362e-34	0	1.8491e-03	1.9261e-02	-1.2832e-01
0	-7.6273e-33	0	5.8715e-03	6.8997e-02	-5.1166e-01
0	-3.5386e-18	0	1.7499e-19	-1.8819e-18	4.8004e-18
0	-4.4899e-18	0	2.2897e-19	-2.4625e-18	6.2813e-18
0	1.1371e-18	0	2.8158e-20	-3.0284e-19	7.7247e-19

Columns 13 through 18

4.8412e+01	9.6898e+00	-3.2653e+01	8.4686e-19	6.3421e-22	7.8621e-22
-3.6255e-02	-7.2567e-03	2.4453e-02	5.3149e-16	3.9803e-19	4.9343e-19
4.4945e-02	8.9959e-03	-3.0314e-02	-3.7203e-16	-2.7861e-19	-3.4539e-19
6.2615e-35	1.2533e-35	-4.2233e-35	6.8679e-24	5.1433e-27	6.3761e-27
2.6995e-01	5.9983e-02	-7.0178e-01	-3.6240e+01	6.9586e-01	1.0490e+00
-1.9420e-02	-4.3150e-03	5.0485e-02	2.6070e+00	-5.0058e-02	-7.5465e-02
3.3351e-01	7.4105e-02	-8.6701e-01	-4.4773e+01	8.5969e-01	1.2960e+00
1.2202e-26	2.4423e-27	-8.2299e-27	-7.1054e-15	0	0
-2.7415e+01	-6.0916e+00	7.1270e+01	3.6804e+03	-7.0668e+01	-1.0654e+02
-9.8310e-03	-1.8491e-03	5.8715e-03	-1.0975e-21	-8.2193e-25	-1.0189e-24
9.0920e-02	1.9261e-02	-6.8997e-02	3.6469e-21	2.7311e-24	3.3857e-24
-5.5625e-01	-1.2832e-01	5.1166e-01	-1.7695e-20	-1.3252e-23	-1.6428e-23
-4.5960e-01	-1.3262e-01	8.1008e-01	-7.8455e-21	-5.8755e-24	-7.2837e-24
-1.3262e-01	-4.7544e-02	8.1311e-01	2.8563e-21	2.1391e-24	2.6518e-24
-8.1008e-01	-8.1311e-01	-8.9101e-01	-3.1081e-20	-2.3277e-23	-2.8855e-23
1.7138e-18	3.4302e-19	-1.1559e-18	-2.7104e+00	-1.1805e-01	-1.4226e-01
2.2425e-18	4.4884e-19	-1.5125e-18	1.1482e-01	-1.1192e-02	-2.1281e-01
2.7578e-19	5.5198e-20	-1.8601e-19	-1.3463e-01	2.1282e-01	-1.9468e-02

$K_B =$

7.5219e-18
4.7208e-15
-3.3045e-15
6.1002e-23
-2.7756e-22
6.1964e-22
-5.6085e-21
3.1097e+02
0
-9.7485e-21
3.2392e-20
-1.5717e-19
-6.9686e-20
2.5370e-20
-2.7607e-19
-1.0187e+00
-2.7992e-02
6.6853e-02

$K_C =$

Columns 1 through 6

 $-8.2845e-02 \quad 3.1515e-01 \quad 9.3227e-01 \quad 6.7952e+03 \quad 7.4146e+02 \quad 1.1314e-01$

Columns 7 through 12

 $-5.5615e-01 \quad -1.1891e+01 \quad -1.1003e+00 \quad 3.5116e-01 \quad -3.7976e+00 \quad 2.7368e+00$

Columns 13 through 18

 $-5.8773e-01 \quad -1.3059e-01 \quad 1.5279e+00 \quad 7.8902e+01 \quad -1.5150e+00 \quad -2.2839e+00$ $K_D =$

0

Multiplicative Uncertainty: System Responses and μ Analysis (High Altitude)

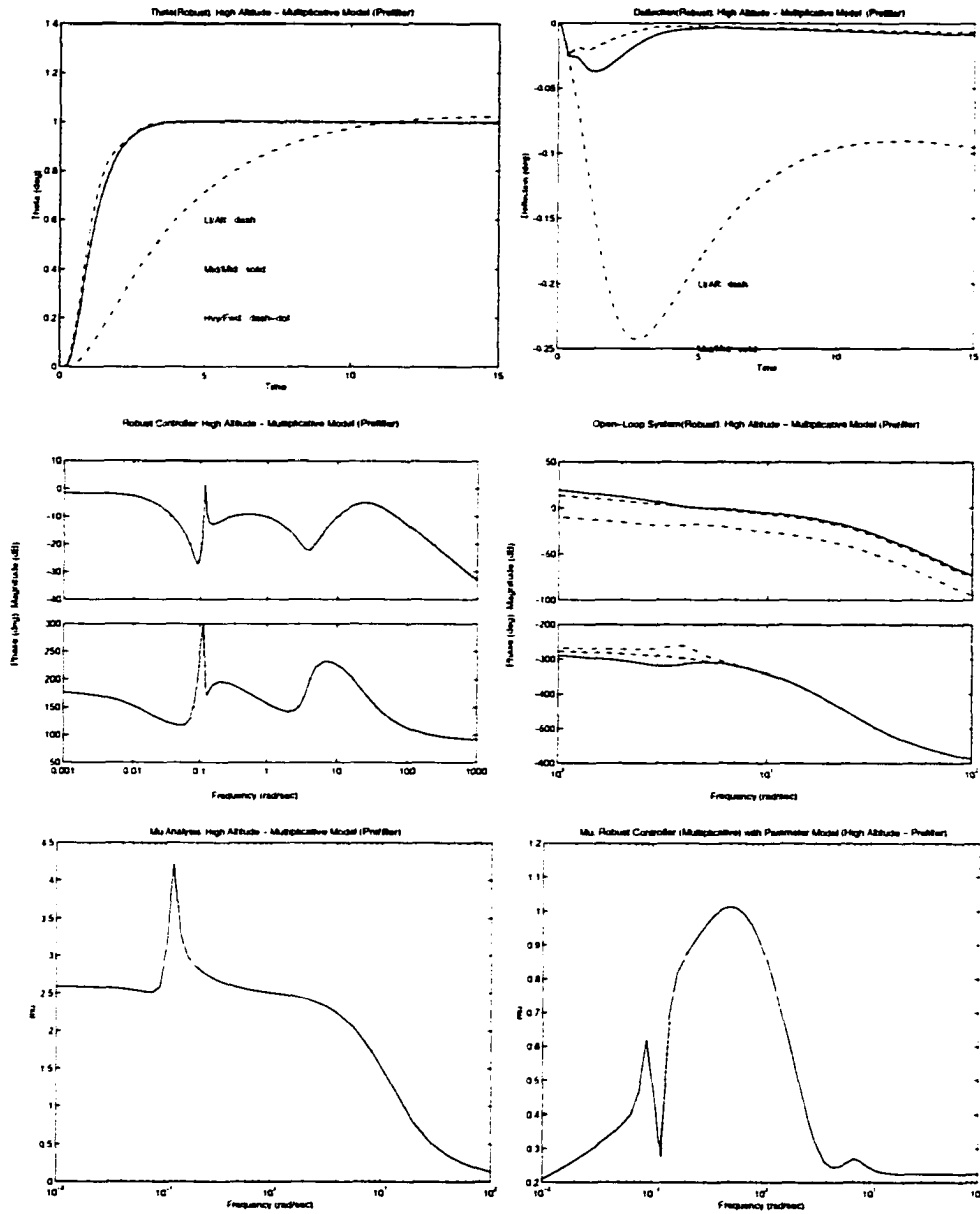


Figure E.2 Robust synthesis: High-altitude/high-air-speed

The state-space representation ($\tilde{K}_A, \tilde{K}_B, \tilde{K}_C, \tilde{K}_D$) of the designed robust controller \tilde{K} at High Altitude/Airspeed:

$\tilde{K}_A =$

Columns 1 through 6

-1.8847e+02	-3.0412e-01	2.2977e+00	2.3200e+03	0	0
3.0412e-01	-8.5296e-04	1.0788e-01	-1.6601e+00	0	0
2.2977e+00	-1.0788e-01	-8.7313e-02	-1.5506e+01	0	0
2.6647e-21	1.9068e-24	-1.7810e-23	-9.5412e-19	1.0000e+00	0
6.8035e+00	-3.6787e-03	-4.7683e-01	-5.6566e+02	-3.3309e+01	-1.5562e-05
1.9633e-02	-1.0616e-05	-1.3760e-03	-1.1438e+01	-3.7880e+00	-1.8674e-02
8.7566e-01	-4.7348e-04	-6.1371e-02	-7.2959e+01	2.2694e+02	-1.1235e-01
3.1959e-21	2.2869e-24	-2.1360e-23	0	0	0
-1.5689e+00	8.4833e-04	1.0996e-01	1.3044e+02	7.5203e+00	1.0328e-03
-1.3839e-21	-9.9028e-25	9.2498e-24	-3.2629e+00	0	0
1.3726e-20	9.8217e-24	-9.1740e-23	-1.5649e+01	0	0
1.8876e-21	1.3507e-24	-1.2616e-23	-1.4235e+01	0	0
6.9622e-19	4.9819e-22	-4.6534e-21	8.1995e+01	0	0
-9.9383e-20	-7.1115e-23	6.6425e-22	-9.1899e-02	0	0
1.0609e-18	7.5916e-22	-7.0910e-21	4.9052e+00	0	0

Columns 7 through 12

0	3.3528e-24	0	2.5519e+00	-1.2239e+01	-1.1133e+01
0	-1.1098e-24	0	-1.8260e-03	8.7579e-03	7.9666e-03
0	2.6698e-25	0	-1.7056e-02	8.1804e-02	7.4412e-02
0	-5.8113e-27	0	-4.0406e-23	1.9379e-22	1.7628e-22
-1.6419e-04	4.7677e+00	9.3602e-04	-7.9783e-02	7.1290e-03	2.3623e-01
1.0748e-02	1.3758e-02	2.7011e-06	-2.3023e-04	2.0572e-05	6.8169e-04
-1.3861e+00	6.1363e-01	1.2047e-04	-1.0269e-02	9.1755e-04	3.0405e-02
0	-2.0000e-01	0	-4.8459e-23	2.3242e-22	2.1142e-22
-1.3797e-02	-1.0994e+00	-1.0002e+00	1.8398e-02	-1.6440e-03	-5.4475e-02
0	-5.5455e-27	0	-9.2097e-04	1.1888e-01	8.7365e-03
0	1.7750e-26	0	-1.1888e-01	-2.2886e-02	-3.8316e-02
0	-3.1268e-28	0	-8.7365e-03	-3.8316e-02	-2.1859e-01
0	-2.1801e-18	0	-1.0557e-20	5.0632e-20	4.6057e-20
0	-1.1027e-17	0	1.5069e-21	-7.2275e-21	-6.5744e-21
0	-1.7493e-17	0	-1.6087e-20	7.7155e-20	7.0183e-20

Columns 13 through 15

6.0462e-17	4.3264e-20	-4.0411e-19
-6.5134e-14	-4.6607e-17	4.3534e-16
-7.4086e-15	-5.3013e-18	4.9517e-17
6.0134e-20	4.3030e-23	-4.0192e-22
6.8355e+00	-2.3434e-01	2.2669e+00
1.9725e-02	-6.7622e-04	6.5417e-03
8.7978e-01	-3.0161e-02	2.9177e-01
-3.5527e-15	0	2.7756e-17
-1.5763e+00	5.4038e-02	-5.2276e-01
5.7887e-21	4.1422e-24	-3.8690e-23
-2.3063e-19	-1.6503e-22	1.5414e-21
-5.7341e-20	-4.1031e-23	3.8325e-22
-2.5542e+01	-1.8754e-01	1.2088e+00
1.8972e-01	-9.3483e-04	1.0865e-01
8.5135e-01	-1.0892e-01	-7.7646e-02

$K_B =$

-1.4704e-16

1.5841e-13

1.8018e-14

-1.4625e-19

4.3168e-19

-7.8287e-19

4.0137e-17

7.3071e+01

0

-1.4078e-20

5.6088e-19

1.3945e-19

1.3071e+01

-1.4650e-02

7.8198e-01

$K_C =$

Columns 1 through 6

-3.4354e-01 1.8575e-04 2.4077e-02 2.8563e+01 1.6467e+00 2.2615e-04

Columns 7 through 12

-3.0211e-03 -2.4074e-01 -4.7263e-05 4.0286e-03 -3.5997e-04 -1.1928e-02

Columns 13 through 15

-3.4515e-01 1.1833e-02 -1.1447e-01

$K_D =$

0

Multiplicative Uncertainty: System Responses and μ Analysis (Middle Altitude)

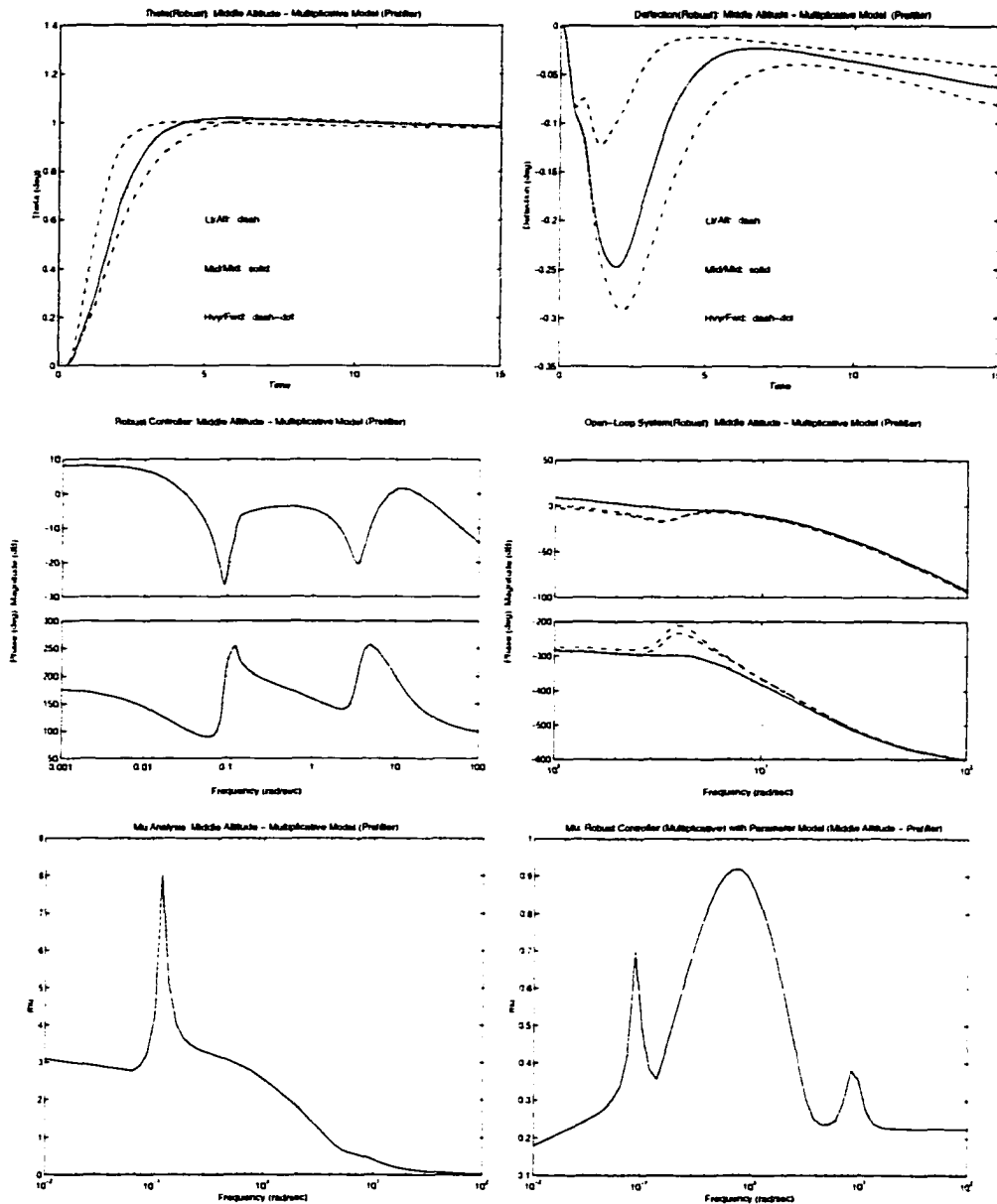


Figure E.3 Robust synthesis: Middle-altitude/high-air-speed

The state-space representation (K_A, K_B, K_C, K_D) of the designed robust controller K at Middle Altitude/Airspeed:

$K_A =$

Columns 1 through 6

-1.3440e-02	-7.7249e-02	-3.5857e+00	0	0	0
7.7249e-02	-1.0437e-02	2.7123e+00	0	0	0
0	0	0	1.0000e+00	0	0
-2.1096e-02	2.0624e-02	-1.7052e+02	-1.7618e+01	-9.7767e-05	-2.6352e-03
-2.2723e-04	2.2215e-04	-1.1643e+01	-2.4455e+00	-1.3617e-02	4.1638e-02
-2.7088e-02	2.6482e-02	-2.1908e+02	1.5279e+02	-9.8664e-02	-1.6268e+00
5.2191e-37	3.9477e-37	-1.4211e-14	0	0	0
7.2925e-03	-7.1293e-03	5.8946e+01	5.7191e+00	1.3733e-03	-3.1176e-02
0	0	9.3630e+00	0	0	0
0	0	2.5314e+01	0	0	0
0	0	1.0464e+02	0	0	0
0	0	-5.4717e+01	0	0	0
0	0	3.4403e+01	0	0	0
0	0	-2.1087e+01	0	0	0
5.1003e-18	3.8579e-18	-3.7704e+00	0	0	0
-9.5587e-19	-7.2303e-19	5.7906e+00	0	0	0

Columns 7 through 12

-6.9340e-36	0	3.6714e-02	-9.9262e-02	-4.1032e-01	-2.1456e-01
2.1271e-36	0	-2.7771e-02	7.5083e-02	3.1037e-01	1.6229e-01
0	0	0	0	0	0
2.7762e+00	-1.8979e-02	-2.2632e-01	-3.4096e-01	-4.5985e+00	-7.3015e-01
2.9903e-02	-2.0443e-04	-2.4378e-03	-3.6726e-03	-4.9532e-02	-7.8646e-03
3.5647e+00	-2.4369e-02	-2.9060e-01	-4.3780e-01	-5.9045e+00	-9.3752e-01
-1.0000e-01	0	3.7829e-37	-1.0228e-36	-4.2278e-36	-2.2107e-36
-9.5969e-01	-9.9344e-01	7.8236e-02	1.1786e-01	1.5896e+00	2.5240e-01
0	0	-3.4938e-03	1.3441e-01	1.5838e-01	2.9773e-02
0	0	-1.3441e-01	-2.9714e-02	-1.5452e-01	-2.2627e-01
0	0	-1.5838e-01	-1.5452e-01	-8.6086e-01	-3.3709e+00
0	0	2.9773e-02	2.2627e-01	3.3709e+00	-3.2115e-01
0	0	-2.7097e-02	-7.6118e-02	-5.1294e-01	4.7028e-01
0	0	1.6301e-02	4.7590e-02	3.2479e-01	-2.7295e-01
2.5398e-18	0	3.6969e-18	-9.9949e-18	-4.1316e-17	-2.1604e-17
-3.6331e-18	0	-6.9284e-19	1.8732e-18	7.7433e-18	4.0489e-18

Columns 13 through 16

-1.3490e-01	8.2687e-02	-5.1220e-29	-3.8743e-29
1.0204e-01	-6.2545e-02	1.5712e-29	1.1885e-29
0	0	0	0
-2.7146e-01	2.5870e-01	1.4312e+00	8.7884e-01
-2.9240e-03	2.7865e-03	1.5416e-02	9.4663e-03
-3.4856e-01	3.3217e-01	1.8377e+00	1.1284e+00
-1.3900e-36	8.5198e-37	0	0
9.3838e-02	-8.9427e-02	-4.9475e-01	-3.0380e-01
2.7097e-02	-1.6301e-02	0	0
-7.6118e-02	4.7590e-02	0	0
-5.1294e-01	3.2479e-01	0	0
-4.7028e-01	2.7295e-01	0	0
-8.9865e-01	6.6396e-01	0	0
6.6396e-01	-5.1216e-01	0	0
-1.3584e-17	8.3260e-18	-4.9257e-02	-1.0434e-01
2.5458e-18	-1.5604e-18	9.2777e-02	1.3089e-03

$K_B =$

7.5223e-28

-2.3075e-28

0

0

0

0

6.6222e+00

0

0

0

0

0

0

0

-2.1789e-01

3.3464e-01

$K_C =$

Columns 1 through 6

2.2024e-02 -2.1532e-02 1.7802e+02 1.7273e+01 4.1477e-03 -9.4155e-02

Columns 7 through 12

-2.8984e+00 1.9814e-02 2.3628e-01 3.5596e-01 4.8009e+00 7.6228e-01

Columns 13 through 16

2.8341e-01 -2.7008e-01 -1.4942e+00 -9.1752e-01

$K_D =$

0

Multiplicative Uncertainty: System Responses and μ Analysis (Middle Altitude with Reduced Controller 5th)

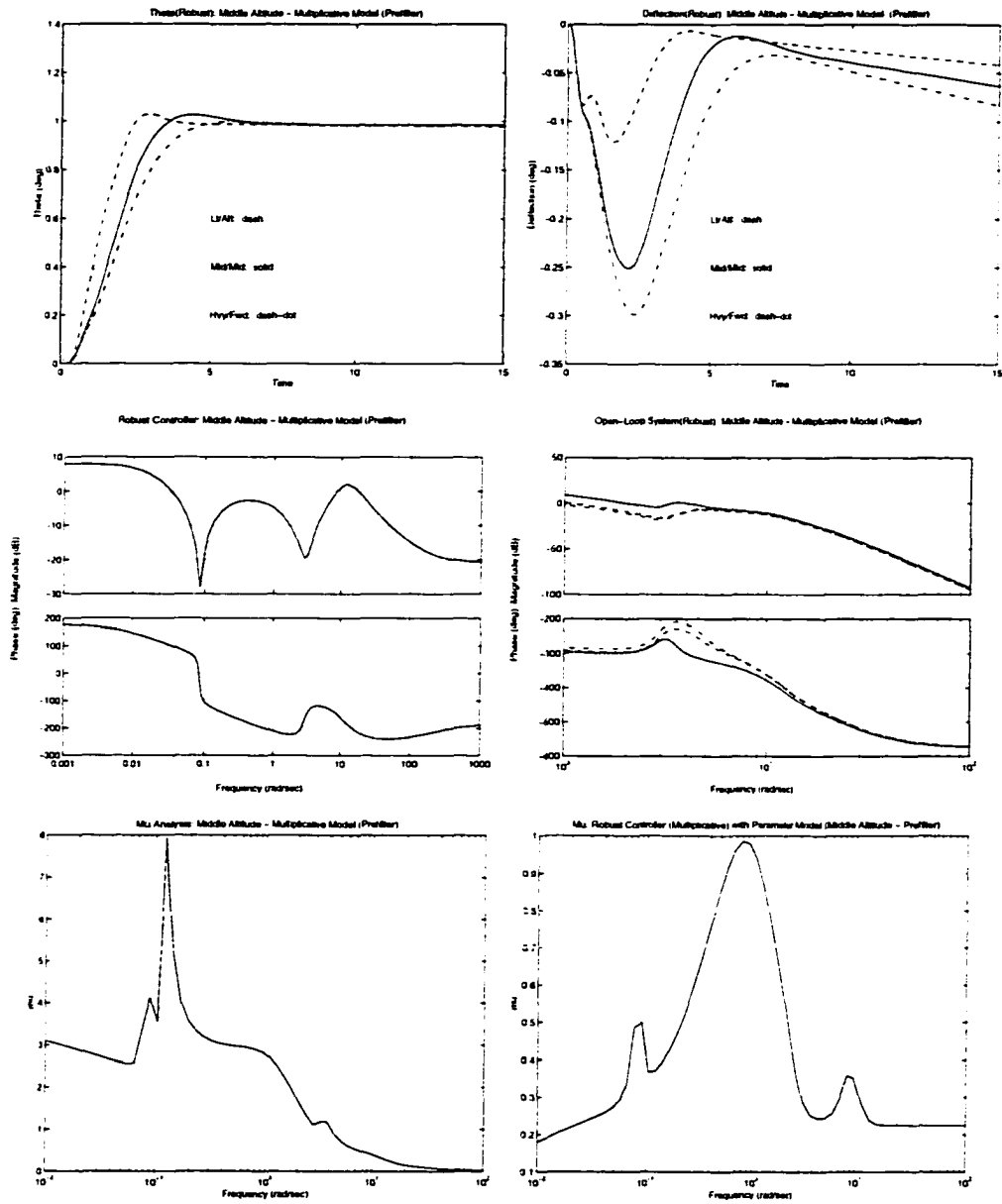


Figure E.4 Reduced robust controller (5th): Middle-altitude/high-airspeed

The state-space representation (K_A, K_B, K_C, K_D) of the reduced robust controller K (5th order) at Middle Altitude/Airspeed:

$K_A =$

-3.9403e-01	1.3741e+01	1.3963e+00	5.5590e-01	1.6410e-01
-9.6335e+00	-1.0473e+01	-6.5654e+00	-2.5424e+00	-8.5174e-01
0	0	-1.0571e+00	-7.8689e-01	-2.5107e-01
0	0	0	-1.4247e-01	-9.6089e-02
0	0	0	0	-1.8328e-02

$K_B =$

-5.8067e-01

3.5659e+00

8.8631e-01

3.6106e-01

2.1136e-01

$K_C =$

5.5692e-01 -3.5740e+00 -8.8366e-01 -2.7071e-01 -1.8505e-01

$K_D =$

-9.2521e-02

BIBLIOGRAPHY

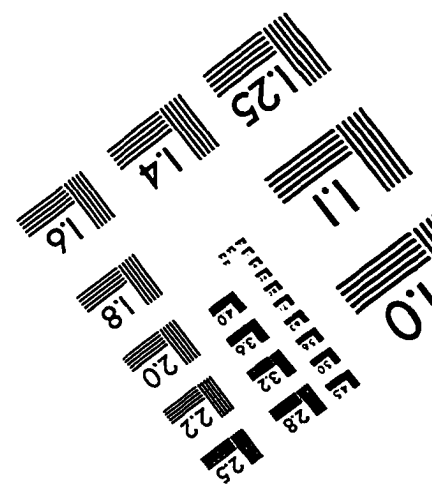
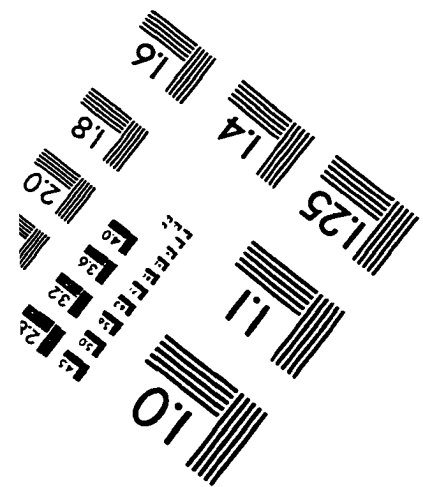
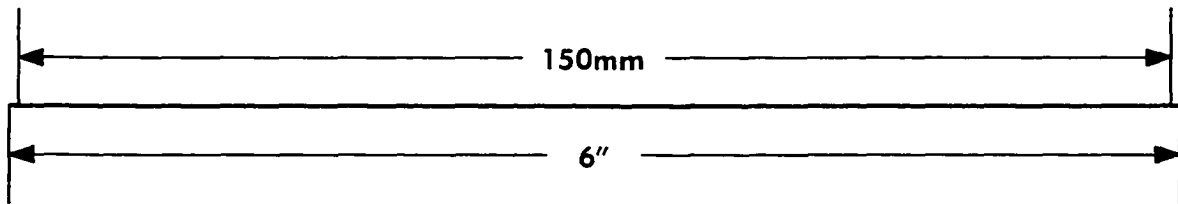
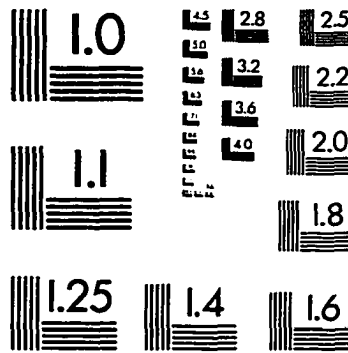
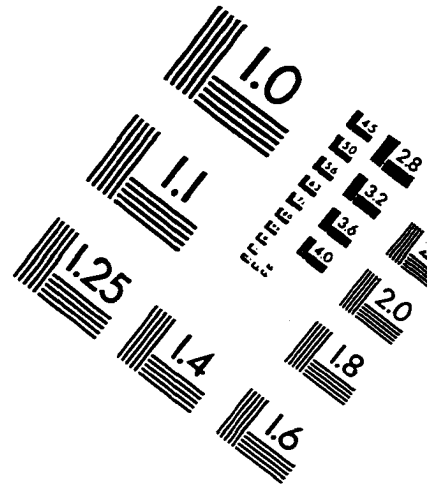
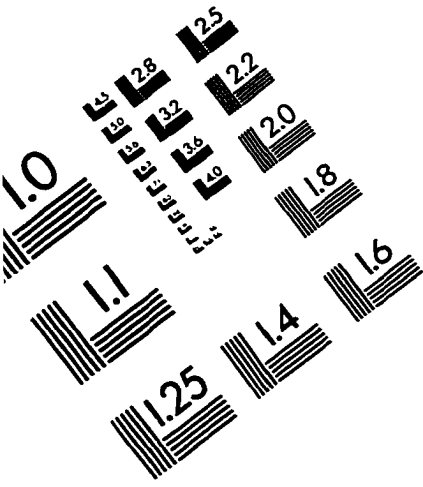
- [1] J. Almquist. *Rockwell/Iowa State University Robust Control Law Design Project*. Rockwell Collins, Inc., Cedar Rapids, Iowa. 1997.
- [2] G. Balas, J. Dolye, K. Glover, A. Packard, and R. Smith *mu-Analysis and Synthesis TOOLBOX*. MUSYN Inc. and The Mathworks Inc. Natick. 1995.
- [3] B. A. Bamieh, M. A. Dahleh, and J. B. Pearson. "Minimization of the \mathcal{L}^∞ -induced norm for sampled-data systems," *IEEE Trans. Auto. Control*. vol.38, no.5, pp.717-732. 1993.
- [4] B. A. Bamieh and J. B. Pearson, "A general framework for linear periodic systems with application to \mathcal{H}_∞ sampled-data control," *IEEE Trans. Auto. Control*. vol.37, pp.418-435. 1992.
- [5] B. A. Bamieh and J. B. Pearson, "The \mathcal{H}_2 problem for sampled-data systems." *Systems & Control Letters*, vol.19, pp.1-12, 1992.
- [6] B. A. Bamieh, J. B. Pearson, B. A. Francis, and A. Tannenbaum, "A lifting technique for linear periodic systems with applications to sampled-data control." *Systems & Control Letters*, vol.17, pp.79-88, 1991.
- [7] R. G. Bartle, and D. R. Sherbert, *Introduction to Real Analysis*. New York: John Wiley & Sons. 1982.

- [8] T. Chen. and B. Francis. "On the \mathcal{L}_2 -induced norm of a sampled-data system." *Systems & Control Letters*, vol.15, pp.211-219, 1990.
- [9] T. Chen. and B. Francis. "Input-output stability of sampled-data systems." *IEEE Trans. Auto. Control*, vol.36, pp.50-58, 1991.
- [10] T. Chen. and B. Francis. *Optimal Sampled-Data Control Systems*. New York: Springer. 1995.
- [11] M. A. Dahleh. and Y. Ohta, "A necessary and sufficient condition for robust BIBO stability." *Systems & Control Letters*, vol.11, pp.271-275, 1988.
- [12] M. A. Dahleh. and J. B. Pearson. " l^1 optimal feedback controllers for MIMO discrete-time systems." *IEEE Trans. Auto. Control*, vol.32, no.4. pp.314-322. 1987.
- [13] M. A. Dahleh. and J. B. Pearson. " \mathcal{L}^1 -optimal compensators for continuous-time systems." *IEEE Trans. Auto. Control*, vol.32, no.10. pp.889-895. 1987.
- [14] J. Dolye. "Lecture notes in advances in multivariable control." 1984.
- [15] J. Dolye. B. Francis. and A. Tannenbaum. *Feedback Control Theory*. Macmillan Publishing Company. New York. 1992.
- [16] G. Dullerud. "Tracking and \mathcal{L}_1 performance in sampled-data control systems." M.A.Sc. Thesis. Dept. of Electrical Engineering, University of Toronto. 1990.
- [17] G. Dullerud. and B. A. Francis, " \mathcal{L}_1 performance in sampled-data systems." *IEEE Trans. Auto. Control*, vol.37, pp.436-446, 1992.
- [18] G. Dullerud. and K. Glover, "Robust stabilization of sampled-data systems to structured LTI perturbations." *IEEE Trans. Auto. Control*, vol.38, pp.1497-1508. 1993.

- [19] B. Francis, and T. Georgiou, "Stability theory for linear time-invariant plants with periodic digital controllers," *IEEE Trans. Auto. Control*, vol.33, no.9, pp.820-832, 1988.
- [20] K. Glover, and J. Dolye, "State-space formulae for all stabilizing controllers that satisfy an \mathcal{H}_∞ norm bound and relations to risk sensitivity." *System and Control Letters*, vol.11, pp.167-172, 1988.
- [21] S. Hara, and H-K Sung, "Ripple-free conditions in sampled-data control systems." *Proc. IEEE CDC*, 1991.
- [22] R. Horn, and C. Johnson. *Matrix Analysis*, Cambridge: Cambridge University Press, 1985.
- [23] P. T. Kabamba, and S. Hara. "On computing the induced norm of a sampled-data system." In *Proc. ACC*, pp.319-320, 1990.
- [24] M. Khammash. "Necessary and sufficient conditions for the robustness of time-varying systems with applications to sampled-data systems." *IEEE Trans. Auto. Control*, vol.38, no.1, pp.49-57, 1993.
- [25] M. Khammash. "Robust steady-state tracking," *IEEE Trans. Auto. Control*, vol.40, no.11, pp.1872-1880, 1995.
- [26] M. Khammash. "Robust Performance: Unknown Disturbances and Known Fixed Inputs," *IEEE Trans. Auto. Control*, to present.
- [27] M. Khammash, and J. B. Pearson. "Analysis and design for robust performance with structured uncertainty," *Systems & Control Letters*, vol.20, pp.179-187, 1993.
- [28] M. Khammash, and J. B. Pearson. "Performance robustness of discrete-time systems with structured uncertainty," *IEEE Trans. Auto. Control*, vol.36, no.4, pp.398-412, 1991.

- [29] G. M. H. Leung, T. P. Perry, and B. A. Francis, "Performance analysis of sampled-data control systems," *Automatica*, vol.27, pp.699-704, 1991.
- [30] N. Sivashankar, and P. P. Khargonekar, "Induced norms of sampled-data systems," *Automatica*, vol.28, pp.1267-1272, 1992.
- [31] N. Sivashankar, and P. P. Khargonekar, "Robust stability and performance analysis of sampled-data systems," *IEEE Trans. Auto. Control*, vol.38, no.1, pp.58-69, 1993.
- [32] M. Vidyasagar, "Optimal rejection of persistent bounded disturbances," *IEEE Trans. Auto. Control*, vol.31, pp.527-534, 1986.
- [33] L. Zou, and M. Khammash, "MIMO robust steady-state tracking". *Fifth Annual Midwest Electro-Technology Conference*, April, 1996.
- [34] L. Zou, and M. Khammash, "Robust steady-state tracking of sampled-data systems". *Proc. ACC Conference*, pp.3616-3620, June, 1997.
- [35] L. Zou, and M. Khammash, "Robust steady-state tracking for periodic systems". *Proc. ACC Conference*, June, 1998.
- [36] L. Zou, and M. Khammash, *Rockwell/Iowa State University Robust Control Law Design Project Report*, Iowa State University, Ames, 1997.

IMAGE EVALUATION TEST TARGET (QA-3)



APPLIED IMAGE, Inc
 1653 East Main Street
 Rochester, NY 14609 USA
 Phone: 716/482-0300
 Fax: 716/288-5989

© 1993. Applied Image, Inc., All Rights Reserved